CHEMICAL SYNTHESIS IN ELASTOMER-BASED INTEGRATED MICROFLUIDICS

Thesis by

Cheng-Chung Lee

In partial fulfillment of the requirements

For the degree of

Doctor of Philosophy

California Institute of Technology

Pasadena, California

2010

(Defended November 23, 2009)

©2010

Cheng-Chung Lee

All Rights Reserved

Acknowledgements

I would like to thank my advisor, Stephen Quake, for his mentorship and guidance over the course of my graduate student career. He has taught me how to think critically as well as work independently in my research. Working for Steve was an invaluable experience and I thoroughly enjoyed the time I spent in his laboratory.

I would also like to thank our collaborators Michael Phelps and Hsian-Rong Tseng for their interest in the application of microfluidics to the synthesis of PET molecular probes and thus opening up this field of work for me. In particular, I would like to thank Guodong Sui in Tseng's lab for sharing his knowledge of organic chemistry techniques and assisting me with all the chemical preparations for synthesis of FDG.

I am also grateful for all the excellent colleagues that I have had an opportunity to work with over the past years. Carl Hansen was a tremendous resource when I was starting out and I learned many tool of the trade regarding microfluids from him. I also really enjoyed working with Yanyi Huang and Piero Castrataro on DNA synthesizer made of PFPE. While the work on peptide synthesis with Yinthai Chan did not pan out, his subsequent work with Thomas Snyder on gene assembly helped tremendously in testing the functionality of oligonucleotides synthesized.

I would also like to thanks the late night crew of Stavros Stavrakis, Jerrod Schwartz, and Aaron Streets for their company in lab. I appreciate all the help that I have received from the rest of the Quake lab over the years. Sebastian Maerkl, Megan Anderson, Ziyang Ma, Jong Wook Hong, Yann Marcy, Rafael Gomez-Sjoberg, Paul Blainey, Doron Gerber, Jenny Ning, Anne Leyrat, Tomer Kalisky, Angela Wu, Christina Fan, and Jianbin Wang have always been extremely generous with their time and knowledge. A special thanks to Jason Imada and Thomas Snyder as proofreaders of my works.

Finally, I would like to thank my family who has always been there for me. I appreciate the continual support and encouragement from my parents, and my brother. Above all, I thank my wife Kathryn for her unending love, patience, and support. Not many could have accepted me with all my little flaws and quirks but she has stuck with me through thick and thin. My life is that much more fulfilled having journeyed down this road together with her.

Abstract

There is wide interest in using the unique properties of microfluidic environments for the production of fine chemicals and pharmaceuticals. Compared to bench top synthesis, microfluidic systems engender the significant advantage of superior control of chemical state functions. The ability to tune reagent concentration, reaction temperature, mixing time, and residence time allows reactions to run more efficiently thus generating products of higher yield and purity. While several microfluidic platforms are actively developed in both academic and industrial laboratories, vast majority are based in rigid materials and have only demonstrated improvements in yield for single reaction steps.

Multilayer Soft Lithography has already found much use in the biological field. For example, several complex devices based upon functional modules have been developed for protein crystallography, nucleic acid processing, FACS, enzyme screening tools, and PCR. Because of the many similarities between operations in organic synthesis and biochemistry, there is widespread interest in extending these newfound successes in the realm of biology to the realm of automated chemical synthesis.

This thesis focuses on the application of Multilayer Soft Lithography to the development and adaptation of microfluidic tools for chemical synthesis. The first successful demonstration of multistep organic synthesis in integrated microfluidics was the production of a molecular image probe, 2-deoxy-2-[18F]fluoro-d-glucose. The nanogram level dosage for imaging probes makes them attractive candidates for small scale synthesis of microfluidics. The reduced synthesis time achieved by using a microfluidic device is especially important because of the relatively short half-life of the radioactive fluoride.

While PDMS remains the material of choice for devices in biological applications, its incompatibility with many nonpolar organic solvents limits the types of reactions that can be performed with it. Through collaboration with Joseph DeSimone's group at the University of North Carolina at Chapel Hill, a suitable substitute for PDMS was found in perfluoropolyethers (PFPE). A solvent-resistant integrated microfluidic device was developed for solid-phase oligonucleotide synthesis using conventional phosphoramidite chemistry. To confirm that the microfluidic platform in development can indeed become a valuable tool in the field of synthetic biology, a 16 column parallel oligonucleotide synthesizer was manufactured that is capable of producing 16 distinct sequences up to 40 bases in length to be used in gene assembly. Successful construction of a gene fragment was completed from a mixture of unpurified and unamplified oligonucleotides synthesized on the device.

Table of Contents

List of Figures

List of Tables

Chapter 1

OVERVIEW

Introduction

There is great interest in exploiting the unique properties of microfluidic environments for producing fine chemicals and pharmaceuticals (1--3). The reduced length scale associated with microfluidic architecture allows access to an extraordinary physical regime that is often counterintuitive yet advantageous to experiences in the macroscopic world.

The most notable effects that manifest in this microenvironment are diminished inertial nonlinearity, enhanced heat transfer, increased surface-to-volume ratio and reduced diffusion time (4). In fact, there are many examples where microreactors have been used to take advantage of each of these effects to facilitate chemical processes.

With the decline in inertial forces, fluid flows at low Reynolds Numbers are almost strictly laminar. Two immiscible fluids can stream side-by-side in concurrent or countercurrent flow arrangements without mixing. By choosing two liquids that have different partition coefficients to the molecule of interest, continuous extraction of solute from one phase to another is achievable as demonstrated by Aota et al. (5).

Also, as a direct result of miniaturization, typical microfluidic devices have reduced thermal masses. High thermal transfer efficiencies allow many exothermic or high

temperature reactions to be performed with unprecedented control. Fluorine chemistry has always been a field plagued with safety issues such as thermal runaway and explosions because the change in enthalpy from a carbon-hydrogen bond to carbon-fluorine bond is so extreme. De Mas et al. have reported direct fluorination of toluene under isothermal conditions at room temperature, which looks promising for future commercialization (6).

The large surface-to-volume ratios characteristic of microfluidic reactors are exceptionally well suited for performing heterogeneous chemistry. Typically, these reactions are difficult to conduct when compared to homogeneous reactions because the efficiency of interaction and mass transfer between different phases is low. To accelerate multiphase catalytic reactions, high interfacial area between the two or three reacting phases needs to be produced through vigorous stirring. By switching from a macro scale setting to microfludics, the interfacial area per unit of volume can increase by 3 to 4 orders of magnitude. Through incorporation of a catalyst into the channel surfaces, Kobayashi et al. reported triphasic hydrogenation with space-time yield considerably higher than that of laboratory-scale reactions (7).

In typical microfluidic devices, mixing is accomplished though diffusion. However, unlike in the macroscopic world, where diffusive mixing is highly inefficient, diffusion time can be very small at a micron length scale. A further advantage of diffusive mixing is that it can be spatially controlled. By manipulating the width of the diffusive length and the flow rate of the streams, one can not only achieve mixing times of less than 10

microseconds, but can also determine the residence time from the distance that the mixture has traveled since it first converged. In fact, ultra-fast chemical reactions have been probed through the use of hydrodynamic focusing (8,9).

The above examples provide persuasive arguments for using microfluidic systems in chemical synthesis. Compared to bench-top synthesis, microfluidic systems engender the significant advantage of superior control of chemical state functions. The ability to tune reagent concentration, reaction temperature, mixing time, and residence time allows reactions to run more efficiently thus generating products of higher yield and purity. However, currently most applications are limited to the implementation of individual reaction units to demonstrate enhanced performance compared with their macroscale counterparts; to date, applications involving total synthesis of molecular compounds involving multiple reactions steps with intermediate workup are almost nonexistent.

There are many reasons why adaptation of microfludics to complete molecular synthesis is not yet possible. Among the major challenges is the inability to manipulate and process diverse reagents and solvents in an efficient manner that can be coupled to perform complex multi-step synthesis. In this regard, microfluidic systems with integrated microvalves represent a device architecture that is much better suited to the execution and automation of multiple, parallel, and sequential chemical processes than the continuous flow devices that are more prevalent in the current literature.

That is not to say that continuous flow reactors are inferior. The use of microfluidics in production applications will ultimately be determined by their ability to generate useful volumes of product on short time scales, and continuous flow reactors in combination with parallelization (scale out approach) have greater potential for large scale production of a single compound. However, there exist many applications in which the ability to generate minute amounts of large number of diverse products is desirable, especially in lead generation for drug discovery or oligonucleotide synthesis for gene or genome assembly (10,11). The work presented here will attempt to fill that niche of molecular synthesis with integrated microfluidics.

Context

The technologies used in this thesis utilize and build upon the multilayer soft lithography (MSL) process developed in the Quake group by Unger et al. (12). MSL uses soft elastomeric rubber such as polydimethylsiloxane (PDMS) to fabricate active monolithic valves, which are the fundamental building blocks used to assemble higher level fluidic components such as pumps, mixers, columns, and multiplexers (13). These high level components (or modules) can then be incorporated to perform complex operations in seamless fashion much like integrated circuits.

At the initiation of this work, MSL has already found much use in the biological field. For example, several complex devices based upon functional modules have been developed for protein crystallography, nucleic acid processing, FACS, enzyme screening tools, and PCR (14--19). Some, such as devices for protein crystal growth and digital PCR, were in the early stages of commercialization. Because of the many similarities

between operations in organic synthesis and biochemistry, there is widespread interest in extending these newfound successes in the realm of biology to the realm of automated chemical synthesis.

The focus of this thesis is the application of multilayer soft lithography to the development and adaptation of microfluidic tools for chemical synthesis. The first successful demonstration of multistep organic synthesis in integrated microfluidics was the production of a molecular image probe, 2-deoxy-2-[^{18}F]fluoro-D-glucose. The nanogram level dosage for imaging probes makes them attractive candidates for small scale synthesis of microfluidic. Gas permeability of PDMS matrix was exploited for successful solvent exchange through evaporation. The reduced synthesis time achieved by using a microfluidic device is especially important because of the relatively short half-life of the radioactive fluoride. Overall, it provides a glimpse of the capabilities of integrated elastomeric-based microfluidic by successfully proving its utility for synthesizing molecular probes.

While PDMS remains the material of choice for devices in biological applications, its incompatibility with many nonpolar organic solvents limits the types of reactions that can be performed with it. The field of chemical synthesis could benefit tremendously from the development of solvent-resistant elastomeric microfluidic devices. Through collaboration with Joseph DeSimone's group at the University of North Carolina at Chapel Hill, a suitable substitute for PDMS was found in perfluoropolyethers (PFPE). With the help of Piero Castrataro, who perfected the fabrication protocol for PFPE

devices, a solvent-resistant integrated microfluidic device was developed for solid-phase oligonucleotide synthesis using conventional phosphoramidite chemistry.

To confirm that the microfluidic platform in development can indeed become a valuable tool in the field of synthetic biology, a 16 column parallel oligonucleotide synthesizer was manufactured that is capable of producing 16 distinct sequences up to 40 bases in length to be used in gene assembly. Successful construction of a gene fragment was completed from a mixture of unpurified and unamplified oligonucleotides synthesized on the device.

In order to produce the tens of thousands of distinct oligonucleotide strands needed for genome synthesis, several technical issues need to be addressed. The ability to address appropriate reactors in each synthetic step becomes increasingly difficult as the number of reactors increases. Two strategies are devised to overcome such problems. The first strategy involves the adaptation of a demultiplexer (demux) to address multiple valves from a single pressure input, termed “control of control” by others. The second strategy takes advantage of the ease of the design and fabrication of PDMS devices to manufacture synthesizers that are tailored to specific sequences. While the startup and fabrication costs of conventional glass or silica microfluidic devices make it unfeasible to design and make devices for single use customized applications, the simplicity of MSL fabrication makes such strategies reasonable.

Organization and Collaborations

Chapter 2 describes an integrated microfluidic device designed for rapid synthesis of a [^{18}F]radio-labeled molecular imaging probe, 2-deoxy-2-[^{18}F]fluoro-D-glucose ([^{18}F]FDG)(20) on a nanogram scale that is sufficient for PET studies in mice. This device integrates valves, peristaltic pumps, an anion exchange column, and reaction loops to perform several sequential processes—fluoride concentration, fluorination, solvent exchange, and hydrolytic deprotection. A modular approach is taken in the design of the device. High level components, such as the anion exchange column and reactions loops are first constructed, tested, and optimized for each process before integration. The results of the development of each component module are presented. The modules are then integrated and the combined design is simplified down to its final state. Work involving fluorination and hydrolytic deprotection was done in collaboration with Guodong Sui from Hsian-Rong Tseng's group at the University of California, Los Angeles. [^{18}F]fluoride from proton-bombarded [^{18}O]water was provided by Nagichettiar Satyamurthy at The Crump Institute for Molecular Imaging. A second-generation device capable of synthesizing [^{18}F]FDG dose sufficient for several human PET scans was designed by Arkadij Elizarov. The product from the second-generation device was utilized for microPET- and microCT-based molecular imaging of two mouse models.

Chapter 3 describes an automated DNA synthesizer made of PFPE (perfluoropolyether) that is capable of synthesizing 60 pmol of DNA oligonucleotides up to 20 nucleotides in length with substantial savings in reagent consumption (by 60-fold). The reaction cycles performed are adopted from the widely used phosphoramidite method (21,22). The

device remains robust and functional even after hours of exposure to organic solvents such as dichloromethane that are incompatible with PDMS. Electrospray ionization liquid chromatography mass spectrometry is used to characterize synthesized oligonucleotides. The sequence is further confirmed through melting curve measure with matched and mismatched complementary strands. Fabrication of PFPE devices was developed and provided by Piero Castrataro, and the adaptation of phosphoramidite chemistry was done by Yanyi Huang.

Chapter 4 describes a second-generation oligonucleotide synthesizer made of PDMS that can produce sixteen distinct sequences in parallel. The scale of synthesis is increased to ~ 100 pmol so there are enough products for both standard analytical methods as well as gene assembly without further amplification. The reagent consumption on a per sequence basis is further reduced by 2-fold compared with a previous generation single reactor microfluidic DNA synthesizer. The development of a new deblocking solution was necessary due to dichloromethane's incompatibility with PDMS. The deblocking efficiency of the new deblocking solution is calculated to be greater than 98.6%, which is substantially higher than that of many other PGA systems (23). We also added an additional capping step that was not used in our original synthesis of short nucleotides. By capping unreacted bases, we prevented truncated sequence from extending further and were able to synthesize oligonucelotides up to 40 bases in length (twice as long as our previous devices). A mixture of 17--24-mers oligos were also synthesized and used in a ligation-mediated assembly method to generate a gene fragment from *Bacillus cereus* approximately 200 base pairs in length. Sequencing revealed that the error rate is

consistent with other assembly methods using unpurified oligonucleotides (24). The gene assembly method used was developed by Thomas Snyder and Yinthai Chan. PCR and cloning of the assembled product was done under guidance from Thomas Snyder.

Chapter 5 describes future strategies for further parallelization of DNA synthesis. Using current device architectures, the number of reactor columns that can be individually addressed is severely limited by the number of solenoid valves. Two solutions are devised to overcome such problem. The first solution involves the adaptation of "control of control", first implemented by Todd Thorsen in our group. The second strategy takes advantage of the ease of the design and fabrication to make custom synthesizers that are tailored to specific sequences. Instead of making the reactors individually addressable and having an outside program control each valve depending on the sequence, information about the specific sequences are directly embedded into the control lines of the device. The difficulty of constructing reactor columns with uniform load and flow rates presents another problem. While dramatic improvements have been made for the device described in Chapter 4, it is difficult to envision a similar column array scaling up to over 100 columns. Some work has been done using sol-gel technologies to make the PDMS surface more glass like, thus allowing further coupling of linker directly onto the column surfaces.

Chapter 2

SYNTHESIS OF POSITRON EMISSION TOMOGRAPHY IMAGING PROBES USING ELASTOMERIC-BASED INTEGRATED MICROFLUIDICS

Introduction

Imaging science has grown exponentially during the past three decades. Many imaging techniques developed during this period have become indispensable both in research and clinical use. Positron emission tomography (PET), a nuclear imaging technique that uses the unique decay characteristics of radionuclides that decay by positron emission, is one such technique. The molecular compounds of interest are labeled with radionuclides and then introduced into the body and distributed in tissues. When the radioactive atom on a molecule decays, a positron is ejected from the nucleus. The positron will combine with a surrounding electron and annihilates into two high energy photons that are emitted simultaneously in opposite directions. A PET scanner detects and localizes these events to reconstruct them into a three-dimensional tomographic image where signal intensity is proportional to the amount of radionuclide.

PET's molecular diagnostics of disease is distinct from anatomical diagnostics using structural imaging techniques such as X-ray computed tomography (CT) and magnetic resonance imaging (MRI). In many ways, molecular imaging is superior to structural imaging for diseases because it provides a way to study the biological process of disease directly, even before the disease has the time to manifest itself anatomically. For example, the loss of regulated expression of genes will precede visible tumor growth of cancers by many years or even decades (25,26). The incorporation of molecular imaging

techniques to aid in the discovery and study of biochemical abnormalities leading to diseases would greatly aid in the detection and treatment of diseases. Indeed, advances in PET technologies and imaging probes for humans and small animals are extending into the realm of drug discovery and development, and have great potential to accelerate these processes (27,28).

A key component in any successful molecular imaging is that the molecular probe specifically targets the process of interest in the body. The probes must be safe, not alter the process being studied, be able to reach the target in sufficient concentration, and be retained long enough to be detected. A successful development of an imaging probe is an iterative process that first requires one to identify a specific receptor site, synthesize a molecular agent for that site, and then label that agent with a radioisotope. While the concept is simple, the process can be arduous and complex. The identification of molecular imaging targets and the development of new radiolabeled molecular probes for those targets are crucial for expanding the capability of *in vivo* molecular imaging for biological research, molecular diagnostics, and drug discovery. The broad range of radiolabeled molecular probes needed in various applications would benefit greatly from optimized synthetic approaches so that they can be obtained rapidly, in high radiochemical yields, with flexible structural diversity, and at low cost.

The synthesis of the [^{18}F]-labeled molecular imaging probe 2-deoxy-2-[^{18}F]fluoro-D-glucose ([^{18}F]FDG) in an integrated microfluidic chip was chosen as a proof of principle since it is a widely used radiopharmaceutical with over a million patient doses produced

in 2004 (PETNet Radiopharmaceuticals, private communication). The short half-life of [^{18}F]fluorine makes rapid synthesis of doses essential, and the synthetic process includes common steps required in many chemical syntheses, including the preparation of other radiolabeled molecular imaging probes. The nanogram mass of PET molecular imaging probes administered to subjects is ideal for miniaturized architecture of integrated microfluidics. Thus, the multi-step synthesis of [^{18}F]FDG and other PET probes represents an interesting opportunity for integrated microfluidics chips.

This chapter describes two integrated microfluidic devices that were developed in an effort to automate and streamline molecular probe synthesis on chip. The first-generation device (Figure 2-1) is capable of executing the five chemical processes of the syntheses of both [^{18}F]FDG and [^{19}F]FDG within an anion exchange column and a nanoliter scale reaction vessel. Each of the components and their operation procedure will be dealt with in more detail in the subsequent sections. More importantly, it demonstrates that the implementation of sequential chemical steps, variable chemical environments, and variable physical conditions on a single chip is possible using elastomeric-based integrated microfluidic platform. The device is also designed to produce sufficient quantities (100--200 μCi corresponding to a few nanograms) of [^{18}F]FDG for mouse imaging. The 2nd-generation device (Figure 2-9) can synthesize larger [18F]FDG doses. The coin-shaped reactor (5 μL volume) is much larger compared to the 40 nL volume reactor volume for the previous device. It was used to synthesize 1.74 mCi [18F]FDG sufficient for several mice experiments and can ultimately synthesize large quantities (i.e.,

100 mCi) of [18F]FDG for imaging patients. However, the concentration of fluoride is performed on a separate device.

Overview of 2-Deoxy-2-fluoro-D-glucose (FDG) Synthetic Steps

The production (29) of [^{18}F]FDG is based on 5 sequential chemical processes (Figure 2-1 A): (i) concentration of the dilute [^{18}F]fluoride solution (1–10 ppm) obtained from the proton bombardment of [^{18}O]water with a cyclotron; (ii) solvent exchange from water to anhydrous acetonitrile; (iii) [^{18}F]fluoride substitution of the D-mannose triflate precursor in dry acetonitrile; (iv) solvent exchange back to water; and (v) acidic hydrolysis of the fluorinated intermediate to obtain [^{18}F]FDG. Presently, [^{18}F]FDG is routinely produced in about 50 min using commercial synthesizers (30). These automated synthesizers have a physical size of approximately 80 × 60 × 40 cm, and can produce ~ 10 to 100 doses for a human in a single run. Inevitably, a considerable decrease in the radiochemical yield of the resulting probe must be tolerated because of the relatively short half-life of [^{18}F]fluorine ($t_{1/2}$ = 110 min). Obtaining high radioactive yields is even more challenging for molecular imaging biomarkers labeled with other important positron emitting radioisotopes with shorter half-lives, such as ^{11}C ($t_{1/2}$ = 20 min) and ^{13}N ($t_{1/2}$ = 10 min).

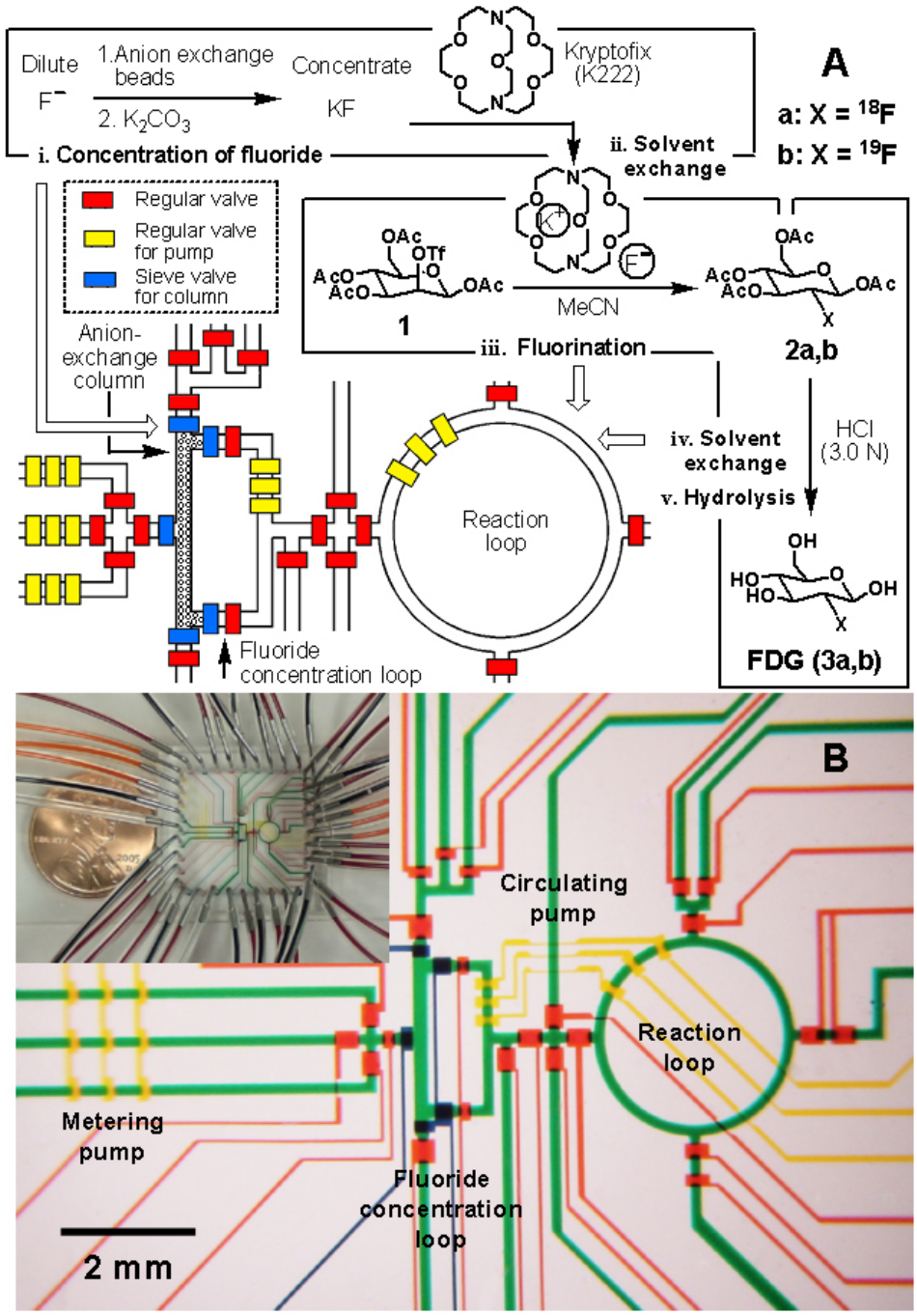

Figure 2-1: (A) Schematic representation of an integrated microfluidic device used in the production of 2-deoxy-2-fluoro-d-glucose (FDG) (3a,b). Three sequential processes—(i) concentration of dilute fluoride ion using a miniaturized anion-exchange column located in a square-shaped fluoride concentration loop, (ii) solvent exchange from water to dry MeCN, (iii) fluorination of the d-mannose triflate precursor 1, (iv) solvent exchange back to water, and (v) acidic hydrolysis of the fluorinated intermediate 2a (or 2b) in a ring-shaped reaction loop—produce nanogram levels of FDG (3a,b). The operation of the device is controlled by pneumatic valves, with their delegate responsibilities illustrated by their colors: red for regular valves (for isolation), yellow for pump valves (for fluidic metering circulation), and blue for sieve valves (for trapping anion exchange beads in the column module). (B) Optical micrograph of the device. The various channels have been loaded with food dyes to help visualize the different components of the microfluidic chip: (red) control channels for regular valves, (blue) control channels for sieve valves, (yellow) control channels for pump valves, and (green) fluidic channels.

Ion Exchange Column for Fluoride Concentration

The concentration of [^{18}F]fluoride obtained from a proton-bombarded [^{18}O]water is usually below 1 ppm, and performing fluorination reaction at such a low [^{18}F]fluoride concentration is not feasible. Because reaction volumes in microfluidic devices are on the level of nL, it would be advantageous if there were ways to concentrate desired reagents within the device to not only boost the overall production but also favor the reaction kinetics. In addition, an ion exchange column can also be used for separation and purification of proteins, polypeptides, nucleic acids, polynucleotides, and other charged bio molecules, making it a versatile module to have in our chemical toolbox.

Thus we sought to create a miniaturized anion exchange column (Figure 2-2) in the microfluidic device to concentrate the [^{18}F]fluoride solution to ~ 100 ppm. Sieve valves, developed by Carl Hansen and Joshua Marcus in our lab, (Figure 2-2 B) were created using a square-profiled fluidic channel and a thin control membrane. Actuation of this membrane prohibits the passage of large particles while still permitting the solution to pass through the edges of the channel. Anion exchange beads (Source 15Q, Amersham Biosciences) were packed into the column module by introducing an aqueous solution containing suspended beads into the microfluidic chamber. The beads were activated by passing 1.0 M of $KHCO_3$ through the column followed by sequential introduction of DI water (18 MΩ).

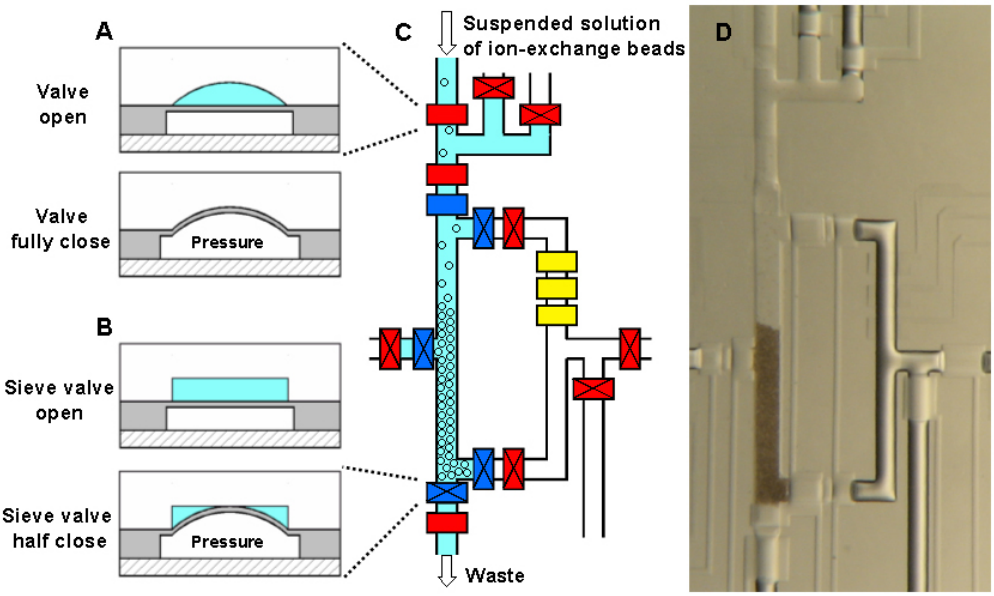

Figure 2-2: Schematic representations illustrate the operation mechanisms of (A) a regular valve having a round-profiled fluidic channel and (B) a sieve valve having a rectangular-profiled fluidic channel. When pressure is introduced into the control channels, the elastic membranes expand into the fluidic channels. In a regular valve, the fluidic channel is completely sealed because of the perfect fit between the expended membranes and the round profile of the fluidic channel. In a sieve valve, the square-profiled fluidic channel is only partially close, which allows fluid to flow through the two edges. Sieve valves can be used to confine solid objects within the fluidic channel, but allow liquid to flow through it. (C) Schematic illustration of the loading of anion exchange beads into a column module incorporating one fluidic channel and five sieve and five regular valves. [□], open valve; [X], closed valve. A suspended solution of anion exchange beads is introduced into the column modules where five sieve valves and five regular valves operate cooperatively to trap anion exchange beads inside the fluidic channel (total volume: 10 nL). A miniaturized anion exchange column for fluoride concentration is achieved when the fluidic channel is fully loaded. (D) A snapshot of the bead-loading process in action

Several iterations of concentration modules were constructed before a final design was settled upon. A layout of the first-generation column is shown in Figure 2-3. After the column is packed and activated, dilute fluoride solution fills the binding path and the eluting loop. Pumps can then be turned to circulate the fluoride solution through the column for a preset amount of time. After the binding of fluoride to the column is complete, the binding path is separated from the eluting loop by closing off valves. 0.25M K_2CO_3 solution is introduced to the eluting loop and circulated until the fluoride ions are competed off the column. The concentrated fluoride is then displaced and recovered from the device using DI water.

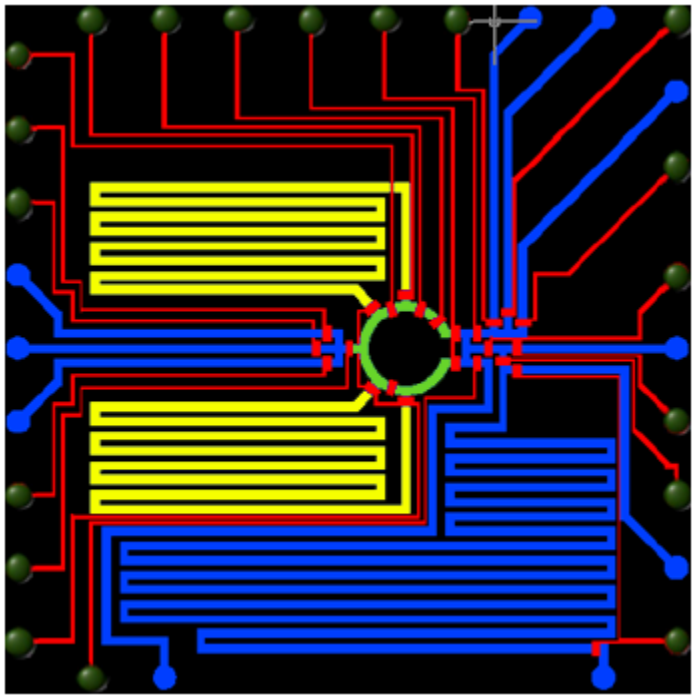

Figure 2-3: Layout of the 1st-generation anion exchange column. Control channels (Red); Fluidic channels (Blue). The column is designed to hold 25.7 ng of fluoride. Dilute fluoride solution and K_2CO_3 solution are loaded from the left. Bead suspension, 1.0 M of $KHCO_3$ and DI water are introduced from the top. The green circular path in the center of the chip is the eluting loop. The yellow serpentine channel to the top left and bottom left of the circle are part of the binding path. The binding path holds 1.28 uL of solution, while the smaller eluting loop holds only 65 nL. Maximum concentration factor is the ratio between volume of binding path and eluting loop or 19.7.

Using the first-generation device, we measured the capacity of anion exchange column and compared it to our expected value. A high concentration of fluoride solution (2000 ppm) is flowed through the column to encourage complete binding. An excess amount of DI water is then used to wash off unbound fluoride. Thereafter, a 1M K_2CO_3 solution is then used to elute off the fluoride completely. 22.9 ng of fluoride ion is recovered when the column is designed to hold 25.7 ng (89.1% yield). Dependence of amount of fluoride bound to the column to the number of times the dilute fluoride solution is passed through the column is also investigated. It is found that increase in the number of times the dilute fluoride solution loops through the column only leads to a modest increase in amount of

fluoride bound to the column. However, the loss of F^{18-} through radioactive decay associated with the extended flow time offsets the gain in fluoride recovery.

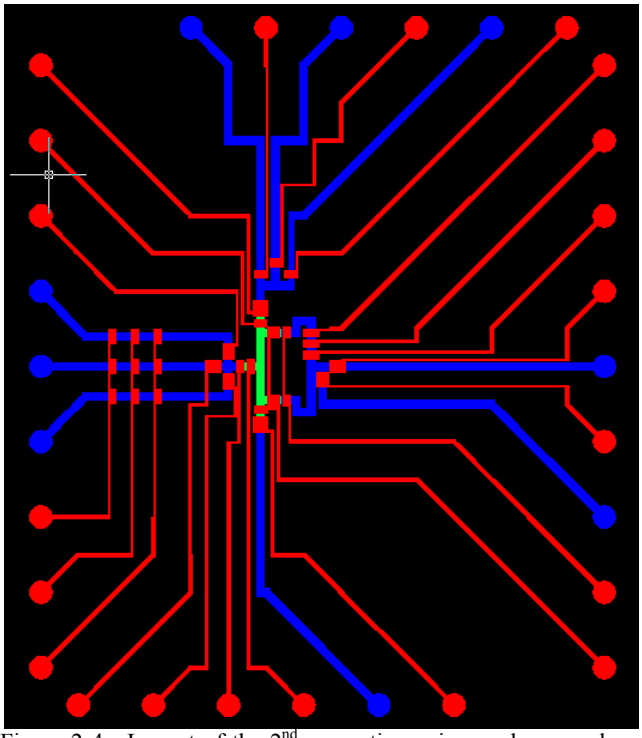

Figure 2-4: Layout of the 2nd-generation anion exchange column. Control channels (Red); Fluidic channels (Blue). The column is designed to hold 55.0 ng of fluoride. Dilute fluoride solution and K_2CO_3 solution are loaded from the left. Bead suspension, 1.0 M $KHCO_3$ and DI water are introduced from the top. The small rectangular path in the center of the chip is the eluting loop. Metering pumps are incorporated at the inlets for precise metering of solutions.

A layout of the 2nd-generation column is shown in Figure 2-4. The binding path is completely taken out because the improvement in fluoride binding is minimal with multiple passing. Pumps are added in the input line to gain improved control on the amount as well as the flow rate at which solutions can enter the anion exchange column (maximum flow rate of 160 nL/sec is achievable). The size of the column is enlarged twofold to increase the binding capacity from 25.7 ng to 55 ng. The size of the eluting loop is minimized (38.4 nL) to increase the concentration of fluoride competed off the column during elution.

Further testing was done using 5 ppm NaF as the dilute fluoride solution and 0.5 M K_2CO_3 as the eluting solution. The results are summarized in Table 0-1. The amount of fluoride loaded is controlled by the volume of dilute fluoride passing through the column. The optimum loading range for the anion exchange column as measured by percent recovery is between 60--90% of the total capacity. An ultra dilute fluoride solution (0.2 ppm) is used to see what factor of concentration is possible using the 2nd-generation column design. 29.4 ng fluoride is loaded onto the column (58% total capacity) and 13 ng fluoride was recovered in final volume of 45 nL (285 ppm). That is a greater than 1400-fold increase in concentration.

Table 0-1: Efficiency of fluoride recovery over different loading range

Capacity Loaded (%)	Amount of Fluoride Loaded (ng)	Amount of Fluoride Recovered (ng)	Efficiency of Recovery
30	16.5	15.1	91.5%
60	33.0	23.2	70.4%
90	49.5	22.8	46.0%
120	66.0	25.9	39.3%
150	82.5	27.0	32.8%
180	99.0	31.8	32.1%
210	115.5	25.5	22.1%
240	132.0	27.7	21.0%

Reaction Loop for Solvent Exchange, Fluorination, and Acid Hydrolysis

The challenges for conducting sequential chemical processes within microfluidic devices are (i) isolating distinct regions on the chip for individual chemical processes, (ii) accelerating diffusion-dominated mixing within an isolated microfluidic environment, and (iii) removing and exchanging solvents specific to each individual synthetic step. Elastomer-based microfluidic reactors (12,31) with integrated micromechanical valves provide elegant solutions to these challenges.

First, integrated valves (12) can isolate distinct regions on the device for distinct chemical processes, a capability that is virtually impossible to design into continuous flow microfluidic systems (7,32). Second, a peristaltic pump, (12) comprised of three adjacent valves in series, can be used to produce active mixing within a short fluidic loop. Continuous flow microfluidic devices, on the other hand, require long winding (33) or highly branched (34) channels to achieve efficient mixing between laminar flows. This requires valuable chip real estate and flow time. Third, the gas permeable PDMS matrix allows solvent exchange to occur within the microfluidic channel through direct evaporation, whereas glass- and silicon- based microfluidic devices have no intrinsic way to exchange solvents. Finally, a solution inside a PDMS-based microfluidic reactor can be heated above its normal (atmospheric) boiling point. This high-temperature and high-pressure environment provides the conditions for accelerated rates of chemical processes. The pressure is not only controlled by the heat supplied to the chip, but it is also mediated by the porosity of the PDMS matrix.

The reaction loop was designed to match the volume of concentrated fluoride solution from the eluting loop to maximize the fluoride concentration in subsequent steps. Because of the short path length of reaction loop, a peristaltic pump is used to enhance the mixing of reagents within the reactor. Following the elution of fluoride, 20 nL of K_2CO_3 solution was introduced into the fluoride concentration loop to displace the concentrated fluoride solution into the reaction loop. The other 20 nL of volume is filled through a dead-end filling process (all the valves are closed except the valve controlling

the loading channel, the air inside the loop is pushed out through the porous PDMS matrix).

Solvent Exchange

With all the valves around the reaction loop closed, the device was heated on a digitally controlled hotplate with a gradient (100 ^{o}C for 30 seconds, 120 ^{o}C for 30 seconds, 135 ^{o}C for 3 minutes). Due to the small thermal mass of the device, the heating is almost instantaneous. Most of the water from the concentrated fluoride solution was removed through the first evaporation; however, a few droplets can be seen clinging to the reactor wall. The device was then cooled down to 35 ^{o}C within 1 minute. The limiting factor is the heating element rather than the device itself. Anhydrous MeCN was introduced into the reaction loop through the bottom middle channel through dead-end filling. This step took less than 20 seconds at 25 ^{o}C. The device was heated again with a gradient (80 ^{o}C for 30 seconds, 100 ^{o}C for 1 minutes) to remove the remaining water inside the loop. It is found that if the temperature is ramped up too fast, there is a chance for pressure inside the chamber to exceed the valve closing pressure and cause the reactor to leak. To prevent such a leakage, double valves are implemented around the reaction chamber and strict heating procedures are followed.

Fluorination

A 40 nL anhydrous MeCN solution containing 1,3,4,6-tetra-*O*-acetyl-2-*O*-trifluoromethanesulfonyl-D-manno-pyranose (mannose triflate) (92 ng, 1.9 x 10^{-10} mol) and 4,7,13,16,21,24-hexaoxa-1,10-diazabicyclo [8,8,8]hexacosane (Kryptofix 222) (364 ng, 9.6 x 10^{-10} mol) was introduced into the reaction loop containing the KF which was dried through the solvent exchange process mentioned in the previous section. Direction

loading of concentrated KF solution is first used to establish the reaction parameter. Later KF concentrated from dilute fluoride solutions using the ion exchange column are also tested. After all the valves around the reaction loop were closed, the reactor was heated at 100 ^{o}C for 30 seconds and maintained at 120 ^{o}C for 50 seconds. Meanwhile, the circulating pump was turned on to provide efficient mixing. After the chip was cooled down to 35 ^{o}C, the reaction residue inside the loop was flushed out with MeCN for GC-MS analysis. Although we cannot obtain an accurate reaction yield from GC-MS analysis, it is obvious the entire peak for D-mannose triflate precursor disappeared after the reaction and the fluorinated intermediate was the only reaction product. (Figure 2-7 B)

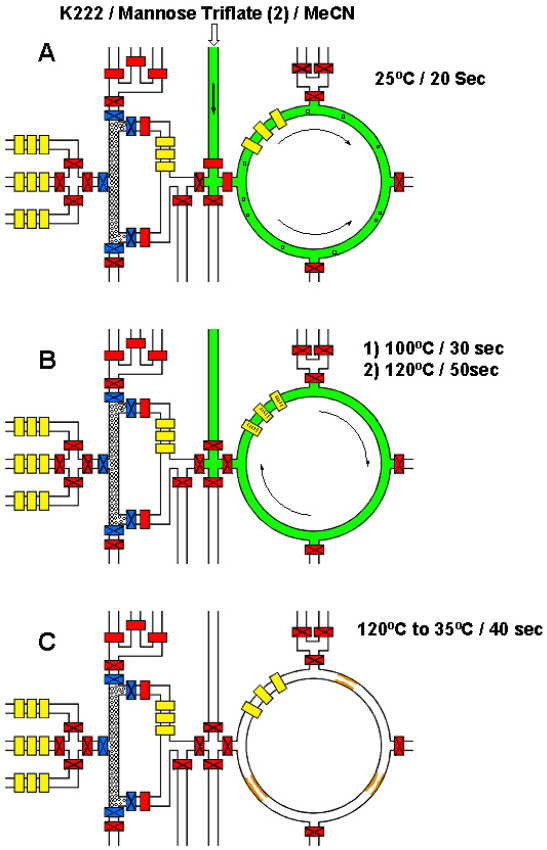

Figure 2-5: Schematic diagrams summarize the fluorine substitution process which is composed of 3-step sequential operations in the microfludic device. (A) Kryptofix 222 / the mannose triflate **1** in anhydrous MeCN were introduced from the top middle channel to the reaction loop by dead-end filling. This step took 20 seconds at 25 ^{o}C. (B) The reaction loop was heated with a gradient (100 ^{o}C/30 seconds, 120 ^{o}C/50 seconds). At the same time, the solution was actively mixed by the circulating pump. The fluorinated intermediate **2a** (or **2b**) was obtained by the end of this step. (C) The reaction loop was cooled down to 35 ^{o}C within 40 seconds.

Acidic Hydrolysis

After the fluorination step, 40 nL of HCl solution (3.0 N) was loaded into the reaction loop. With all the valves closed and circulating pump running, the hydrolysis of the fluorinated intermediate was finished in 1 minute at a temperature of 60 ^{o}C. After cooling down to 35 ^{o}C, the final product, [^{19}F]FDG was flushed out from the reactor by water. The final aqueous solution was removed. Due to the low volatility, [19F]FDG was derivatized with TMSCl prior to GC-MS analysis. The GC-MS result indicated that the hydrolytic reaction of the intermediate results in [19F]FDG > 90% purity. (Figure 2-7 C)

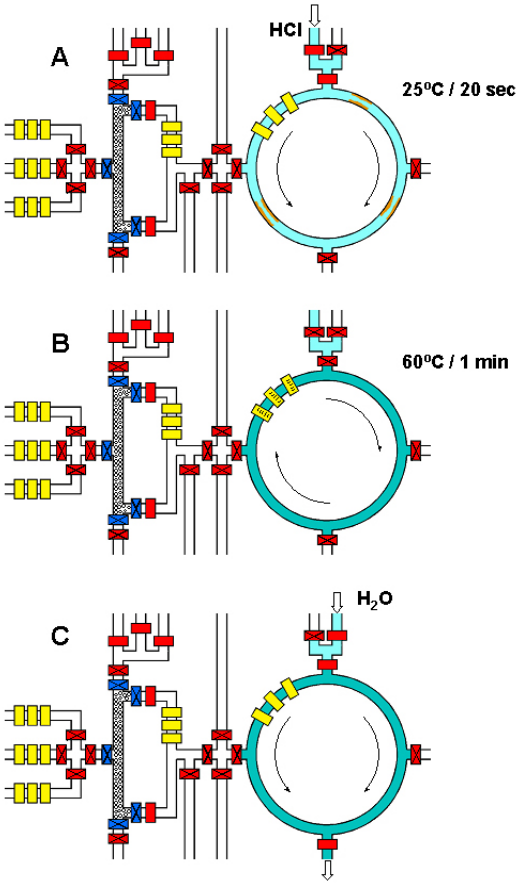

Figure 2-6: Schematic diagrams summarize the hydrolytic process which is composed of 3-step sequential operations in the microfluidic device. (A) HCl aqueous solution (3.0 N) was introduced from the top right channel (in light blue) to the reaction loop by dead-end filling. This step took 20 seconds at 25 ^{o}C. (B) The HCl and the fluorinated intermediate 2a (or 2b) were mixed by the circulating pump for 1 minute at 60 ^{o}C. In this step, the intermediate 2 (or 2b) was hydrolyzed to yield the final product FDG (3a,b). (C) The solution containing FDG (3a,b) (in dark blue) was flushed out of the device though the product line located at the bottom of the device.

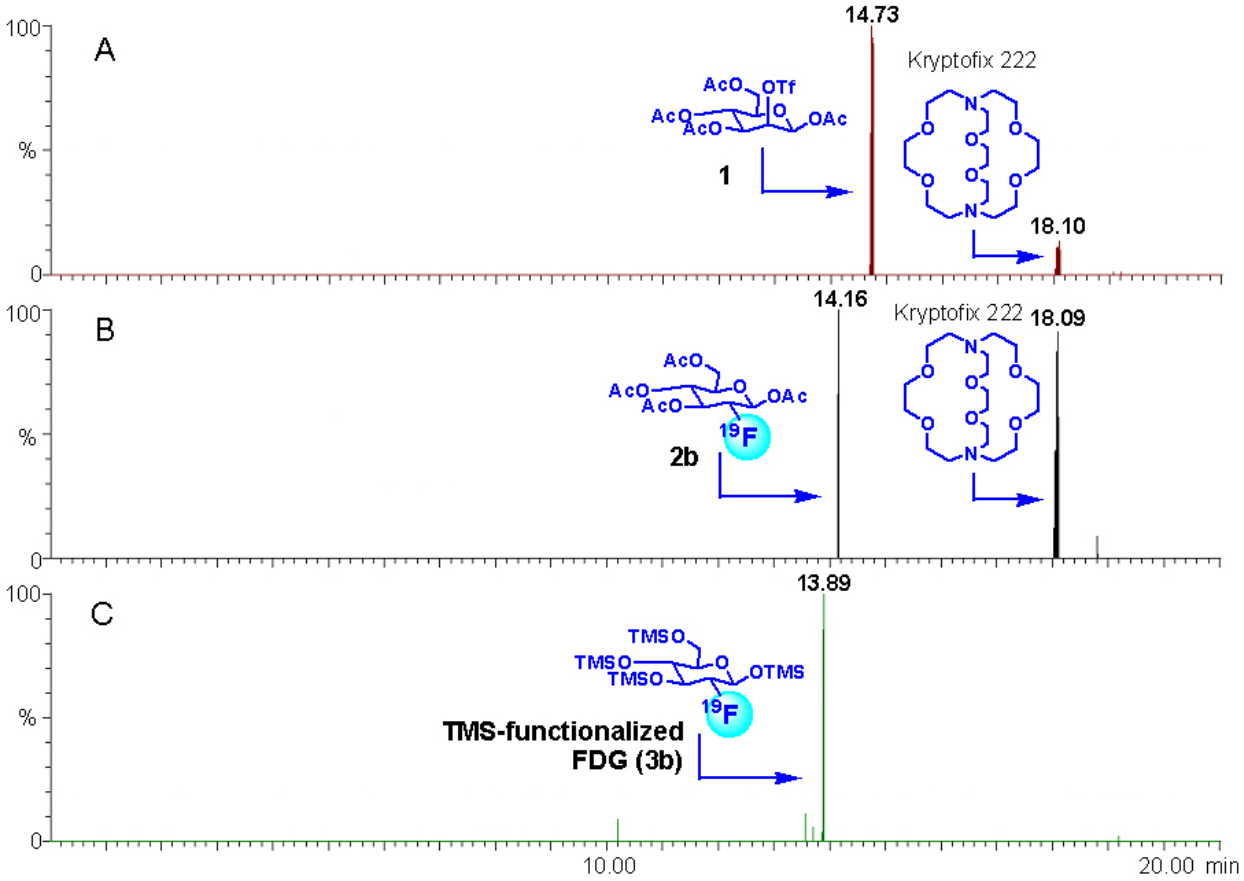

Figure 2-7: (A) GC-MS plot of a mixture containing MeCN, mannose triflate **1,** and Kryptofix 222. The two peaks at retention times of 14.73 and 18.10 min correspond to mannose triflate **1** and Kryptofix, respectively. (B) GC-MS plot of the mixture in (A) after its reaction with concentrated fluoride in the device. The peak having a retention time of 14.16 min corresponds the formation of the fluorinated intermediate **2b**. A calibrated integration of the chromatogram suggests a conversion yield of 95%. (C) GC-MS plot of a TMS-functionalized [^{19}F]FDG (**3b**) which is obtained by treating crude [^{19}F]FDG (**3b**) with TMSCl. The calibrated integration indicates that the hydrolytic reaction of intermediate 2b resulted [19F]FDG (3b) in > 90% purity.

Cold 2-Deoxy-2-[^{19}F]fluoro-D-glucose ([^{19}F]FDG) Synthesis

We performed a proof-of-concept trial using non-radioactive [^{19}F]fluoride to test the feasibility of producing [^{19}F]FDG within the device. The acquired experimental parameters are employed directly for the production of radioactive [^{18}F]FDG. For the first process, concentration of dilute fluoride, a 5 ppm NaF solution was loaded into the anion exchange column. The loading rate (5.0 nL/sec) was controlled using a metering pump. After the fluoride solution was loaded completely, a K_2CO_3 solution (0.25 M, 18 nL) was introduced to fill the rectangular loop. The circulating pump module was then

turned on so that the K_2CO_3 solution (0.25 M, 18 nL) could loop through the column continuously to produce a concentrated KF solution. Because the fluorination of the D-mannose triflate requires anhydrous conditions, a digitally controlled hot plate was used to heat the device for removing water from the concentrated KF solution. To completely extrude any remaining moisture, dry MeCN was loaded into the reaction loop and the device was heated again. Moisture and MeCN vapor can penetrate and escape the gas-permeable PDMS matrix. Once the device had cooled to room temperature, an anhydrous MeCN solution (40 nL) containing the D-mannose triflate (92 ng, limiting reagent) and Kryptofix 222 (364 ng) was introduced into the ring-shaped reaction loop containing the dried KF. This heterogeneous reaction mixture was mixed inside the loop using the circulating pump. During this step, the device was heated (100 °C for 30 s and then 120 °C for 50 s) to yield the fluorinated intermediate, as analyzed by GC-MS. This analysis indicated that the conversion yields for the fluorination process were 98%. After removing MeCN by direct evaporation, 3 N HCl solution (40 nL) was injected into the device and the hydrolysis of the intermediate was conducted at 60 °C to obtain [^{19}F]FDG, in > 90% purity, according to GC-MS analysis. The PDMS materials were compatible (35) with MeCN and the entire synthesis was demonstrated on multiple chips.

Hot 2-Deoxy-2-[^{18}F]fluoro-D-glucose ([^{18}F]FDG) Synthesis

720 μCi of [^{18}F]fluoride in ca. 1 μL of [^{18}O]water was introduced into the fluoride concentration loop of the device. Because of the relatively high loading rate (65 nL/sec) as well as other competing anions present in the bombarded water, only 500 μCi of [^{18}F]fluoride (ca. 3.3 x 10^{-11} mol, limiting reagent) was trapped in the column. An 18 nL of K_2CO_3 solution (0.25 M, 4.5x10^{-9} mole) was introduced to fill the rectangular loop,

and the circulating pump module was then turned on so that the K_2CO_3 solution could loop through the column continuously to produce a concentrated [^{18}F]KF solution. After circulation, 20 nL of K_2CO_3 solution was introduced into the fluoride concentration loop to displace the concentrated [^{18}F]fluoride solution into the ring-shaped reaction loop. With all the valves around reaction loop closed, the device was heated on a digitally controlled hotplate. The device was cooled down to 35 ^{o}C within 1 minute, and anhydrous MeCN (40 nL) was introduced into the reaction loop. The device was heated again to remove the water residue inside the loop. Kryptofix 222 (1.4 μg, 3.7 x 10^{-7} mol) and the mannose triflate (324 ng, 6.7 x 10^{-10} mol) in anhydrous MeCN were introduced into the reaction loop. The device was heated with a gradient (100 ^{o}C for 30 seconds, 120 ^{o}C for 50 seconds). At the same time, the solution was actively mixed by the circulating pump to give [^{18}F]fluorinated intermediate in the device. After cooling the device down to 35 ^{o}C within 1 minute, HCl aqueous solution (3.0 N) was introduced into the reaction loop. The mixture was mixed by the circulating pump for 1 min at 60 ^{o}C. In this step, the intermediate was hydrolyzed to yield the final product [^{18}F]FDG. After cooling down to room temperature, the final product, 190 μCi of [^{18}F]FDG (ca. 1.25 x 10^{-11} mol, 38% yield) was flushed out from the chip by water for the analyses of radio-TLC and radio-HPLC. The analyses of radio-TLC (Figure 2-8) and radio-HPLC suggested that the unpurified mixture obtained upon the sequential production of [^{18}F]FDG has a radiochemical purity of 97.6 %. Similar results were observed across multiple runs.

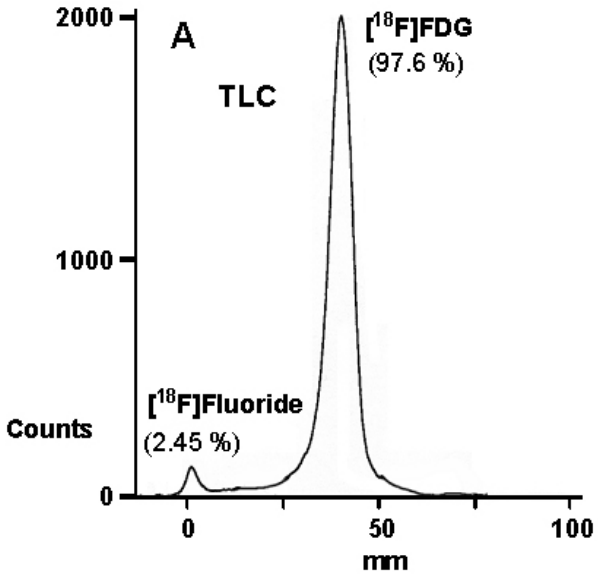

Figure 2-8: Analytical TLC profile of the unpurified mixture obtained upon the sequential production of [18F]FDG (3a) in the first generation microfluidic device indicating that the radiochemical purity of the FDG production is up to 97.3 %. The two peaks with values for Rf of 0.0 and 0.4 correspond to [18F]fluoride and [18F]FDG (3a), respectively.

2nd-Generation FDG Synthesizer

A second-generation synthesizer was also designed with the capacity to synthesize larger [18F]FDG doses. This chip has a coin-shaped reactor (5 μL volume) equipped with a vacuum vent. It was used to synthesize 1.74 mCi [18F]FDG sufficient for several mice experiments. From the purified and sterilized product (Figure 2-10 A), two doses (375 μCi and 272 μCi) were utilized for microPET- and microCT-based molecular imaging of two mouse models of cancer. One of the mouse images is shown in Figure 2-10 B as a 2-dimensional projection image. This new design should ultimately be able to synthesize large quantities (i.e., 100 mCi) of [18F]FDG that is sufficient for several human PET scans.

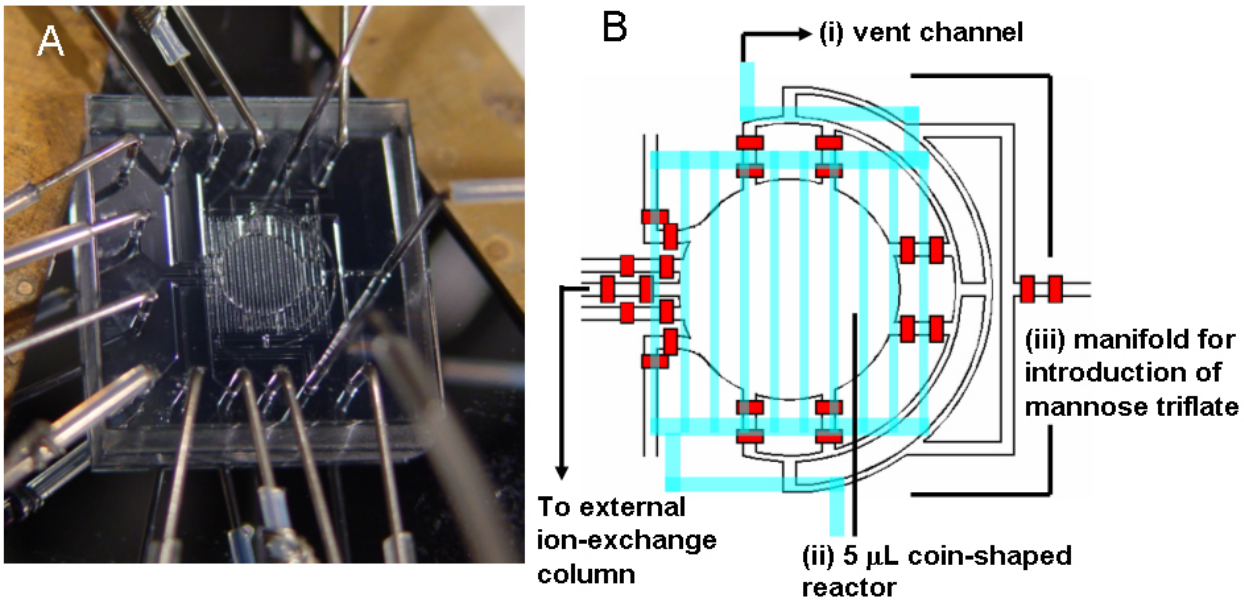

Figure 2-9: (A) A second-generation device is in action for the [18F]FDG (3a) production. (B) Schematic representation of the second-generation device composed of three major functional components, including (i) vent channel, (ii) coin-shaped reactor, and (iii) manifold for introduction of the mannose triflate 2a solution

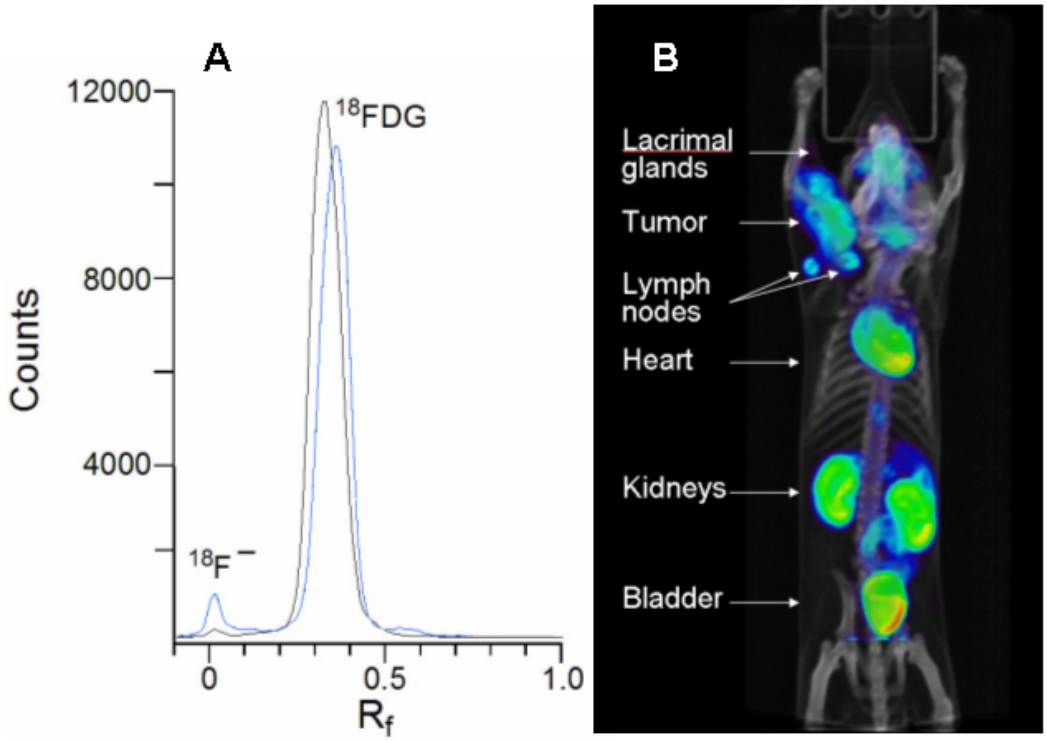

Figure 2-10: (A) Analytical TLC profile of the unpurified mixture (blue curve) obtained upon the production of [18F]FDG (3a) in the second-generation device indicating that the radiochemical purity of the FDG production is up to 96.2%. The two peaks have Rf values of 0.0 and 0.36 corresponding to [18F]fluoride and [18F]FDG (3a), respectively. After purification and sterilization, the [18F]FDG (3a) (black curve) with 99.3% radiochemical purity was employed for mouse microPET/microCT imaging. (B) Projection view of microPET/microCT image of a tumor-bearing mouse injected with [18F]FDG produced in a microfluidic chip. Organs visible are the bladder, kidneys, heart, tumor, and two lymph nodes.

Materials and Methods

Fabrication of the First-Generation Device

The chip was fabricated using the multi-layer soft lithography method. (12,36) Two different molds were first fabricated by photolithographic processes to create the fluidic channels and the control channels for actuating the values located in the respective layers of the PDMS-based device. The mold used to create the fluidic channels was made by following a two-step photolithographic process. In the first step, a 45-μm-thick negative photoresist (SU8-2025) was spin coated on to a silicon wafer (Silicon Quest, San Jose, USA). After UV exposure and development, a square-profiled pattern for the miniaturized anion exchange column was obtained. In the next step, a second layer of 45-μm-thick positive photoresist (AZ 100XT PLP) was then spin coated on the same wafer. Prior to the UV exposure the mask was aligned (Karl Suss AmericaInc., Waterbury, VT) to ensure a good match between two sets of patterns of the control and fluid channels. Once the positive photoresist was developed, the wafer was heated above the glass transition temperature of the positive photoresist. As a result, the surface profile of the patterned positive photoresist was transformed into a round profile while the profile of the negative photoresist remained unchanged (square profile). This device has a channel height of 45 μm and width of 200 μm. The control channels mold was made by introducing a 25-μm-thin negative photoresist (SU8-2025) pattern on a silicon wafer. In order to achieve reliable performance of each valve, the width of the control channel was set at 250 μm in sections where the valve modules are located.

Before fabricating the device, both the fluidic and control molds were exposed to trimethylchlorosilane (TMSCl) vapor for 2--3 minutes. A well-mixed PDMS (GE, RTV 615 A and B in 5 to 1 ratio) was poured onto the fluidic mold located in a petri dish to give a 5-mm-thick fluidic layer. Another portion of PDMS (GE, RTV 615 A and B in 20:1 ratio) was spin-coated onto the control mold (1600 rpm, 60 s, ramp 15 s) to obtain the control layer. The thick fluidic layer and thin control layer were cured in an 80 ^{0}C oven for 50 minutes. After incubation, the thick fluidic layer was peeled off the mold, and holes were introduced onto the fluidic layer for access of reaction solutions. The fluidic layer was then trimmed, cleaned, and aligned onto the thin control layer. After baking at 80 ^{o}C for 60 minutes, the assembled layer was peeled off the control mold, and another set of holes were punched for access of control channels. These assembled layers were then placed on top of a glass slide that was coated (1600 rpm, 60 s, ramp 15 s) with PDMS (GE RTV 615 A and B in 20:1 ratio) that had been cured for 45 minutes in the oven. The device was done after overnight incubation.

Control Interface

The pneumatic control setup consists of 4 sets of eight-channel manifolds controlled through a BOB3 breakout controller board (Fluidigm, San Francisco, USA). Argon gas that was pre-dried through a gas purifier (Hammond Drierit, Xenia, USA) provides pressure (30 psi) to the manifolds. 32 control lines from the device are individually connected to the corresponding channels on the manifolds with metal pins (23 Gauge, New England Small Pin Corp, USA) using Tygon microbore tubing (Cole-Parmer East, Bunker Court, USA). When a channel on the manifold is activated, argon gas enters the

control line connected with the specific channel, providing pressure to close valves in the microfluidic device. The control interface was created using the Labview program on a PC. A National Instruments card (AT-DIO-32HS) digitally controls the switching of manifolds through the BOB3 breakout controller board. The Labview program allows for manual control of individual valves and for automation of the synthesis processes.

Materials

All reagents were purchased from Sigma-Aldrich. Solvents purchased from VWR/EMD were purified according to literature procedure. GC-MS was performed with GC/EI Time-of-Flight mass spectrometer (Micromass GCT). A DBS-MS capillary column (40 m long, 320 μm of OD) was employed for GC analyses of [^{19}]FDG intermediate and product using helium as carrier gas at flow rate of 1.2 mL/min. No-carrier-added [^{18}F]fluoride (specific activity: > 10,000 Ci/mmol) was produced by 11 MeV proton bombardment of 95% ^{18}O-enriched H_2O via $^{18}O(p,n)^{18}F$ nuclear reaction using a RDS-112 cyclotron. HPLC analysis was performed using a Rainin-HP system equipped with a γ-detector. A Phenomenex column (Econosphere-NH_2, 5 μm, 250 × 4.6 mm) was used with a solvent system of 85% MeCN and 15% H_2O. Radio-TLC analysis was performed on silica plate (EM Separation Technology, Silica gel 60) with an eluent system of 85% MeCN and 15% H_2O.

Concluding Remarks

Micro-reactors based upon integrated multilayer elastomeric microfluidics offer the potential for executing a sequence of chemical events, each carried out under different

solvent and/or physical conditions. In addition, rates and yields of the chemical syntheses can be improved over standard procedures, and multiple distinct chemical syntheses can be executed on a single chip under fully automated and parallel operation. This technology enables acceleration of the synthetic process and the reduction of reagents and solvents required. These integrated microfluidic chip platforms can be extended to other radiolabeled molecular imaging probes (37), and also to other chemical compounds produced by sequential synthetic processes. This concept can be enabling of a number of applications, and the one specific application explored here is the preparation of biomarkers for PET-based molecular imaging. Chips designed to produce both small animal and human-level doses of the common radiopharmaceutical, [^{18}F]FDG were demonstrated, and both chip designs yielded enhanced operational efficiency and chemical economy.

Chapter 3

SOLVENT RESISTANT ELASTOMERIC-BASED INTEGRATED MICROFLUIDICS: PROOF OF PRINCIPLE OLIGONUCLEOTIDE SYNTHESIS

Introduction

Synthetic chemistry presents numerous instances in which it would be useful to automate and miniaturize reactions. Many synthesis problems require trial and error efforts in order to optimize yield. A miniaturized, automated chemical synthesizer would reduce manpower, reagent consumption, and cost. Reducing reagent consumption for chemical synthesis also offers the possibility of reducing waste proportionately and is thus environmentally friendly.

Microfluidic devices have shown great potential in realizing these goals (38). However, because chemical synthesis requires the use of a wide variety of solvents, most microfluidic work in this area has been limited to continuous flow reactors fabricated in glass or silicon (39). These platforms suffer from several disadvantages. While simple manipulation of solvents and reactive species has been demonstrated in devices fabricated from hard materials, it remains difficult to scale up these devices to the levels of integration seen in recent elastomeric-based devices. In addition, glass- and silicon-based microfluidic devices are often designed from scratch for each new application because of the lack of generality in the fabrication and fluid manipulation methods (40). Coupled with the exuberant cost in the fabrication of these devices, the application and commercialization of glass- and silicon- based microfluidics for fine chemical synthesis,

especially in the developmental stage where many iterations of designs need to take place, is still distant.

In special cases where the solvents are mild, it has been possible to use integrated elastomeric micromechanical valves to perform batch synthesis at the nanogram scale of radiopharmaceuticals as demonstrated in the previous chapter. Even though other impressive devices have been demonstrated, fundamental incompatibilities of PDMS with many solvents have limited this platform to applications involving only aqueous media (41,42). Drawing inspiration from PDMS microfluidic device technology and the many qualities that have led to its success, our group has developed a novel technology based on a photocurable perfluoropolyether (PFPE) elastomer material. Due to their elastomeric properties, these devices share many of the same advantages of PDMS devices with the added advantage that they are resistant to most solvents (43).

The synthesis of oligonucleotide was chosen to demonstrate the capability of PFPE devices. The recent boom in synthetic genes and long DNA construct has been fueled by a broad cross-section of applications within molecular biology, such as the design of genetic circuitry (44,45), the engineering of entire metabolic pathways for target molecule manufacturing (46), and the construction and re-engineering of viral and bacterial genomes (47,48). While these applications require thousands or even hundreds of thousands of oligonucleotides, the amount of each sequence needed is actually very small. For example, as little as a pico-mole of oligonucleotides are needed for successful gene assembly (49). Commercially available synthesizers prepare DNA on a micromole

scale; this amount far exceeds what is needed. Currently, oligonucleotides are available at a cost on the order of USD 0.1 per nucleotide. This makes applications such as the de novo synthesis of bacterial genomes (10^6 bp in size) prohibitively costly, requiring on the order of USD 100,000 in oligonucleotides alone. By scaling reactions down to volumes of less than a microliter, reagent costs can be substantially reduced.

Also, the deblocking solution commonly used in phosphoaramidite chemistry contains dichloromethane (DCM). DCM is a solvent that poses severe challenges with conventional elastomers such as PDMS (35). Microfluidic channels made in PDMS will swell and become clogged within seconds when exposed to DCM. By choosing an application that requires repeated exposures to such solvent over its operation, we wish to demonstrate that PFPE is a viable choice of material for production of devices to be used in other organic syntheses as well.

This chapter describes a microfluidic DNA oligonucleotide synthesizer (Figure 3-1) made of PFPE which performs reaction cycles adopted from the widely used phosphoramidite method (Figure 3-2). The device is capable of synthesizing 60 pmol of DNA oligonucleotides while consuming less than 500 nL of 0.1 mol/L phosphoramidite solution in each reaction cycle, thus filling in the void between the commercial synthesizers' micromole scale and the sub-femtomole scale of the emergent microarray technology. The reduction of reagent consumption is significant: a 60-fold reduction over conventional automation on a per sequence basis. This approach demonstrates the usefulness of integrated micromechanical valves for complicated multi-step organic

synthetic reactions and enables automated chemical experiments with a wide variety of solvents.

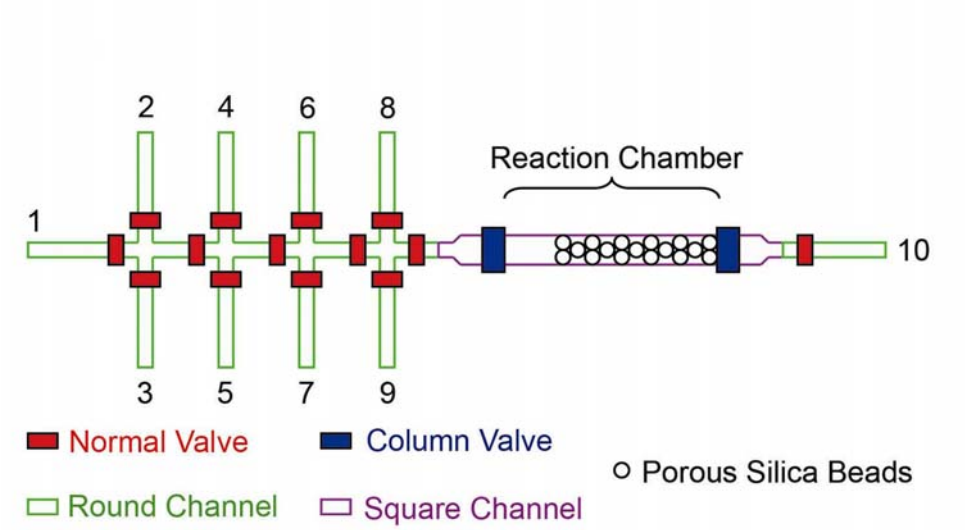

Figure 3-1: Schematic of microfluidic oligonucleotides synthesizer. The fluidic channels consist of both rounded and squared profiles. The first eight channels are assigned to specific reagents: 1) acetonitrile, 2) deblocking reagent, 3) oxidizing reagent, 4) activator, 5) dT-CE phosphoramidite, 6) Pac-dA-CE phosphoramidite, 7) iPr-Pac-dG-CE phosphoramidite, and 8) Ac-dC-CE phosphoramidite. The ninth channel serves two functions. During experimental setup it is used as an inlet for silica beads. During the experiment it is used as an outlet for unwanted reagents that are left in the main channel. A solid-phase reaction column is formed in situ using partially closed column valves to trap the silica beads (5 μm in diameter).

Overview of Solid-Phase Oligonucleotide Synthesis

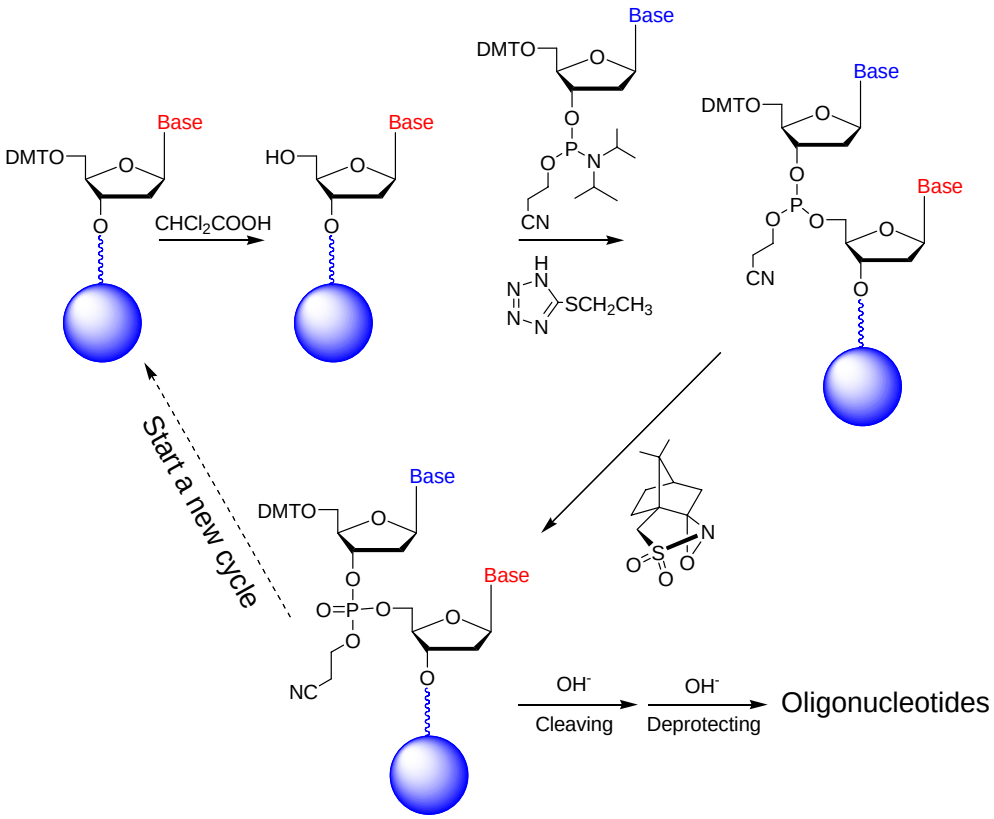

Figure 3-2: The synthetic cycle of DNA oligonucleotides

Almost all oligonucleotide synthesis is now done on a solid support, which allows for the elongation of the chain without intermediate purifications. The 3′-OH group of the first nucleoside is attached to the solid support through a cleavable linker, and the synthesis proceeds by coupling the 5′-OH group of the growing chain to the 3′-phosphorus of the monomer being added.

The synthesis is cyclical in nature and generally involves 4 steps with proper washing inbetween them. Step 1 is deblocking. The first base that is attached to the solid support has a DMT group protecting the 5'hydroxyl group, making it inactive. DMT groups are

removed under acidic conditions. By introducing 3% dichloroacetic acid (DCA) in dichloromethane (DCM), the 5'-hydroxyl group in the growing chain is now exposed.

Step 2 is coupling. The next base monomer cannot be added until it has been activated. This is achieved by adding tetrazole, a weak acid to the monomer. Tetrazole protonates the phosphoramidite nitrogen on the incoming base, leaving its 3'-hydroxyl susceptible to nucleophilic attack by the active 5'hydroxyl group of the preceding base. They then loosely bind to form an unstable phosphite linkage.

Step 3 is capping. During a coupling step, not all active 5'-hydroxyl sites of the previous base will form a phosphate linkage. If this unreacted hydroxyl group is left alone, it is possible for it to react in a later coupling step. This would result in oligonucleotides with truncated sequences. To prevent this from occurring, the unbound, active 5'-hydroxyl group is capped with a protective group which subsequently prohibits that strand from growing again. We have elected to leave out the capping step in our synthesis because we were satisfied with the purity of our oligonucleotides. However, in Chapter 4 where longer sequences were made, a capping step is implemented to reduce the amount of truncated sequences.

Step 4 is oxidation. The phosphite linkage formed in the coupling step is unstable. Traditionally, a solution of dilute iodine in water, pyridine, and tetrahydrofuran is added to oxidize the phosphate trimester into a tetracoordinated phosphate. However, we substituted iodine with (1S)-(+)-(10-Camphorsulfonyl)oxaziridine (CSO) (50), as the

oxidizing reagent because it allows the entire reaction cycle to carried out in anhydrous conditions.

These steps are repeated until the desired sequences have been synthesized. When the synthesis is completed, the chain must be cleaved from the support and the base and terminal 5′-OH-protecting groups removed. The final product is a mixture of full length and truncated oligonucleotides, cleaved protective groups, and ammonium ions from the final cleavage. Depending on the application, additional purification steps might be needed before the oligonucleotides can be put to use.

Oligonucleotide Synthesis

Preparation of Controlled Porous Glass Support

The porous silica beads were modified with the first nucleoside (thymidine in our experiments) attached. We added 0.5 g of silica beads into 10 mL 8 mol/L HNO_3, and refluxed it for 4 hours. The beads were washed with water and then dried in an oven at 120 °C overnight. The dried beads were re-suspended into 10 mL anhydrous toluene and then 0.6 mL APTMS was added into the system. The mixture was refluxed for 24 hours and then filtered and washed with toluene and acetone. All beads were then transferred into a new vial with 75 mg 5'O-DMT-2'-dT-3'-O-succinate, 40 mg HATU, 100 μL DIEA, and 5 mL MeCN. The reaction vial was sealed and the mixture was stirred overnight at room temperature. Finally the beads were filtered, washed with MeCN and acetone, and then dried under vacuum. We suspended the beads in MeCN and then packed the column as we described in Chapter 2.

Preparation of Reagents and Device

All the phosphoramidite compounds were dissolved into anhydrous MeCN to form 0.1 mol/L solutions. The CSO was dissolved in anhydrous MeCN (0.1 g/mL) and filtered through a 0.45 μm filter. All the reagents were flushed through the microfluidic channels during setup to remove unwanted air bubbles. Each synthesis cycle contained 3 reaction steps and 3 washing steps as described earlier (Figure 3-2). The total time of each synthetic cycle is 9 min.

The coupling step requires two reagents, phosphoramidite and 5-ethylthio-1H-tetrazole, as activators. The two reagents were piped into the synthetic column in an alternating fashion (Figure 3-3): one reagent flowed continuously for 1.8 s then the other one flowed for 1.8 s. For the labeled oligonucleotides, we replaced one of the phosphoramidite solutions with Cy3-phosphoramidite and increased the coupling time to 5 min. Final "DMT-off" ("MMT-off" for Cy3-phosphoramidite) was done by flowing deblocking reagent into the column for 2 min.

After the MeCN wash, we released the "column valve" and flushed the beads out of the chip and into a micro-centrifuge tube. The MeCN was evaporated using centri-vap. We added 0.3 mL concentrated ammonium hydroxide into the tube and then incubated the tube at room temperature for 1 hour. The beads were spun down to the bottom of the tube by a centrifuge and then the liquid phase was transferred into a new tube and kept at room temperature for 3 hours for removal of the side-protection groups on the oligonucleotides. Finally the tube was lyophilized to yield solid-form oligonucleotides.

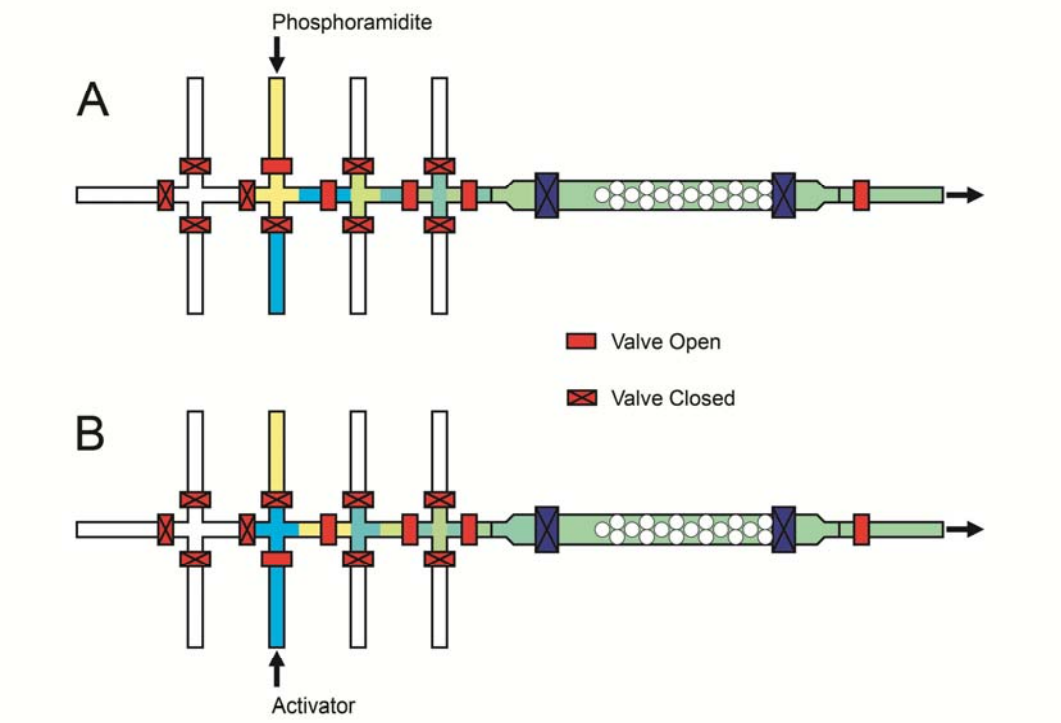

Figure 3-3: Schematic diagram of the coupling step. (A) Phosphoramidite is flowing through the column. (B) Activator is flowing through the column.

Characterization of Synthesized DNA

Electrophoresis

The synthesized oligonucleotides were re-suspended into pH 7.5 TE buffer and mixed with a TBE-Urea sample loading buffer (Invitrogen). The samples (typical volume is 20 μL) were loaded onto a TBE-Urea gel. 1X TBE running buffer (Invitrogen) was used. The temperature was set to ca. 60 ºC and the voltage was set to 175 V. Usually a running time of 45 min to 1 hour was enough to achieve single-base resolution of the gel bands. For unlabeled samples, we used SYBR gold dye to stain the gels for 30 min. A Typhoon 9410 (GE Health) scanner was used to scan the gel images. The final images were processed using Matlab (Mathworks).

5’-Cy3-TTT TTT TTT TTT TTT TTT TT-3’ (Poly-dT 20-mer, Cy3 labeled)

Synthesized poly(dT) DNA oligonucleotides (20 mer, with Cy3 labeled at the 5’-end) are compared to the standard sample purchased from IDT. The standard sample is a mixture of identical amounts of the HPLC purified poly(dT) 10-mer, 15-mer, and 20-mer. The gel image (Figure 3-4) indicates that the major product of our synthesis is the poly(dT) 20-mer.

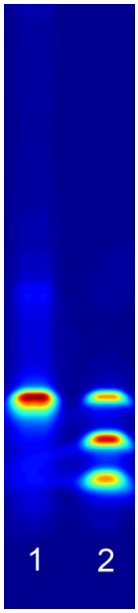

Figure 3-4: Lane 1 is the 5’-Cy3-labeled poly-dT 20-mer sample we synthesized from the PFPE microfluidic chip, without purification. Lane 2 is the mixture of the HPLC purified Cy3-labelled poly-dT 10-mer, 15-mer, and 20-mer (all ordered from IDT)

5’-CCG ACC TGG ATA CTG GCA TT-3’ (DNA 20-mer)

We also synthesized the DNA 20-mer without fluorescent labels. We used both gel electrophoresis and LC/MS to test our product. Figure 3-5 is the gel image. Figure 3-6 through Figure 3-9 are LC/MS data. The gel was stained with SYBR gold. Lane 2 contains 1 pmol of DNA molecules, while lane 1 contains 10% of the product from a single reaction on the microfluidic chip. By comparing the fluorescent intensity of the bands, we can estimate that the total amount of the DNA oligonucleotides produced by

each run of the reaction is ca. 60 pmol. The reaction of the labeled DNA oligonucleotides has a similar yield.

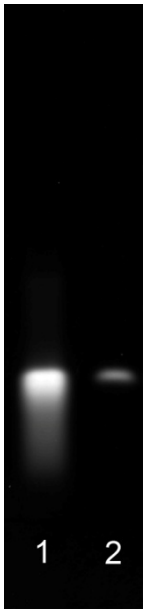

Figure 3-5: Lane 1 is our synthesized unlabeled DNA 20-mer without purification. Lane 2 is the HPLC purified unlabeled DNA 20-mer ordered from IDT

Mass Spectrometry

The synthesized oligonucleotides were sent to Novatia, LLC (Monmouth Junction, NJ) for HPLC/MS characterization. The LC column was a 2 × 50 mm Clarity C18 3 μm from Phenomenex and the experimental temperature was 40 °C. The gradient was 5--25% B in 20 min at 200 μL/min. A = 0.075% hexafluoroisopropanol (HFIPA) / 0.0375% DIEA in water, B = 90% methanol with 0.075% HFIPA / 0.0375% DIEA. The MS data were acquired on an LTQ mass spectrometer from Thermo. The samples were analyzed by electrospray ionization (ESI) mass spectrometry. The detected signal was deconvoluted to generate the final mass spectra.

Table 0-1: Chromatogram summary

Retention Time (min)	Base Peak Mass (Da)	Intensity	LC/MS Area Percent
14.13	5475.4	1.61E+004	7.57
14.53	5788.2	1.16E+005	24.64
14.74	5803.3	1.92E+005	25.55
14.96	6092.5	8.94E+005	42.24

From the deconvoluted mass spectra of product from various retention times of HPLC, one can conclude that the major impurities are DNA sequences with deletion of single nucleotides. No obvious results were observed regarding material leached from fluoropolymers. However, due to the inert nature of the fluoropolymer as well as complete curing of the device, leached material should have minimal or no effect on solid-phase synthesis of DNA.

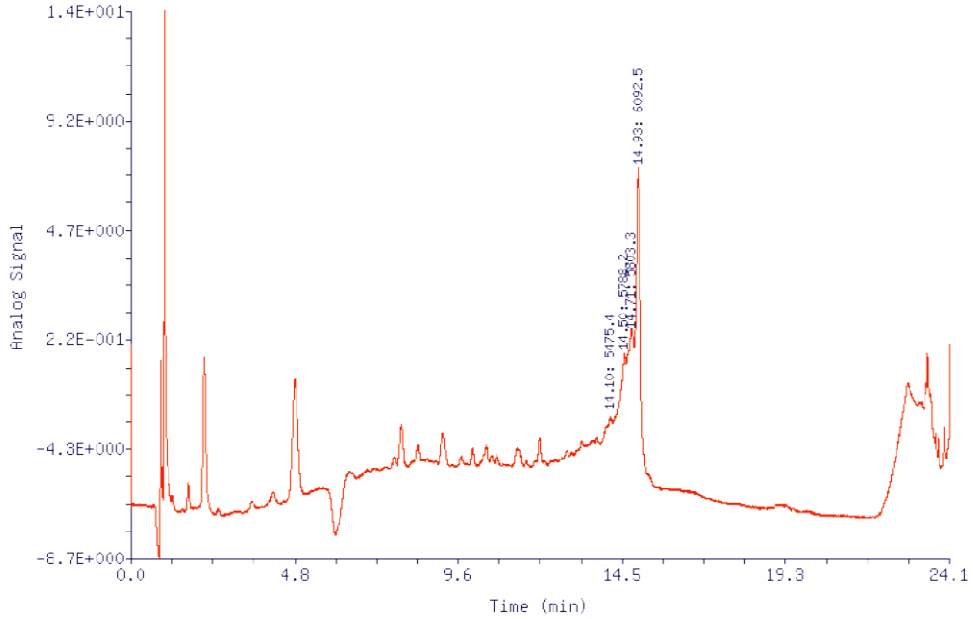

Figure 3-6: LC/UV chromatogram of the synthesized DNA 20-mer at 260 nm

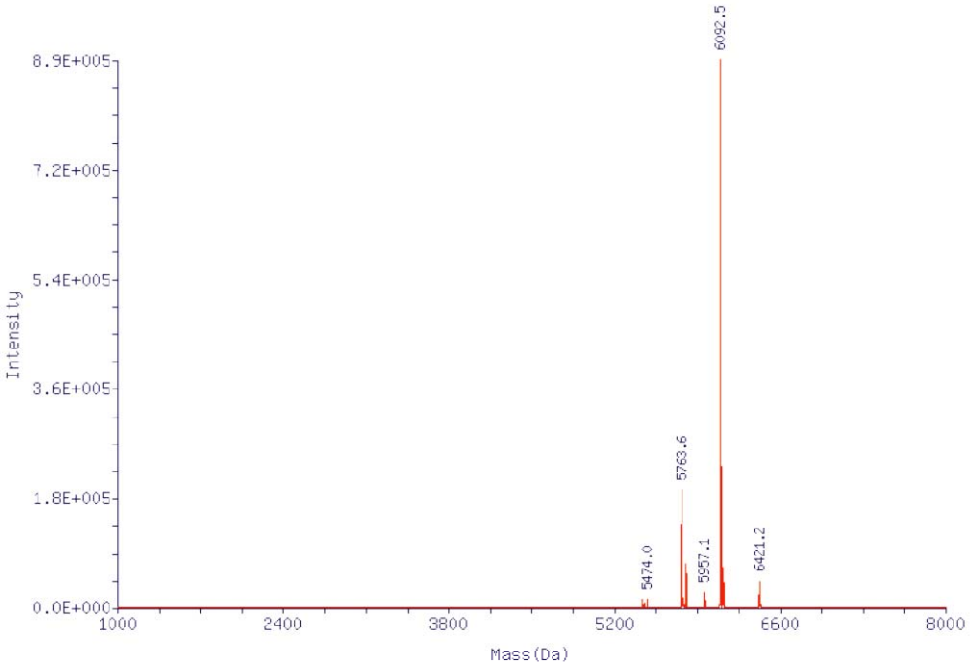

Figure 3-7: The deconvoluted mass spectrum of the synthetic DNA 20-mer at the retention time of 14.96 min. The calculated molecular weight of the DNA 20-mer is 6093 and the detected molecular weight from MS is 6092.5. The smaller peak with molecular weight of 5763.6 comes from a single deletion of nucleotide G in the expected sequence.

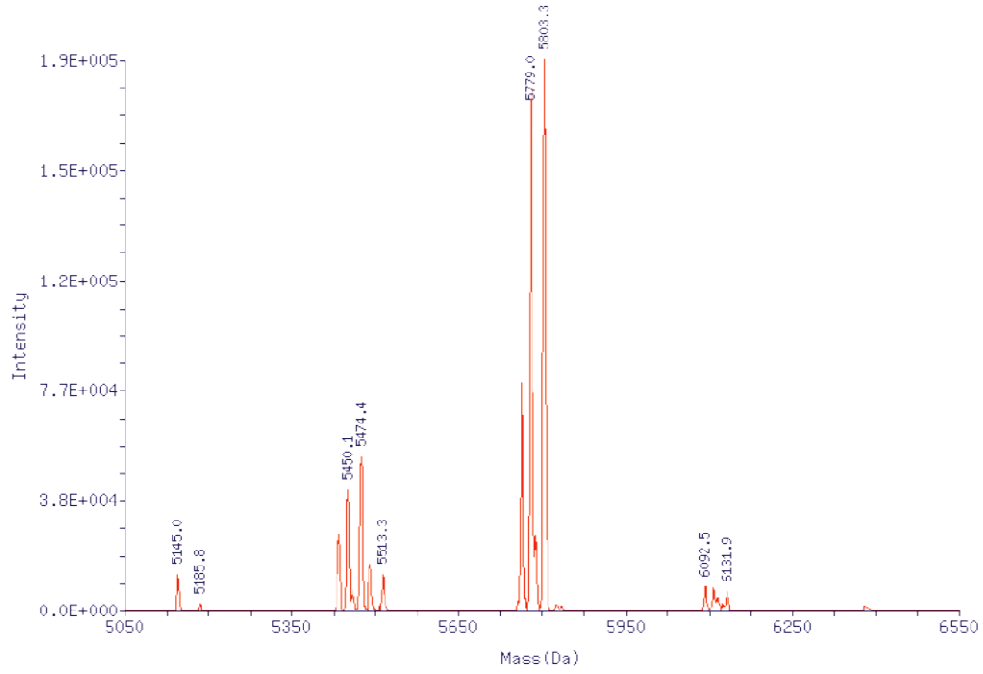

Figure 3-8: The deconvoluted mass spectrum of the synthetic DNA 20-mer at the retention time of 14.74 min. The two large peaks with molecular weight of 5779.0 and 5803.3 correspond to single deletions of nucleotide A or nucleotide C from the expected sequence, respectively.

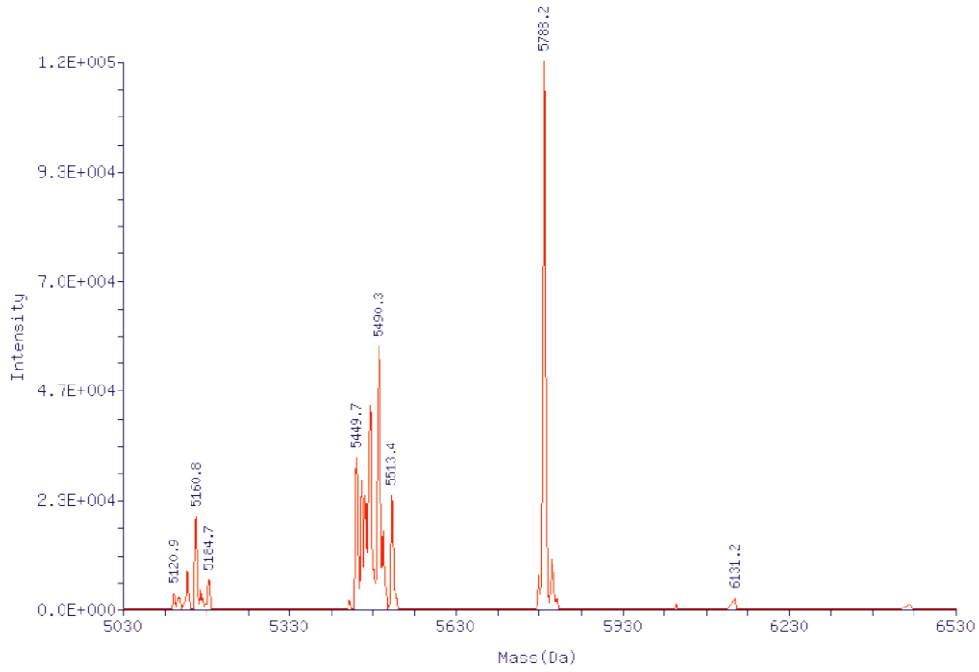

Figure 3-9: The deconvoluted mass spectrum of the synthetic DNA 20-mer at the retention time of 14.53 min. The large peak with molecular weight of 5788.2 corresponds to a single deletion of nucleotide T in the expected sequence.

Melting Curve Measurement

To further test that our synthesized oligonucleotides had the correct sequence, we measured the melting curve of the sample with complementary strands and oligonucleotides containing a single-base mismatch. Our synthesized DNA was labeled at the 5'-end with Cy3-phosphoramidite. The two HPLC purified strands, complementary and single-mismatched, are purchased with FAM-labels at the 3'-ends. When the two strands are hybridized, the fluorescent intensity of FAM is significantly reduced through FRET interaction between FAM and Cy3 fluorophores. When the temperature is elevated above the melting temperature, the two strands separate and the FAM signal recovers. By monitoring the fluorescent intensity of the FAM versus different temperatures, we measured the melting curve of the oligonucleotides (Figure 3-11). The measurement was

carried on a commercial microfluidic chip (Digital Isolation and Detection Chip, Fluidigm, South San Francisco, CA).

1 pmol of standard DNA sample or the DNA sample synthesized from the microfluidic chips (same sequence, with 5'-Cy3 labeled, 5'-Cy3-CCG ACC TGG ATA CTG GCA TT-3') and 1 pmol of FAM-labeled complementary strand (5'-AAT GCC AGT ATC CAG GTC GGT TT-FAM-3') or 1 pmol of FAM-labeled single nucleotide mismatched strand (5'-AAT GCC AGT AAC CAG GTC GGT TT-FAM-3') were mixed with Taq PCR buffer (doped with VOX dye for internal reference) to form 10 μL solutions. The complementary and single nucleotide mismatched strands had 3 extra Thymidine bases at the 3'-end because the fluorescent quantum efficiency would decrease drastically if the FAM was directly coupled to Guanosine. Negative control experiments (solutions containing only FAM-labeled samples or only Cy3-labeled samples, or none of the labeled samples) were also carried out on the same chip simultaneously. We heated the samples to 95 ºC for 5 min and then cooled them down to the room temperature to hybridize the DNA strands in the solutions.

We loaded the samples into the chip by following manufacturer's instructions. Each sample was delivered into 1200 isolated reaction cells (Figure 3-10). The chip was placed on a computer-controlled thermo-cycler and was excited by a band-filtered mercury lamp. The fluorescent signal was captured by CCD camera and both FAM and VOX channels were recorded. We cooled down the chip to 15 °C and then slowly increased the temperature from 15 ºC to 75 ºC. We captured the images while the chip was heated. The

VOX image at each temperature was used to correct for in-homogeneity of the excitation intensity over the chip area (~ 4 cm × 4 cm). The fluorescent signal for each sample integrated over ~ 250 individual cells was used for the data processing. Each intensity point was calibrated with a VOX channel signal, background-corrected with the negative control experiments, and then normalized.

Compared with the standard samples, our synthesized oligonucleotides show similar melting temperatures but higher fluorescent intensity at lower temperatures, indicating that there is impurity in the product. This observation coincides with the results of electrophoresis and mass spectrometry.

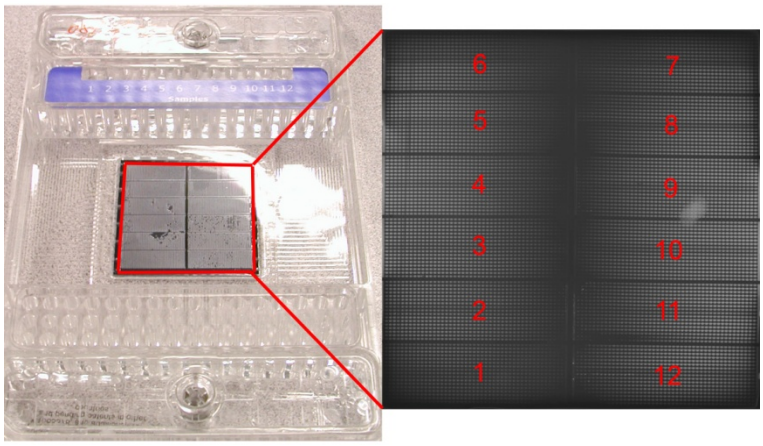

Figure 3-10: The DID chip and a sample fluorescent image of the chip. Each bright square section in the fluorescent image indicates an isolated reaction well.

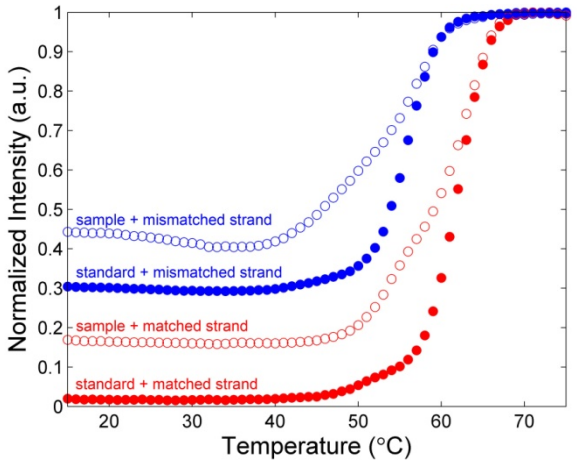

Figure 3-11: Melting curve measurements of single strand (ss)-DNA 20-mer with complementary strand and oligonucleotides with a single mismatch, respectively. The four curves represent the mixture of standard purified ss-DNA + purified complementary strands (●), standard purified ss-DNA + purified mismatched strands (●), unpurified synthesized ss-DNA + purified complementary strands (○), and unpurified synthesized ss-DNA + purified mismatched strands (○), respectively.

Materials and Methods

Synthesis of Perfluoropolyethers (PFPEs)

In a typical synthesis, Fluorolink D4000 (1000 g, 0.24 mol) was added to a dry 2 L round bottom flask and purged with argon for 15 minutes. EIM (67.56 mL, 0.48 mmol) was then added via syringe along with Dichloropentafluoropentane (319 mL) and DBTDA (8 mL). The solution was immersed in an oil bath and stirred at 50 ^{o}C for 24 h. The solution was then passed through a chromatographic column (silica, Dichloropentafluoropentane, 5 × 5 cm). Evaporation of the solvent yielded clear, colorless, viscous oil (PFPE DMA) which was further purified by passage through a 0.22 μm polyethersulfone filter.

In a typical cure, 1 wt% or 0.1% wt of DMPA (0.5 g or 0.05 g, 20.0 mmol or 2 mmol) was added to PFPE DMA (50 g, 12.0 mmol) along with 20 mL Dichloropentafluoropentane until a clear solution was formed. After removal of solvent, the viscous oil was passed through a 0.22 μm polyethersulfone filter to remove any

DMPA that did not disperse into the PFPE DMA. The filtered PFPE DMA was then irradiated with a UV source (Electrolite UV curing chamber model no. 81432-ELC-500, λ = 365 nm, with only one of the four lamps operating to produce 7 mW/cm^2 power flux) while under an oxygen-free nitrogen purge.

Fabrication of the Microfluidic Chips

All the fabrication steps were conducted in a glove box purged with N_2. The PFPE DMA was prepared with 2 different concentrations of photoinitiator, 0.1% and 1.0%. Before use, the polymer was bubbled with N_2 for 30 min. A thick layer (2 mm) of PFPE DMA containing 0.1% of photoinitiator was poured onto the Si wafer having the desired flow pattern made of AZ50 (AZ Electronic materials) and SU-8 2025 features (only the reaction chamber for trapping beads). The thick layer was irradiated with a UV source (Electrolite UV curing chamber, ELC-500, λ = 365 nm, 7 mW/cm^2) for 12 sec. Then PFPE DMA with 1.0% of photoinitiator was spin coated to a thickness of 30 μm (800 rpm for 20 s) onto a Si wafer with the desired control pattern made of AZ50. This wafer was placed in the UV chamber and irradiated for 5 sec. The thick layer was removed, aligned to the thin layer and then irradiated for another 24 sec to bond them together. The chip was peeled off and taken out of the glove box to punch inlet and outlet holes, then it was placed back into the glove box. A 40 μm thick layer of PFPE DMA with 1.0% photoinitiator was spin coated (600 rpm 20 s) onto a glass slide and then irradiated for 4 sec. The chip was placed on top of the coated glass slide and then irradiated for 5 min.

Operation of the Microfluidic Chips

All the inlets and outlets of the chips are inserted with steel tubes (New England Small Tube Co., Litchfield, NH) and connected with either microbore PTFE tubing (for

chemical reagents) or Tygon tubing (for control valves). All the tubing is purchased from Cole-Parmer (Vernon Hills, IL). The valves are filled with Krytox oil. Both reagent delivery (10 psi) and valve actuation (30–40 psi) are pressured by argon. The pressure is switched on and off by computer-controlled solenoid valves (Pneumadyne, Plymouth, MN).

Materials

Porous silica beads (5 μm in diameters, pore size 200 nm) were purchased from Sepax Technology (Newark, DE). Fluorolink D4000 was purchased from Solvay Solexis (Thorofare, NJ). Dichloropentafluoropropane was purchased from SynQuest Laboratories (Alachua, FL). Isocyanatoethyl methacrylate (EIM, 95%) was purchased from Monomer-Polymer & Dajac Labs (Feasterville, PA). 3-Aminopropyl-trimethoxysilane (APTMS), N,N-diisopropylethylamine (DIEA), (1S)-(+)-(10-camphorsulfonyl)oxaziridine (CSO), anhydrous toluene, 2,2-Dimethoxy-2-phenyl acetophenone (DMPA, 99%), and Dibutyltin diacetate (DBTDA, 99%) were purchased from Aldrich (Milwaukee, WI). 5-Ethylthio-1H-tetrazole (activator, 0.25 mol/L solution in anhydrous acetonitrile), deblocking mix (3% dichloroacetic acid (DCA) in dichloromethane (DCM)), anhydrous acetonitrile (MeCN), 5'-dimethoxytrityl-N-phenoxyacetyl-2'-deoxyAdenosine-3'-[(2-cyanoethyl)-(n,N-diisopropyl)]-phosphoramidite (Pac-dA-CE phosphoramidite), 5'-dimethoxytrityl-N-acetyl-2'-deoxyCytidine-3'-[(2-cyanoethyl)-(N,N-diisopropyl)]-phosphoramidite (Ac-dC-CE phosphoramidite), 5'-dimethoxytrityl-N-p-isopropyl-phenoxyacetyl-deoxyGuanosine-3'-[(2-cyanoethyl)-(N,N-diisopropyl)]-phosphoramidite (iPr-Pac-dG-CE phosphoramidite), 5'-dimethoxytrityl-2'-deoxyThymidine-3'-[(2-cyanoethyl)-(N,N-diisopropyl)]-phosphoramidite (dT-CE phosphoramidite), and 1-[3-(4-

monomethoxytrityloxy)propyl]-1'-[3-[(2-cyanoethyl)-(N,N-diisopropyl)phosphoramidityl]propyl]-3,3,3',3'-tetramethylindocarbocyanine chloride (Cy3-phosphoramidite) were purchased from Glen Research (Sterling, VA). 5'-O-(4,4'-dimethoxytrityl)-thymidine-3'-O-succinic acid (5'O-DMT-2'-dT-3'-O-succinate) was purchased from Monomer Science, Inc. (New Market, AL). 2-(7-Aza-1H-benzotriazole-1-yl)-1,1,3,3-tetramethyluronium hexafluorophosphate (HATU) was purchased from Anaspec (San Jose, CA). SYBR Gold nucleic acid gel stain, pre-cast 15% TBE-Urea denaturing polyacrylamide gels (1.0 mm, 10 well), and ultrapure water were purchased form Invitrogen (Carlsbad, CA). Tris-EDTA (TE) buffer (pH 7.5) was purchased from Integrated DNA Technologies (IDT, Coralville, IA). All the DNA oligonucleotides, except the ones we synthesized from the microfluidic chips, were ordered from IDT and HPLC purified.

Concluding Remarks

In conclusion, we have demonstrated that microfluidics can be used for batch synthesis of DNA using phosphoramidite reagents and conventional solvents. We envision a number of direct applications, in spite of the fact that only picomoles of products are produced. First, DNA is special in that it can be biochemically amplified and it has been shown that one can perform whole gene synthesis with as little as femtomoles of the source oligonucleotides (49). Second, if the assay is to be performed on the chip, it is possible to elute the product DNA in nanoliter volumes, thus creating concentrations that are comparable to what are used on the benchtops. This may be useful, for example, in screening siRNA sequences (51), creating DNA nanostructures (52), and for DNA computing (53,54)

Chapter 4

PDMS-BASED PARALLEL MICROFLUIDICS OLIGONUCLEOTIDE SYNTHESIZER: OPENING TO HIGH-THROUGHPUT SYNTHESIS APPLICATIONS

Introduction

De novo gene synthesis is a powerful tool that can be used in a broad cross section of applications, including the study of large sets of genes, the design of genetic circuitry, and the engineering of metabolic pathways for the production of small molecules. The basic concept of *de novo* gene synthesis involves taking a pool of short oligonucleotides and assembling them into larger constructs using some form of polymerase chain assembly or approach involving ligase chain reactions (55,56).

The source of these short oligonucleotides has remained relatively unchanged for the past twenty years. Traditional methods of solid-phase oligonucleotide synthesis (21,22), where each oligonucleotide is synthesized individually on a separate column or in a multi-well plate, produce high yields but are costly. For the assembly of long genes or even whole genomic sequences, the cost of the starting oligonucleotides alone is prohibitive for most applications in academia, as discussed in Chapter 3. Smaller-scale synthesis strategies are needed to bring down the cost of starting oligonucleotides before *de novo* gene synthesis can be widely adopted.

The development of optical and electro-chemical deprotection strategies heralded a new era of parallel oligonucleotide synthesis methods. These technologies have led to a

number of commercially available DNA microarrays (57). Depending on the chip platform being used, several thousand to several hundred thousand distinct oligonucleotides can be synthesized on a single chip. In principle, these massive parallel microarrays can reduce the cost of oligonucleotides by several orders of magnitude.

Despite these promising advancements, there are still several problems inherent in microarray technologies which hinder their direct adaptation to synthesizing oligonucleotides for gene assembly. Because of their small feature size and flat reaction surface, current microchips produce very small amounts of oligonucleotides (10^7--10^8 molecules per sequence) (11). Such low yields of oligonucleotides are insufficient to drive a gene assembly reaction. To overcome this problem, the oligonucleotides can be designed with two flanking adapter sequences and amplified by PCR. These adapter sequences are then removed using a type II restriction enzyme after amplification, making the effective length of the oligonucleotides used in the gene assembly process 30--40 nucleotides shorter than what is synthesized on the microarray (24).

Another problem associated with microarray synthesis technology is that all the oligonucleotides must be cleaved off the chip as a single mixture. While the ability to synthesize thousands or even hundreds of thousands of oligonucleotides on a single chip is beneficial, the sheer number of different strands synthesized on a chip requires careful planning to handle the complexity of all the possible interactions from the various sequences in the mixture (49).

The oligonucleotides obtained from microarray technologies are also of a lower quality compared to those produced with existing solid-phase strategies due to a deblocking step which is less efficient. While many advances have been made since the use of the photo-cleavable protection group 5'-(α-methyl-6-nitropiperonyl-oxycarbonyl), or "MeNPOC", which was first proposed by Fodor (58), the average stepwise efficiency of synthesis from new PGA (photogenerated acid) systems still only approaches ~ 97% (23) compared to the 99.5% stepwise yield cited by Integrated DNA Technologies using conventional solid-phase technology. At these efficiencies, the yield of full-length 30-mer product (compared to truncated sequences) falls from 86% for solid-phase methods to 40% for microarray-based methods. For the longer 50—60-mer nucleotides with adapters synthesized on the microarray the yield is even lower, resulting in synthesis impurities which become a significant concern. An ink-jet oligonucleotide synthesizer, which uses conventional solid-phase chemistry, fares better with a step-wise efficiency between 96.7% to 98.8% (59,60). However, as this method also uses planar substrates, longer sequences still need adapters to allow amplification before use.

This chapter describes a programmable microfluidic synthesis platform made of PDMS that addresses many of the limitations inherent to current microarray DNA synthesis technologies. This device is capable of synthesizing ~ 100 pmol of an oligonucleotide sequence per column while consuming less than 250 nL of 0.1 M phosphoramidite solution per column in each reaction cycle. This is a twofold reduction in reagent consumption coupled with a twofold increase in products when compared to the PFPE microfluidic synthesizer in Chapter 3. As a proof of principle, we synthesized 16

oligonucleotides on a single device; without further purification, we successfully used these sequences to assemble a DNA construct approximately 200 bp long. This microfluidic platform can potentially reduce the cost of DNA synthesis for gene assembly and enable greater accessibility of this methodology in research. The microfluidic architecture with integrated valves also provides a means to individually manipulate and collect products from each column. Sets of oligonucleotides with potentially disruptive interactions can be separated into different pools to avoid problems in gene assembly. Furthermore, this platform lends itself to further integration with other processes including gene assembly, cloning, or purification on chip (49,61,62).

Microfluidic Oligonucleotide Synthesizer

The PDMS-based parallel microfuidic DNA synthesizer, shown in Figure 4-1, was fabricated using a standard multilayer soft lithography (MSL) method (12,63). PDMS is advantageous over other materials such as PFPE as it is readily available and straightforward to use in fabrication, thus allowing the manufacturing of devices that are much more complex than our single reactor chemical DNA synthesizer (64). The device can be roughly divided into three components.

The front component handles all the reagents and has remained mostly unchanged compared to the previous microfluidic DNA synthesizer made of PFPE. In each synthesis step, the valve for the desired reagent opens while others remain closed, delivering the appropriate reagent by means of back pressure.

The middle component consists of a binary tree which produces a uniform flow rate across all reaction columns. Squared profile channels are used in the construction of binary tree because flow velocity is much more constant across the width of a square channel compared to the parabolic velocity profile associated with a rounded channel. The herringbone topology within the binary tree facilitates proper mixing of reagents. The total volume of the binary tree is 1.49 μL.

The end component consists of a sixteen nanoliter-scale reaction chamber array as illustrated in Figure 4-1B. Smaller, more compact reaction columns are also possible using the same fabrication method. The column array was designed to allow parallel loading of solid supports. Purge lines were implemented to avoid cross contamination between synthesis steps by properly purging residual reagent within the binary tree. Each reaction column measures 4500 μm long, 200 μm wide, and 30 μm high to give a column volume of 27 nL. The 100 pmole synthesis scale is chosen to achieve sufficient product yields for several ligation assembly reactions after standard analysis methods. Additional sieve valves (denoted as compression valves) were added to the middle of the columns to prevent rearrangement of closely packed spherical beads when a pressure drop occurs between synthesis steps, minimizing bead loss. Over 95% of resin was retained after 40 cycles (20 hr) of synthesis.

During operation, appropriate reagents are driven by pressure into binary trees that precede the reaction columns. Each reaction column is gated by an individually addressable valve that not only controls which phosphoramidite solution enters the

column but also allows varied exposure time of solutions to that column, if necessary. Because each reaction column is physically separated from the others, the reaction cross-talk between adjacent columns is minimized. While contamination is possible between synthesis steps when residual reagents enter the reactors, the problem is eliminated by adequate flushing of the binary tree after each step. In addition, by physically separating the columns, the contents of each column can be selectively eluted. This is unlike microarray technologies in which all the products are cleaved off into a single mixture.

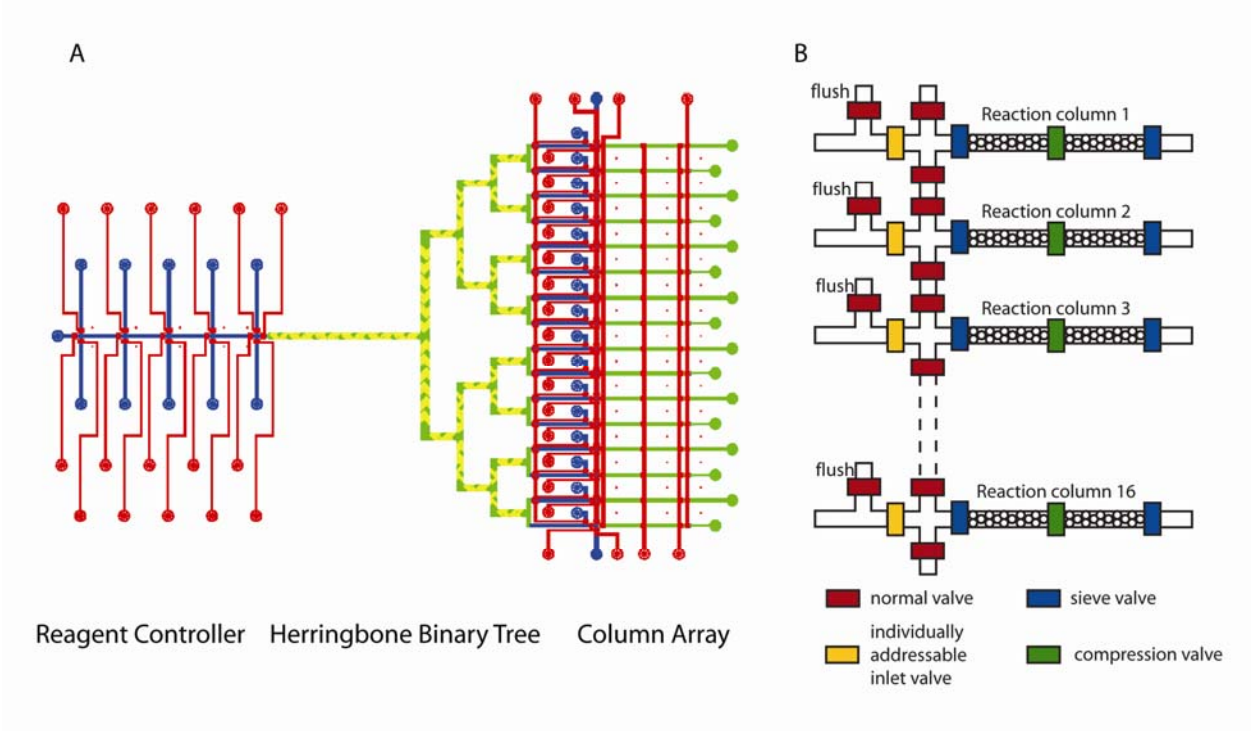

Figure 4-1: (A) Schematic diagram of a 16 column microfluidic DNA synthesizer. The control lines are shown in red, the fluidic lines in blue, the herringbone mixers in yellow, and the square profiled binary tree and reactor columns in green. (B) Close-up schematic of the column array. The red and yellow valves close fully when activated; the blue and green valves are sieve valves that allow fluid flow while trapping CPG beads. The column flush valves open and close in unison to allow residual reagent in the binary tree to be washed away between steps to avoid contamination. The addressable inlet valve controls which columns the reagents enter. The compression valves prevent rearrangement of closely packed spherical beads when a pressure drop occurs between steps.

Microfluidic Oligonucleotide Synthesis

The synthesis method carried out in the PDMS-based device is similar to the standard phosphoramidite chemistry (21,22) described in Chapter 3. However, the standard

solution of 3% dichloroacetic acid in dichloromethane used during the normal deblocking step was replaced by 10% trifluoroacetic acid in acetonitrile to ensure solvent compatibility with PDMS. Also, oligonucleotide synthesis starts on universal linker-derivatized control porous glass beads (65), thus the 1st nucleotides no longer have to be coupled to the CPG beforehand.

Short oligonucleotides approximately 15--25 nucleotides in length can be synthesized without any capping step. Oligonucleotides greater than 40 nucleotides in length required capping steps to achieve high yield of full-length product. Each synthesis cycle contained 7 reaction steps and 4 washing steps. The step-sequence and times are as follows here: deblocking (1.8 min), washing (4 min), coupling T (2.5 min), coupling G (2.5 min), coupling A (2.5 min), coupling C (2.5 min), washing (1 min), capping (2.5 min), washing (2 min), oxidizing (2 min), washing (2 min).

An extended deblocking condition of 2.5 min instead of the normal 1.8 min was used for the initial removal of the DMT group from the secondary hydroxyl group of the universal linker. The initial coupling step to the universal linker was run for 3 min instead of the normal 2.5 min. During the coupling step, the two coupling reagents (phosphoramidite and activator) were sent through the reaction columns alternately, with one reagent flowing continuously for 0.27 s followed by the other for 0.27 s before cycling. The final deblocking of the finished oligonucleotides was done by flowing deblocking reagent into reaction columns for 2 min. After an extended acetonitrile wash, we released the "column valves" and flushed the beads out of the chip and into micro-centrifuge tubes.

The acetonitrile was evaporated using centri-vap. In the final cleavage step, 75 μL concentrated ammonium hydroxide was added into the tubes and then incubated at 55 ºC for 12 h. The beads were centrifuged and then the liquid phase was transferred into new tubes and lyophilized to yield oligonucleotides as pellets.

Modeling of Oligonucleotide Synthesis

A simple computational model is developed to predict the length distribution of product oligonucleotides to better understand how each chemical step affects the overall yield. The three reaction steps taken into consideration are deblocking, coupling, and capping. The effects of depurination or consecutive couplings that would give longer products are not considered. The efficiencies of each reaction step are assumed to be constant throughout the entire synthesis reaction.

Three species are tracked in the model: oligonucleotides with free OH groups (FREE), oligonucleotides with the DMT group attached (DMT), and oligonucleotides that have been capped (CAPPED).

The oligonucleotide can be predicted by iteration of the following equations:

$$DMT_{j+1}(n) = DMT_j(n)*(1\text{-}deblock_{eff}) + DMT_j(n\text{-}1)*deblock_{eff}*couple_{eff} + FREE_j(n\text{-}1)*couple_{eff}$$

$$FREE_{j+1}(n) = [FREE_j(n) + DMT_j(n)*deblock_{eff}]*(1\text{-}couple_{eff})*(1\text{-}cap_{eff})$$

$$CAPPED_{j+1}(n) = CAPPED_j(n) + FREE_j(n)*(1\text{-}couple_{eff})*cap_{eff} + DMT_j(n)*deblock_{eff}*(1\text{-}couple_{eff})*cap_{eff}$$

where n = the length of the nucleotide and i = the cycle number in the synthesis reactions.

At the start of the synthesis, only protected universal linkers are present inside the reaction column, which correspond to oligonucleotide length of 0. The initial condition is therefore DMT(0) = 1, FREE (0) = 0, and CAPPED (0) = 0.

In the first synthesis cycle, the products from the deprotection step are

$DMT(0) = 1\text{-}deblock_{eff}$
$FREE(0) = deblock_{eff}$

The free hydroxyl groups from the universal linkers are allowed to react in the coupling reaction. $DMT(1) = deblock_{eff} * couple_{eff.}$ Those hydroxyl groups that did not react remain as $FREE(0) = deblock_{eff}*(1\text{-}couple_{eff})$.

Capping only affects the free hydroxyl groups remaining. Thus, after the capping step, we have $CAPPED(0) = deblock_{eff}*(1\text{-}couple_{eff})*cap_{eff,}$ and free hydroxyl group remaining in the system is further reduced to $FREE(0) = deblock_{eff}*(1\text{-}couple_{eff})*(1\text{-}cap_{eff})$.

At the end of the first synthesis cycle the species in our system are:

$DMT_1(0) = 1\text{-}deblock_{eff}$ $DMT_1(1) = deblock_{eff} * couple_{eff}$
$FREE_1(0) = deblock_{eff}*(1\text{-}couple_{eff}))*(1\text{-}cap_{eff})$
$CAP_1(0) = deblock_{eff}*(1\text{-}couple_{eff})*cap_{eff}$

To predict the distribution of different species at the end of two cycles, one only has to repeat the analysis using the end product distribution of cycle one as the initial condition. We simulated a synthesis length of 40, which is longer than what is needed for most applications. Graphs for a few tested parameters are shown below:

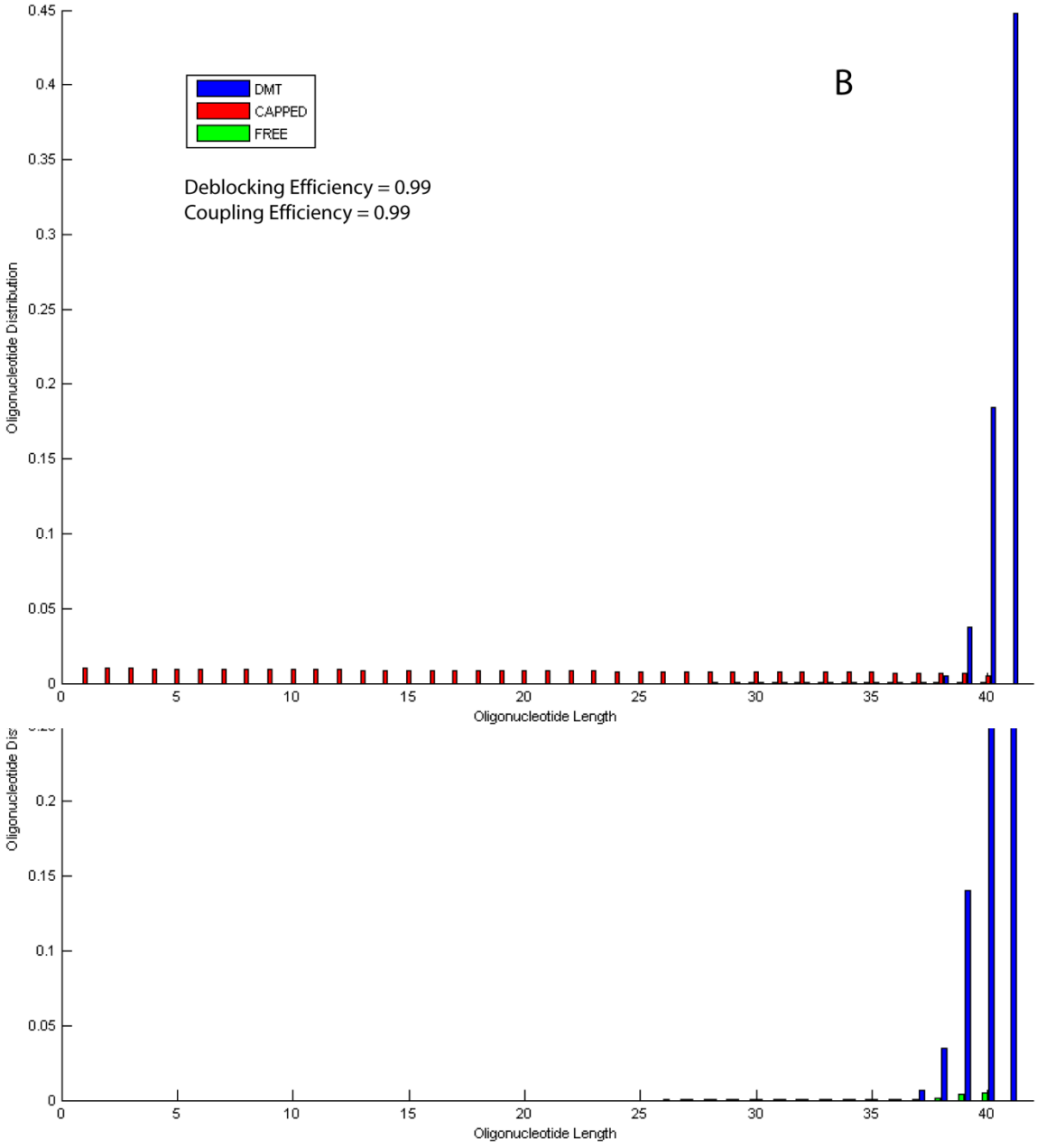
B
DMT
CAPPED
FREE
Deblocking Efficiency = 0.99
Coupling Efficiency = 0.99
Oligonucleotide Distribution
Oligonucleotide Length
Oligonucleotide Length

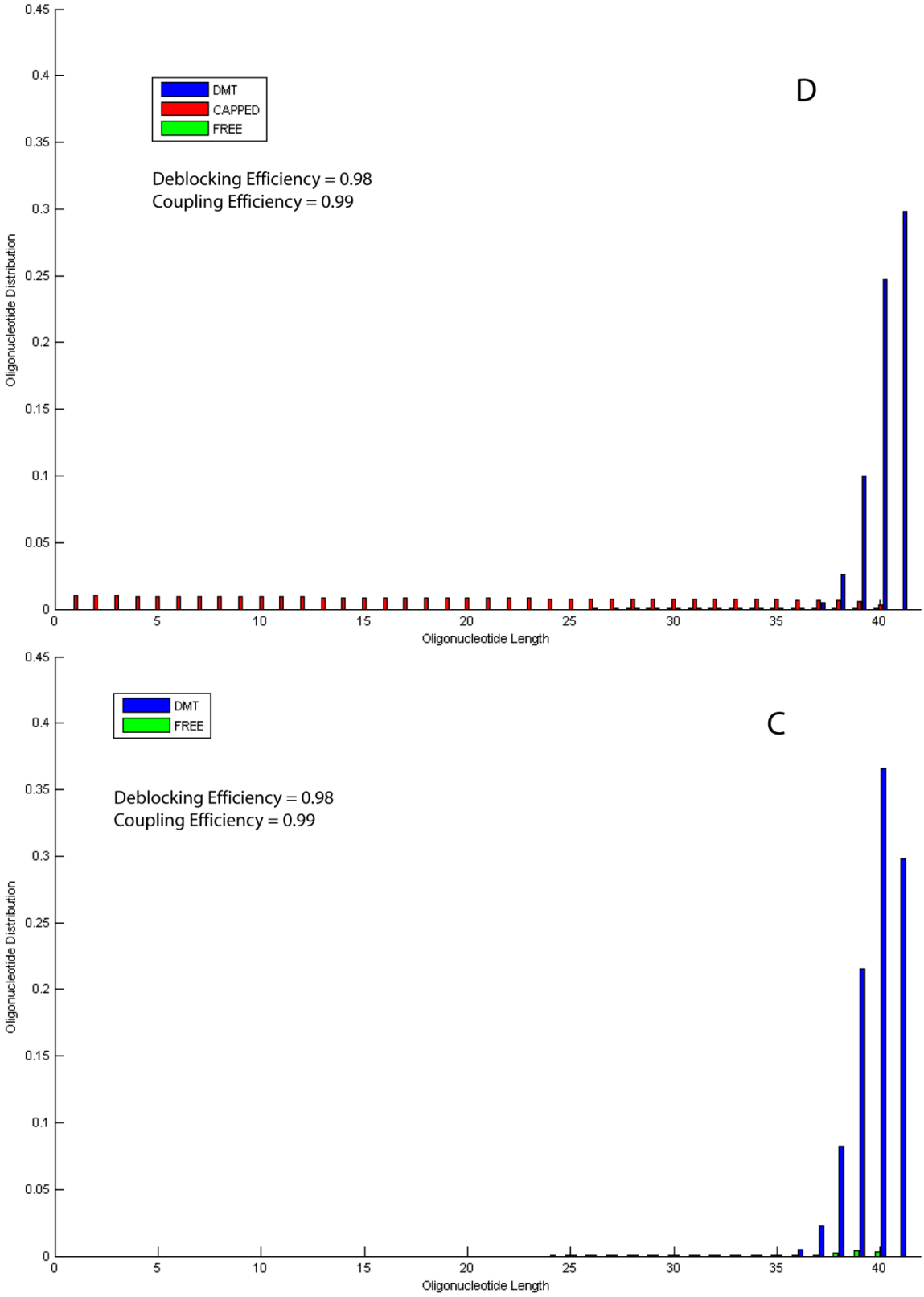

Figure 4-2: The product distribution of oligonucleotides predicted by the model. (A) High yield synthesis conditions (without capping) with coupling and deblocking efficiency of 99%. The major product is the full length oligonucleotide. (B) Same high yield conditions as in A, now with capping at an efficiency of 99%. The total yield on

the full length product does not change between the two cases; however, the amount of truncated product (N-1 mer) is reduced. (C) Low yield synthesis conditions (without capping) with coupling efficiency of 99% and deblocking efficiency of 98%. The major product is the truncated sequence (N-1 mer). (D) Low yield synthesis conditions with an additional capping efficiency of 99%. The additional capping step successfully reduces N-1 mer and the full length oligonucleotide is once again the full length product.

The differences in the qualities of oligonucleotides synthesized with and without capping are compared using our model, with different values for the reaction parameters sampled to reveal the effect of individual reaction steps. The metric chosen to evaluate the qualities of the synthesized oligonucleotides is the ratio between the full length product N mers and N-1-mers. The reason this metric is chosen is that it is very difficult to discriminate between the N-1-mers and N-mers by either physical separation or other biochemical means. While much shorter truncated sequences will not participate further in gene assembly reactions because they would be less likely to anneal properly at the set temperature, N-1-mers behave very similarly to the full length product and could be incorporated in the ligation reaction.

The results from the different modeling parameters are summarized in Table 0-1 and Table 0-2. The numbers given in the table are the ratio of full length product (N-mer) to products with a single deletion (N-1-mers). The capping efficiency is set to 0.99 for the capped system and 0 for system without capping.

Table 0-1 Summary of oligonucleotide synthesis using different parameters in a model system without capping. The metric is the ratio of full length product (N mer) to side product with a single deletion (N -1 mer)

Without Capping		**Deblock Efficiency**			
		0.995	**0.99**	**0.98**	**0.97**
Coupling Efficiency	**0.995**	2.475	1.642	0.975	0.690
	0.99	1.642	1.225	0.809	0.600
	0.98	0.975	0.809	0.600	0.475
	0.97	0.690	0.600	0.475	0.392

Table 0-2 Summary of oligonucleotide synthesis using different parameters in a model system with capping. The metric is the ratio of full length product (N mer) to side product with a single deletion (N -1 mer)

With Capping		**Deblock Efficiency**			
		0.995	**0.99**	**0.98**	**0.97**
Coupling Efficiency	**0.995**	4.926	2.457	1.217	0.804
	0.99	4.829	2.426	1.207	0.798
	0.98	4.514	2.332	1.177	0.782
	0.97	4.090	2.203	1.137	0.761

In synthesis without capping steps, the ratios of N-mer compared to N-1-mer forms a square matrix. The deblocking efficiency is just as important as the coupling efficiency. However, if a capping step is introduced to the synthesis cycle, the coupling efficiency becomes less crucial to synthesizing high quality oligonucleotides because the capping step is able to remove truncated species with free hydroxyl groups and prevent them from being elongated further. This essentially removes oligonucleotides that have failed to couple from going further. However, if the truncated species still has the protecting group attached due to poor deblocking, the capping step has no effect.

As the Table 0-2 reflects, in a system with capping, given a set deblocking efficiency, the ratio of N-mer to N-1-mer does not change as much even if the coupling efficiency is reduced by 2%. However, given a set coupling efficiency, if the deblocking efficiency were to drop by 2%, the ratio is reduced by more than 5-fold. Thus, efficient deblocking is very crucial to making high quality oligonucleotides, even in a system with capping.

Development of Novel Deblocking Solution Compatible with PDMS

By switching to a PDMS-based device for the ease of fabrication, we once again have to address the issue of limited solvent compatibility. In traditional phosphoramidite chemistry, deblocking solution consists of 3% dichloroacetic acid (DCA) in dichloromethane (DCM). However, DCM is incompatible with PDMS and leads to swelling and possible delamination of multilayer devices (35). There are two logical substitutes that have shown to work well with PDMS: acetonitrile and water. Each, however, has its own drawbacks.

While traces of water are used in conjunction with iodine and pyridine in the oxidative step of synthesis, its presence can greatly hamper the efficiency of the coupling step. From our previous work, we found that by switching from the traditional oxidative solution which contains water to CSO in acetonitrile, the purity of our oligonucleotides improved dramatically. We attributed this to the residual water that had not been removed completely from the reaction columns between washing steps. This problem can potentially be addressed by extending the washing step with anhydrous acetonitrile between the deblocking step and the coupling step.

Acetonitrile is a mild solvent that is already used in the coupling and washing step of traditional oligonucleotide synthesis. However, the active acid traditionally used for deblocking (DCA) forms a complex with acetonitrile that drastically slows detritylations (66). Therefore, if one were to use acetonitrile in the deblocking step, a novel deblocking solution using a different acid or concentration must be formulated.

Heterogeneous phase detritylation processes are complex with many chromatography effects, such as the retardation of detritylation due to acid binding with the oligonucleotides and the recapture of free DMT cation by 5'-OH group. In addition, the interplay of incomplete deblocking and losses of oligonucleotide bases due to depurination make rigorous kinetic modeling and analysis difficult. We adopted a practical approach of analyzing the end product of the synthesis and using the ratio of full-length product to truncated byproducts as a benchmark to evaluate the success of the deblocking step.

Aqueous Deblocking Solution

Moocroft et al. (67) have successfully demonstrated a system in which oligonucleotides are synthesized on linker derivatized on planar PDMS surfaces using 10% trifluoroacetic acid (TFA) in aqueous solution as deblocking agent. We attempted to apply their deblocking strategy for our device. The monitoring of detritylation in aqueous solution is much more difficult than in DCM because the characteristic orange color caused by trityl cations is quickly quenched. A rough estimate of deblocking time cannot be made by visual inspection, thus a long deblocking time of 4 min is chosen to ensure detritylation is

driven to completion. Synthesis of the homopolymers A_{20}, G_{20}, C_{20}, and T_{20} are carried out.

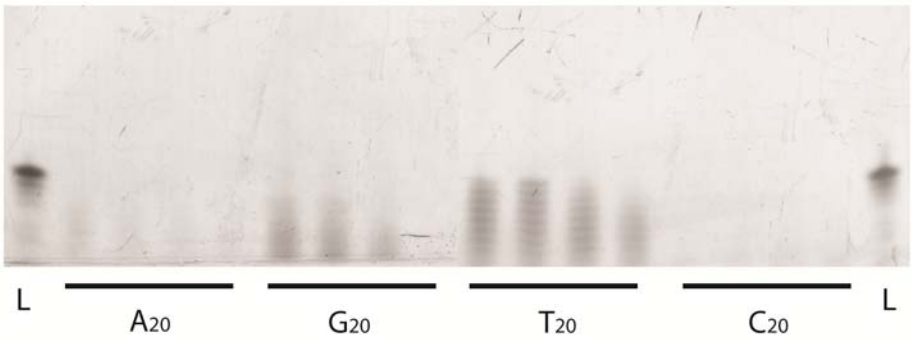

Figure 4-3: Polyacrylamide gel electrophoresis of different homopolymers with length of 20 bases using 10%TFA in aqueous solution as deblocking solution. L denotes a ladder that is 20 nucleotides in length. Both A_{20} and G_{20} samples contain no full length product due to poor coupling as well as depurination. T_{20} lanes contain some full length product but with oligonucleotides which are mostly truncated, indicating poor coupling efficiency.

Gel electrophoresis of the products in Figure 4-3 shows that no full length materials are observed in lanes for A_{20} and G_{20}. While the T_{20} lane does exhibit full length oligonucleotides, the majority of products are truncated sequences. No products are observed for C_{20} because of inefficient staining homopolymer of cystine using SYBR Gold (68). Because homopolymers of purines (A_{20} and G_{20}) are of a much lower quality compared to homopolymers of pyrimidines (T_{20}), the time of exposure to deblocking solution may have been excessively long and allowed extensive depurination to take place. Assuming that deblocking is indeed complete, the poor synthesis of T_{20} can be attributed to insufficient coupling. Extending washing time of anhydrous acetonitrile from 2 min to 4 min did not result in improved yield. These experiments showed that keeping the entire synthesis process water-free would result in better yield as well as require less time. Hence, the pursuit of an aqueous deblocking solution was abandoned.

Deblocking Solution Based in Acetonitrile

We then broadly surveyed several deblocking solutions composed of different organic acids in acetonitrile during the synthesis of the homopolymer A_{20}. Adenine was chosen because it is the base most sensitive to depurination (69). We found that trifluoroacetic acid was most suitable (Figure 4-4). Initially, we established that 5% TFA in acetonitrile with a deblocking time of 2.0 minutes was sufficient for synthesis of short oligonucleotides. However, in experiments where long oligonucleotides (longer than 35-mers) were synthesized, we observed that the orange color of DMT cation persists well over the 2.0 min deblocking time at later synthesis cycles. We believe that acid binding to the growing oligonucleotide depletes free acid from the deblocking solution at higher oligonucleotide mass densities due to the increased length. We addressed this problem by increasing the deblocking acid concentration to 10%. The use of higher acid concentration allows quicker saturation and gives faster and more complete detritylation. Additional experiments were performed using 10% TFA in acetonitrile in the synthesis of homopolymer A_{40} with capping. The deblocking time was varied at 30 second intervals from 0 to 3.5 minutes; the optimum deblocking time was found to be between 1 min and 2 min (Table 0-3). At longer deblocking times, losses of full-length nucleotide product through depurination exceeded gains from increased deblocking efficiency.

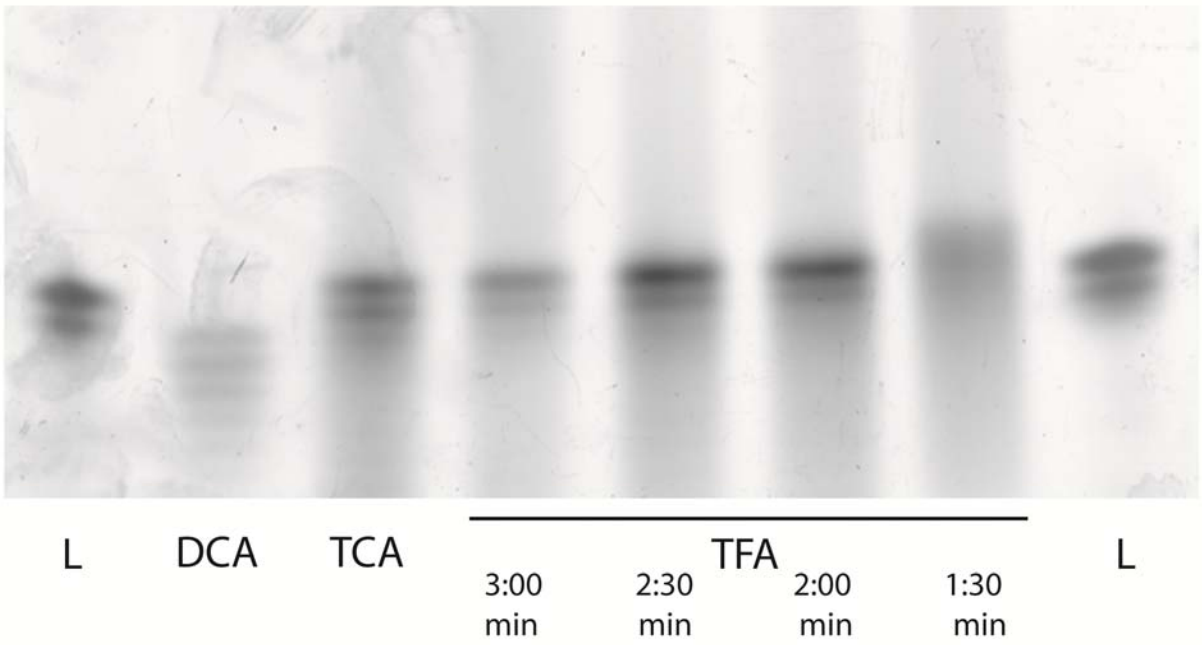

Figure 4-4 Effect of different deblocking acids and deblocking time on the quality of A_{20} homopolymer. A selection of organic acids is broadly surveyed as candidates to be used in a acetonitrile based deblocking solution. 5% TFA is found to be most suitable with a optimal deblocking time between 2 min and 2.5 min.

Table 0-3: Effect of deblocking time on the quality of A_{40} homopolymer using 10% TFA in acetonitrile. A minimum of 1 min deblocking time is needed for successful deblock. The quality of the homopolymer starts to drop with deblocking time above 2.5 min. This suggests that the increased deblocking efficiency at longer times are offset by losses of full-length product through depurination.

	0 sec	30 sec	1 min	1.5min	2.0min	2.5min	3.0min	3.5min
N	0	0.351	0.671	0.651	0.656	0.644	0.644	0.598
N-1	0	0.284	0.329	0.349	0.344	0.356	0.356	0.402
N-2	0	0.214						
N-3	0	0.151						

Construction of Gene Fragment from *Bacillus Cereus*

A gene fragment from *Bacillus cereus* was selected for synthesis through a ligation mediated assembly method. Oligonucleotide sequences were derived from a custom-developed program that first divides the sequence into oligonucleotides with a desired melting temperature range while keeping track of the melting temperature variation between the pieces. The set of pieces with the least variation in melting temperature was chosen. The program then generated the sequence of the sense strand by stitching every

two pieces together, and the anti-sense strand using the same method but with an offset of a single piece. A summary of the oligonucleotide set is provided in Table 0-4.

Table 0-4: Oligonucleotide sequences used for the ligation-mediated assembly of a gene fragment of *Bacillus cereus.* The similar starting sequences of F3 and F9 that led to side products during the assembly are highlighted in red.

	Forward Sequence		Reverse Sequence
F1	GTATACTTCCAATCCAATGCA	R1	TCGCTTTCATTGCATTGGAT
F2	ATGAAAGCGAAGAAAAAAGATAAA	R2	ATATTCAGAAGTTTTATCTTTTTTCT
F3	ACTTCTGAATATCAGTACGTTG	R3	ACCATGCGTCAACGTACTG
F4	ACGCATGGTACTCTAATCAG	R4	CGGCCGTTCTGATTAGAGT
F5	AACGGCCGTAGCATCCC	R5	ACGTTTCCACGGGATGCTA
F6	GTGGAAACGTATCCCGTCC	R6	CACTTCGCTGGACGGGAT
F7	AGCGAAGTGAAACAGTTCCA	R7	CACCGGTCTGGAACTGTTT
F8	GACCGGTGAGGCGTTCA	R8	ACAGTTGAAGTTGAACGCCT
F9	ACTTCAACTGTTTCGCAACTGTTCAGCGTTTC		

Using the established synthesis protocol with our new deblocking conditions, we proceeded to synthesize the oligonucleotides needed to assemble a gene fragment from *Bacillus cereus.* Each oligonucleotide product was verified though gel electrophoresis. The gel image (Figure 4-5) shows that the chip products had the same motility as commercially ordered standards from IDT. The lanes with chip products were partially smeared because no desalting step was taken; however, the major products all corresponded with full-length oligonucleotides.

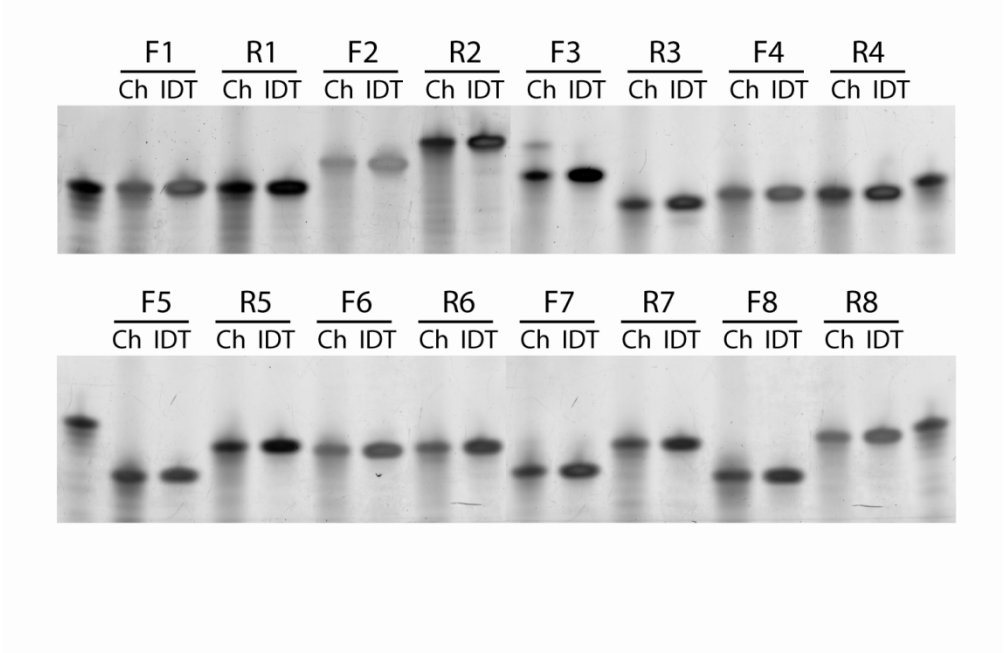

Figure 4-5: Polyacrylamide gel electrophoresis comparing oligonucleotides synthesized from the microfluidic platform (Ch) to oligonucleotides purchased from IDT. The chip products have the same motility as the commercially prepared standards. However, the chip products are also partially smeared because of excess salt as no desalting step was performed after cleavage from the beads.

Ligation Assembly of DNA Constructs

To confirm the identity of synthesized sequences and to determine whether the eluted oligonucleotides were functional without further amplification or purification, a gene fragment from *Bacillus cereus* was assembled from a mixture of oligonucleotide 17—24-mers that were obtained using the microfluidic synthesis method described earlier. The general strategy of gene assembly used involves ligation of oligonucleotides into a complete construct followed by PCR amplification of the full-length product (Figure 4-6). The oligonucleotides were each collected in a 10 μL volume; the material produced from one synthesis is sufficient for 50--100 ligation reactions.

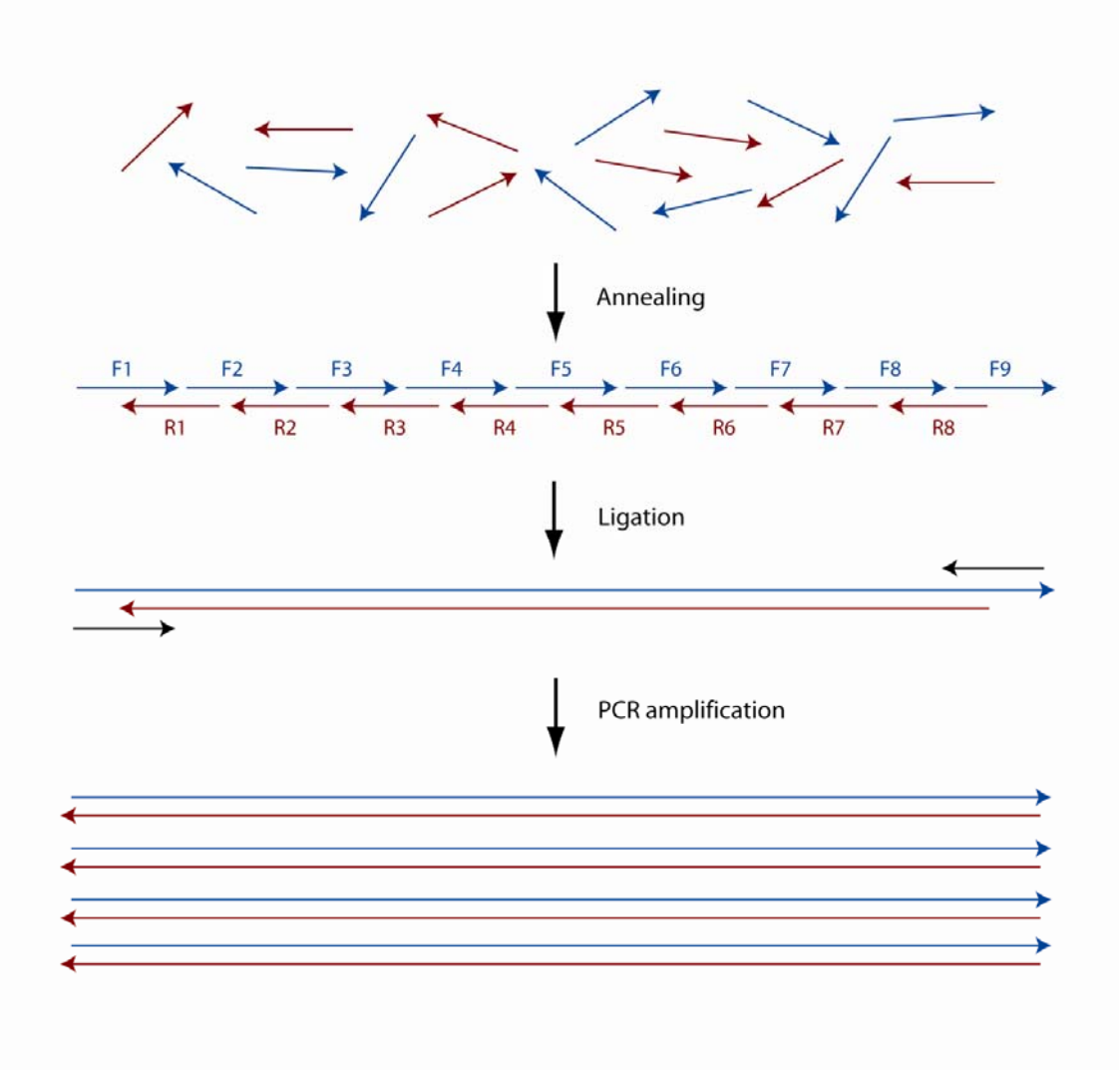

Figure 4-6: Schematic of gene assembly by ligation. The starting oligos are placed in a single mixture and allowed to anneal and ligate into complete constructs. Primers are than added to amplify the full-length product by PCR.

A special set of ligation reactions with Cy3-labeled F1 strands was performed to examine the ligation reaction in detail by gel electrophoresis without the need of amplification (Figure 4-7). Reaction pots with increasing numbers of strands that form products of increasing length were prepared. We expected species of various starting and ending strands to be ligated in each reaction. However, only species that included the Cy3-labeled F1 strand could be visualized after electrophoresis.

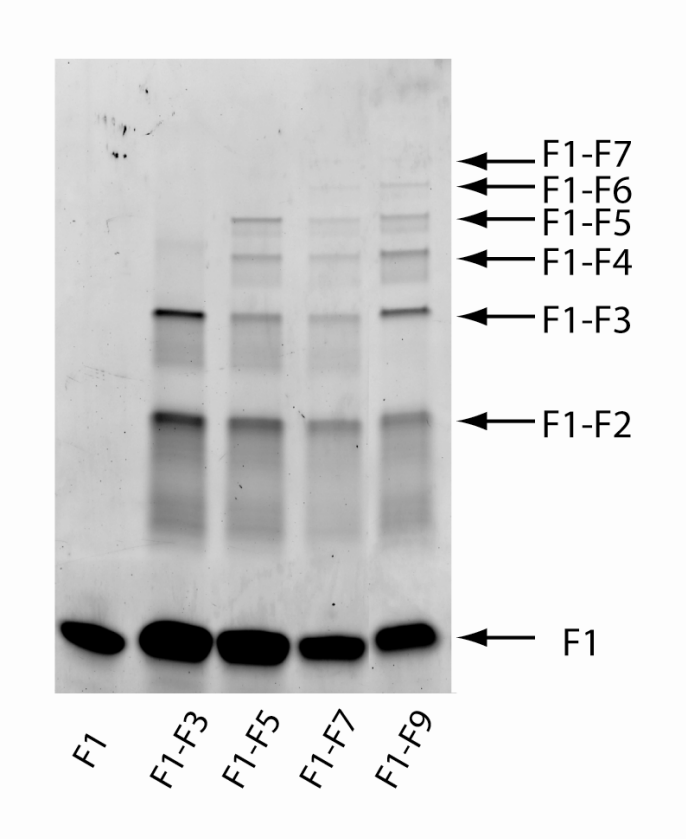

Figure 4-7: Polyacrylamide gel electrophoresis for a series of ligations reactions with a Cy3-labeled F1 strand in combination with different numbers of starting oligonucleotides. No products longer than the expected length are present in each reaction mixture. For example, in the mixture containing F1 through F5, only F1, F1-F2, F1-F3, F1-F4 and F1-F5 are observed. No products longer than F1-F7 can be visualized without further amplification. In general, the amount of ligation product decreases as the number of ligation steps needed to form a particular product increases.

Our results show that no products longer than the expected length are present in each reaction mixture. In general, the amount of ligation product decreases as the number of ligation steps needed to form a particular product increases. The majority of the Cy3-labeled F1 strands failed to take part in any ligation reaction to form longer products. The longest detectable ligation product without further amplification is F1-F7. The yield of this ligation reaction was not optimized.

PCR of Ligation Product

We performed PCR of the ligation reactions and analyzed the results on an agarose gel. Strong, dominant bands were evident for the desired product in lanes with the full set of

starting oligonucleotides. "Primer-only" and incomplete oligonucleotide sets used as controls yielded no product-length bands confirming that the presence of desired-length species was not a consequence from amplifying a contaminating species. We observed a weak band in the main reaction lanes that indicated there were lower molecular weight species present suggesting there could be assembly intermediates present in the ligation product (Figure 4-8).

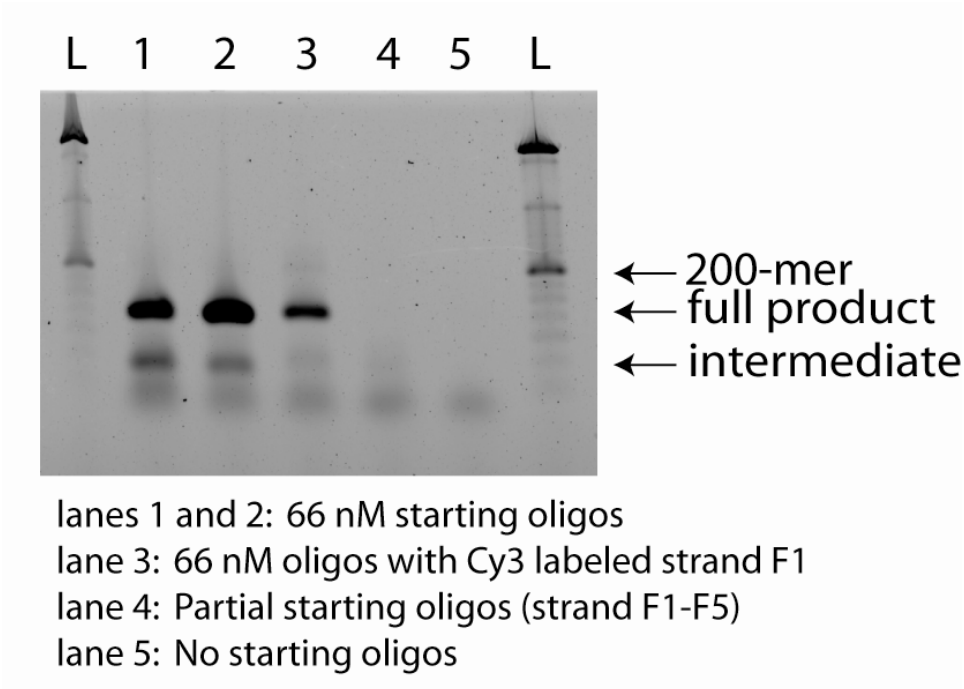

Figure 4-8: Agarose gel electrophoresis showing fell-length assembly of a gene fragment from *Bacillus cereus*. In the presence of the full set of starting oligos, full-length products are observed following amplification. "Primer-only" and incomplete oligonucleotide sets used as controls yielded no product-length bands. Weaker bands with lower molecular weight indicate assembly intermediates present in the ligation product.

DNA Sequencing of Assembled Sequence

Sequencing of microfluidic gene synthesis products unambiguously confirmed the identity of the gene construct. Even though such sequencing does not directly report on the quality of the starting synthesized oligonucleotides, errors present in the starting oligonucleotides would be a source of deletions and other errors in the assembled

sequences. The fidelity of the polymerase used in the amplification step may also contribute to any observed errors (61).

Gel purification of the resulting assembled sequence was omitted to prevent the masking of errors. The clones were also not screened prior to sequencing other than to confirm successful insertion into the cloning vector. Thus, gene assembly products including both full-length species along with other incomplete, intermediate products should be detected in the clones.

Ten clones of DNA constructs assembled from purified oligonucleotides purchased from IDT were sequenced. Eighteen clones of DNA constructs assembled from oligonucleotides synthesized on the microfluidic synthesis chip (Chip) were also sequenced. The results of this sequencing are summarized in Table 0-5.

Out of the 10 IDT clones, 8 had perfect sequence while 2 had single deletions. Out of the 18 Chip clones, 4 had perfect sequences, 5 had single deletions, 2 had single point mutations, 1 had a single deletion and insertion, and 1 had a single point mutation and a single insertion. More interestingly, 3 of the Chip clones were missing a stretch of sequence from F3-F8. Looking more closely at the sequences of the starting oligonucleotides, we found that the 5 starting bases for F3 were identical to F9. Thus, F9 can incorrectly ligate to F2 instead of F3. Such a problem could be avoided with more careful design of the starting oligonucleotide pool.

For the IDT clones, a total of 2 errors were found out of 1300 bases sequenced resulting in an error rate of 1 per 650 bp or 0.15%. Excluding clones with incompletely assembled sequences, the Chip clones had 11 errors out of 1690 bases sequenced. That is an error rate of 1 per 153 bp or 0.65%. This error rate is very similar to the error of 1 in 160 bp given by Tian (24).

Table 0-5: Summary of errors in the assembly of a gene fragment of *Bacillus cereus* using purified oligonucleotides purchased commercially (IDT clones) versus the synthesis products from the microfluidic device (Chip clones)

Error Type	**IDT Assembly of Oligos**	**Chip Assembly of Oligos**
None	8/10	4/18
Single Deletion	2/10	5/18
Single Mutation		2/18
Single Insertion and Deletion		1/18
Single Insertion and Mutation		1/18
Sequence Truncation (missing oligos)		5/18
Total Bases Sequenced	1300	1690 (*without truncation*)
Overall Assembly Success Rate	80%	22%
Total Number of Errors	2	11
Per Base Error Rate	1 in 650	1 in 153

Synthesis of Long Oligonucleotide

To test the limits of our synthesis method, we also synthesized oligonucleotides up to 40 bases in length. We found that at these lengths, the resulting oligonucleotides were not of sufficiently high quality. We therefore added an additional capping step that was not used in our original synthesis of shorter oligonucleotides. By capping unreacted bases, we prevented truncated sequences from further extending. This eliminated most of the N-1 and N-2 oligonucleotides observed in the uncapped synthesis. These sequences can lead to deletion errors in the gene assembly reaction which are problematic.

Synthesis of the homopolymer A_{40}, G_{40}, $C_{40,}$ and T_{40} are carried out. Results for C_{40} are not shown because of the inefficient staining of homopolymer of cystine using SYBR

Gold (68). Homopolymer of guanine G_{40} forms a secondary structure with itself at room temperature and hence its motility is greatly increased. By running the gel at an elevated temperature (60 ºC), the secondary structure is eliminated and the motility returns to normal. However, single base resolution is not possible at such a high temperature. A randomly chosen mix sequence is synthesized to esure that guanine and cytosine are successfully incorporated in the synthesis cycle.

PAGE analysis of the reactions (Figure 4-9 and Figure 4-10) shows that the dominant bands in the capped synthesis are from full-length product as opposed to truncated products from the uncapped synthesis. By comparing the ratio of full-length product to the N-1-mers, we successfully calculated our deblocking efficiency to be greater than 98.6%, which is substantially higher than that of many other PGA systems.

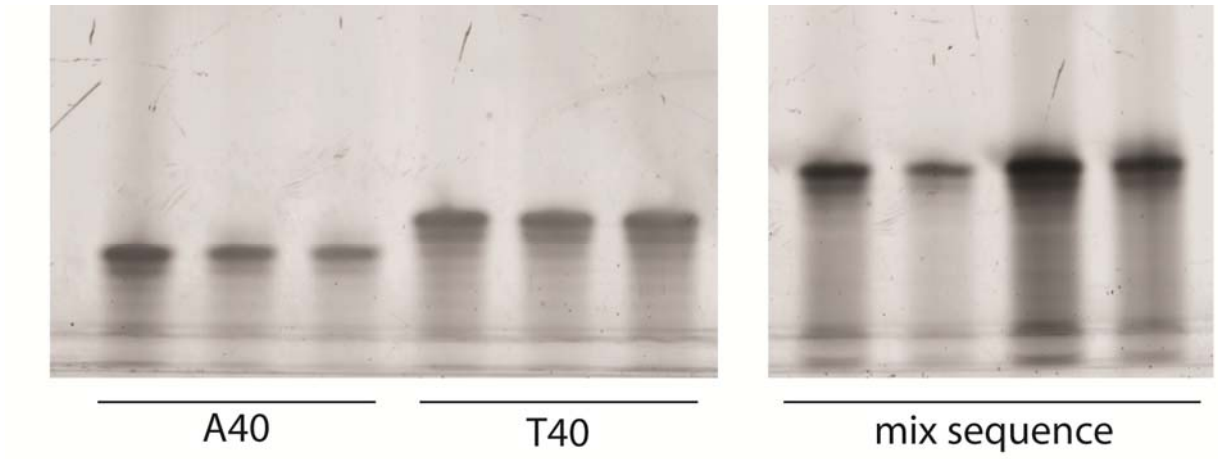

Figure 4-9: Polyacrylamide gel electrophoresis showing successful synthesis of oligonucleotides 40 bases in length

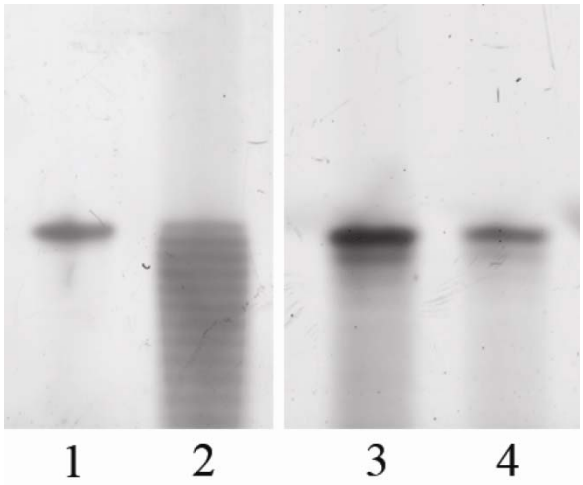

Figure 4-10: Polyacrylamide gel electrophoresis showing oligonucleotides 40 bases in length synthesized under different conditions. Lane 1 is a purified standard purchased from IDT. Lane 2 is product synthesized using the microfluidic chip using 5% TFA deblocking solution without any capping during the synthesis. Lanes 3 and 4 are products from different reaction columns synthesized using 10% TFA deblocking solution with capping after each synthesis cycle. The gel image shows that the dominant bands in the capped synthesis are from full-length products, whereas there is a large number of truncated products in the uncapped synthesis.

Materials and Methods

Device Preparation and Operation

Microfluidic devices were stored in a desiccator overnight before use. Glass vials filled with molecular sieves and steel tubes (New England Small Tube Co., Litchfield, NH) were dried in a 180 °C oven overnight and allowed to cool to room temperature 15 min prior to use. The control lines were interfaced with computer-controlled solenoid valves (Pneumadyne, Plymouth, MN) through steel tubes connected to Tygon tubing. The control lines were primed with Krytox oil through dead-end filling. All reagents were prepared fresh prior to experiments. Glass vials filled with reagent were connected to the device via microbore PTFE tubing through the septa. 5 μm, 500Å control porous silica beads functionalized with universal linker (SynGen) were used to construct the bead columns. Both reagent delivery (10 psi for acetonitrile, 5 psi for others) and valve actuation (35 psi) were controlled using argon gas.

Polyacrylamide Gel Electrophoresis

The synthesized oligonucleotides were re-suspended in water and normalized to a concentration of 50 ng/μL using a NanoDrop 1000 (Thermo Scientific). Before gel loading, the oligonucleotides were mixed with TBE-Urea sample loading buffer (Invitrogen) and heated to 70 ºC for 3 minutes. 1.5 μL of samples were loaded onto polyacrylamide gel (15% Novex® TBE-Urea gel, Invitrogen). Samples approximately 20 nucleotides in length were run at room temperature at 175 V for 75 min. Samples approximately 40 nucleotides in length were run under the same conditions but for 100 min. The gels were stained with SYBR Gold dye and visualized using Typhoon 9410 (Amersham Biosciences). Final images were analyzed using ImageQuant (Amersham Biosciences).

Ligation Assembly of DNA Constructs

Each oligonucleotide strand (8 μL, 5 μM) was mixed with 1 μL of T4 polynucleotide kinase reaction buffer (New England Biolabs) and 1 μL of 10 mM ATP and then cooled to 4 ºC. Afterwards, 0.7 μL of T4 polynucleotide kinase was added. The mixture was allowed to react for 1 hr at 37 ºC and then terminated by heating the reaction mixture to 65 ºC for 15 min. The phosphorylated oligonucleotides were then added together and diluted into a 75 nM solution. 1 μL of Taq DNA ligase reaction buffer and 0.75 μL of Taq DNA ligase were added to 9 μL of phosphorylated oligonucleotide solution. The mixture was heated to 65 ºC for 30 sec to ensure all the oligonucleotides were melted off. The ligation reaction was then allowed to take place at 42 ºC for 4 hrs.

PCR of Ligation Product

Polymerase chain reaction was performed with 100 μL of reaction mixture including 10 μL PCR buffer, 3 μL of 50 mM $MgCl_2$, 2 μL of Primer A1 (10 μM), 2 μL of Primer B1 (10 μM), 1 μL of dNTPs, and 1 μL of ligation mixture. The PCR was conducted using the following conditions: 2 min initial denaturation at 94 ºC, followed by 20 cycles of 94 ºC for 45 s, 55 ºC for 30 s, and 72 ºC for 1.5 min.

DNA Sequencing

PCR products were sequenced to check for errors. The DNA construct was cloned using plasmid vector pCR®4-TOPO (Invitrogen) and transformed into OneShot® TOP10 Chemically Competent *E. coli* cells. The cells were spread on prewarmed LB plates containing 50--100 μg/ml ampicillin and incubated at 37 ºC. After overnight growth, the plates were sent to MCLab where individual colonies were amplified and sequenced.

Conclusion

This novel microfluidic synthesis platform addresses many of the limitations associated with microarray technology such as reduced product purity due to poor deprotection, insufficient synthesis scale, and adverse interactions in large oligonucleotide pools, while keeping many of its advantages (such as reduced cost). Our chip is programmable for synthesis of any desired sequence, easy to operate, and consumes very minute quantities of reagent and solvent on a per sequence basis.

The new deblocking scheme used in our platform rivals optical and electro-chemical deprotection strategies which are currently in development in both cost and efficiency. Unlike other systems where complex mixtures of custom chemicals are needed (70), our

deblocking solution only uses dilute trifluoroacetic acid which is commercially available. The efficiency of our deblocking step is estimated at > 98.6% which is higher than the PGA system used by Affymetrix (97%) as well as other photocleavable protecting groups (94 %) (23).

The physical separation of individual reaction chambers eliminates the potential problem of cross contamination. Having individually addressable valves gating each reaction chamber also allows for easy recovery of specific sequences synthesized for direct use in the subsequent gene assembly. This is especially useful for multiplex reactions where sequences with adverse interactions with each other can be eluted into different mixtures. Such precise fluid handling is not available in microarray technologies and will help allow the integration of this chip into other processes in the future.

The oligonucleotides synthesized from our device were directly used for ligation to give DNA constructs about two hundred base pairs long. Employing such direct synthesis without concentration or an initial amplification step not only reduces the time and cost of the overall synthesis protocol, but also eliminates the possibility that additional errors will be generated during the amplification procedure. While the error rate of 1 in 153 bp from chip product is higher than that observed for a product assembled from purified oligonucleotides ordered from IDT, it is consistent with the 1 in 160 bp error rate given by Tian for assembly of DNA constructs using unpurified oligonucleotides. The 17—24-mer synthesis also lacked capping. Given the improvement in purity for longer syntheses (Figure 4-9), performing capping during the synthesis of the oligonucleotides used for

ligation should similarly improve error rate. Optimized ligation conditions, including varied temperature, may also be able to minimize the incorporation of errors into the full-length product.

These results demonstrate significant progress towards high-throughput gene synthesis and could help meet the growing demands of the emergent field of synthetic biology. Substantial improvements are still needed but many can still be achieved through further optimization of reaction conditions. Systems integration of other processes that have already been demonstrated in stand-alone units, such as purification, cloning, and protein expression (71), will greatly increase the range of suitable applications for this technology.

Chapter 5

FUTURE STRATEGIES FOR MASSIVE PARALLEL OLIGONUCLEOTIDE SYNTHESIS

Introduction

Microfluidic devices have evolved rapidly from early single-channel structures to complex devices that perform hundreds of assays in parallel and that integrate multiple sample preparation and analysis operations. The development of pneumatic valves that allow for dense fabrication and parallel actuation of hundreds or even thousands of valves has been instrumental in the creation of more complex devices. However, independent control of large numbers of valves is still very difficult because in most cases each independent valve requires a dedicated off-chip solenoid valve. The size and cost of these off-chip controllers impose a practical limit on the number of independent pneumatic valves in a device.

In the synthesis of oligonucleotides, each reactor column must be independently addressable for the operation to be parallelized. Using the current design architecture, one off-chip solenoid valve would be needed for each desired sequence to be synthesized. However, for the assembly of a gene of moderate size, hundreds of distinct oligonucleotides would be needed. Given the cost of 20 USD for a typical solenoid valve used for microfluidic devices, a system capable of synthesizing so many oligonucleotides would cost upwards of 2,000 USD without consideration of the additional cost of the digital I/O cards needed to interface the valves to a computer.

If valve control circuitry could be integrated onto the microfluidic device, then the number of off-chip controllers needed for complex control tasks could potentially be reduced to a much smaller number. In principle, a large number of independent valves can be actuated by a single pressure controller using time-division multiplexing. This can be implemented provided that a valve can remain actuated for a period of time sufficient for the external control to cycle back to it.

Another strategy is to embed the sequence information of oligonucleotides to be synthesized in the layout of the control lines themselves. A device utilizing this strategy can only be used to synthesize a specific set of oligonucleotides. However, while the high start-up and fabrication costs of silica microfluidic devices make it infeasible to make single-use devices, the fast turnaround time and economical fabrication costs of MSL devices make such a strategy reasonable.

Novel Control Scheme for Reactor Addressability

Time-Divison Multiplexing through "Control of Control"

In electronics, a multiplexer (mux) selects one of the many analog or digital input signals and forwards the selected input into a single output line. A microfluidic multiplexer serves the same function and is a powerful tool that addresses a large number of lines with a small number of connections to outside controls. The most common way in which a multiplexer is implemented is through an array of complementary valve pairs organized in a binary architecture to select 1 of 2^N flow lines using 2N control lines. Each selection

bit corresponds to two control lines, and the lines for each bit will always be in complementary states, for example $Bit\ 1$ and $\overline{Bit\ 1}$.

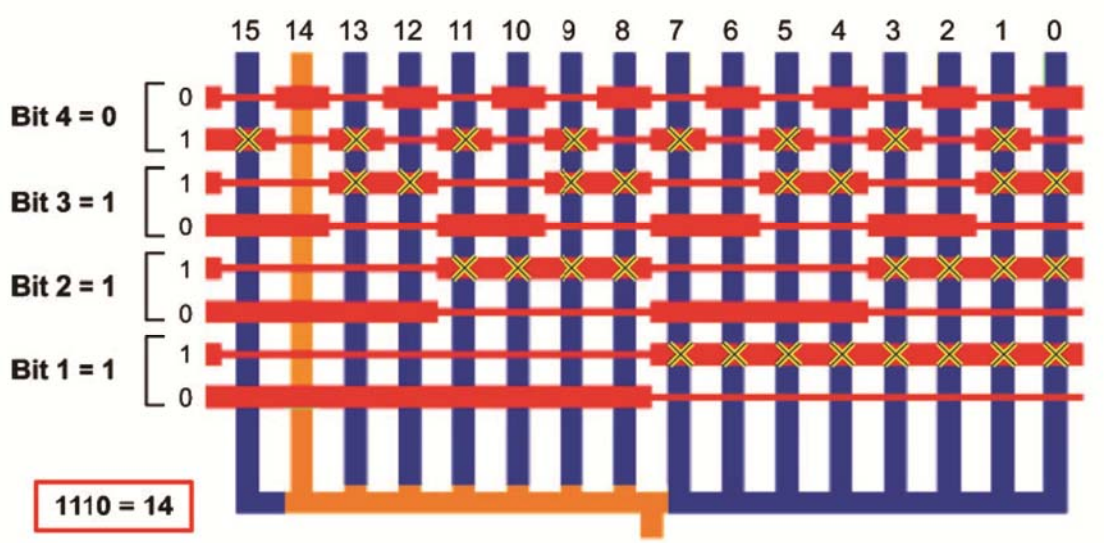

Figure 5-1: Schematic of a binary multiplexer

While a multiplexer with even higher efficiency than the binary multiplexer has been demonstrated that uses a strategy that allows $N!/(N/2)!^2$ lines to be addressed using N control lines (72), it is very difficult to decode the exact line being addressed from the select bits. In the case of the binary multiplexer, the binary value of the selected bits specifies which line is being addressed. For example, a set of selection bit valves can be represented in binary as 1110, which corresponds to a decimal value of 14, and line 14 is being selected (Figure 5-1). Conversely, a demultiplexer (demux) takes a single input signal and selects which one of multiple outputs the input is passed to. In microfluidics, the implementation of a demux is exactly the same as a mux but the direction of flow is reversed.

Normally, the use of muxes and demuxes is used primarily in the fluidic layer. However, Todd Thorsen proposed and demonstrated the concept of using a demultiplexer to selectively actuate control lines which in turn actuate valves, termed “control of control”. “Control of control” can more easily be understood if one were to imagine an intermediate component that is a microfluidic analog of an electronic dynamic random access memory (DRAM). An electronic DRAM is an array of memory cells that stores information as voltage potentials, with the defining characteristics of being randomly accessible and dynamic. The random access aspect of a DRAM is expressed as the ability of each cell to be uniquely addressed and written to with the same ease as other cells. And because the stored potentials decay over time, requiring that they be actively refreshed at regular intervals, the memory can be described as dynamic. A microfluidic DRAM has both of these characteristic.

For a microfluidic DRAM, each cell is a control line, and the demux in the base level is used to address specific cells. By connecting a high pressure source to a cell, one sets the state of the cell to be high, and by connecting a low pressure source to a cell one sets the state of the cell to be low. Since each cell inside the DRAM corresponds to a control line on the top level, if the cell is in a high pressure state, then all the valves associated with that control line are closed. If the cell is in a low pressure state, then all the valves associated with that control line remain open. One actuates the valves on the top level by changing the states of the cells inside the DRAM in the intermediate level. Because only one demux output is being controlled at once, the pressure in the cells not currently being

controlled will decay as the control fluid leaks (through opening in valve or evaporation), and so the values of all of the cells must periodically be refreshed.

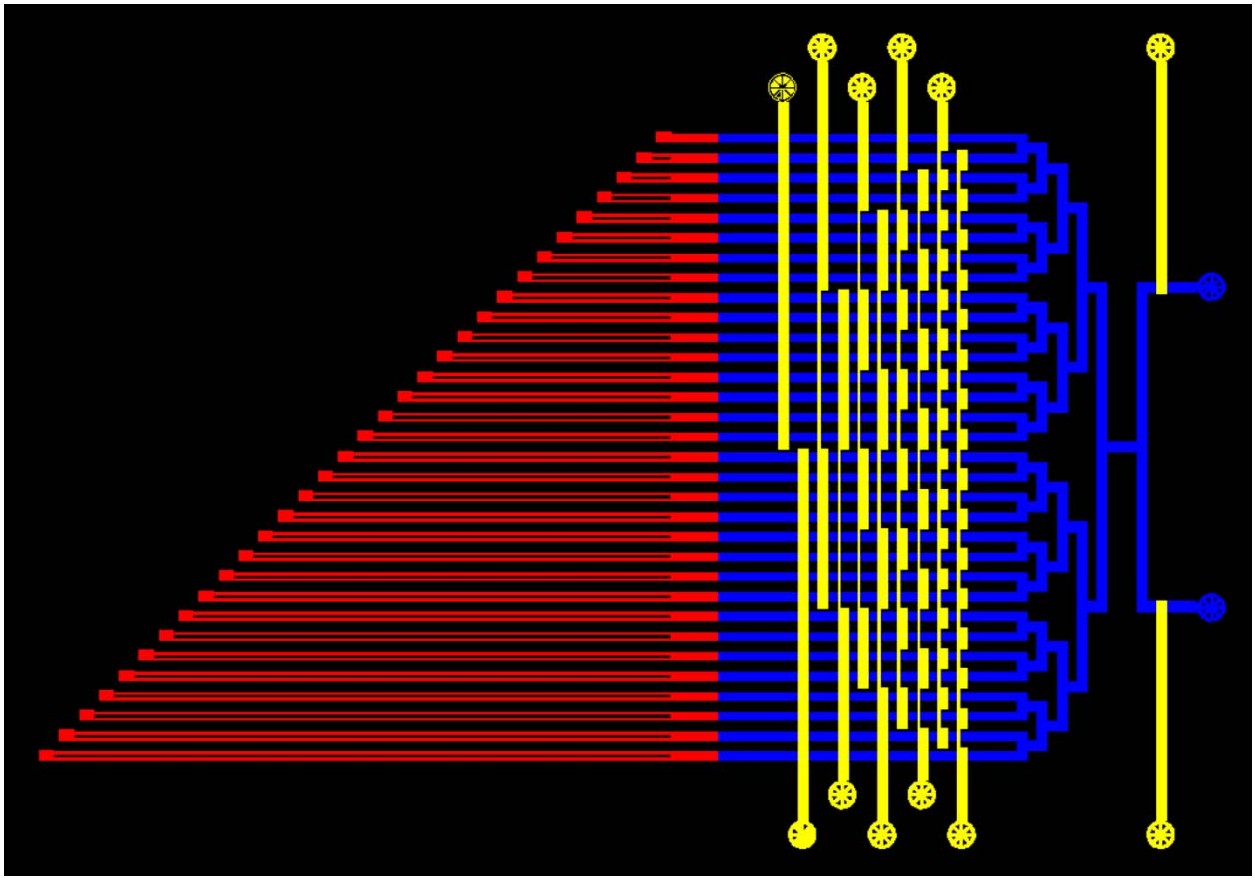

Figure 5-2: A 32 compartment DRAM. The simplest DRAM can be implemented using only a single demux. The two inputs to the right correspond to a high pressure source and a low pressure source. The top five control lines (yellow) correspond to the 5 select bits needed to address the 32 compartment, the bottom five control lines are their complements. The 32 channels (red) in the row array are the compartments and the large pads at the end of each compartment are the valves.

The Use of DRAM for Actuation of Valves

To demonstrate the functionality of the DRAM for actuation of valves, a fluidic layer with 32 channels is added on top of the DRAM to make actual valves. The threshold pressure for the valve is highly dependent on the geometry of the intersection, thus valves are only formed at the end of each row. This array of 32 valves is used to characterize the performance of valves with dimension and operating conditions similar to those found on the microfluidic DNA synthesizer.

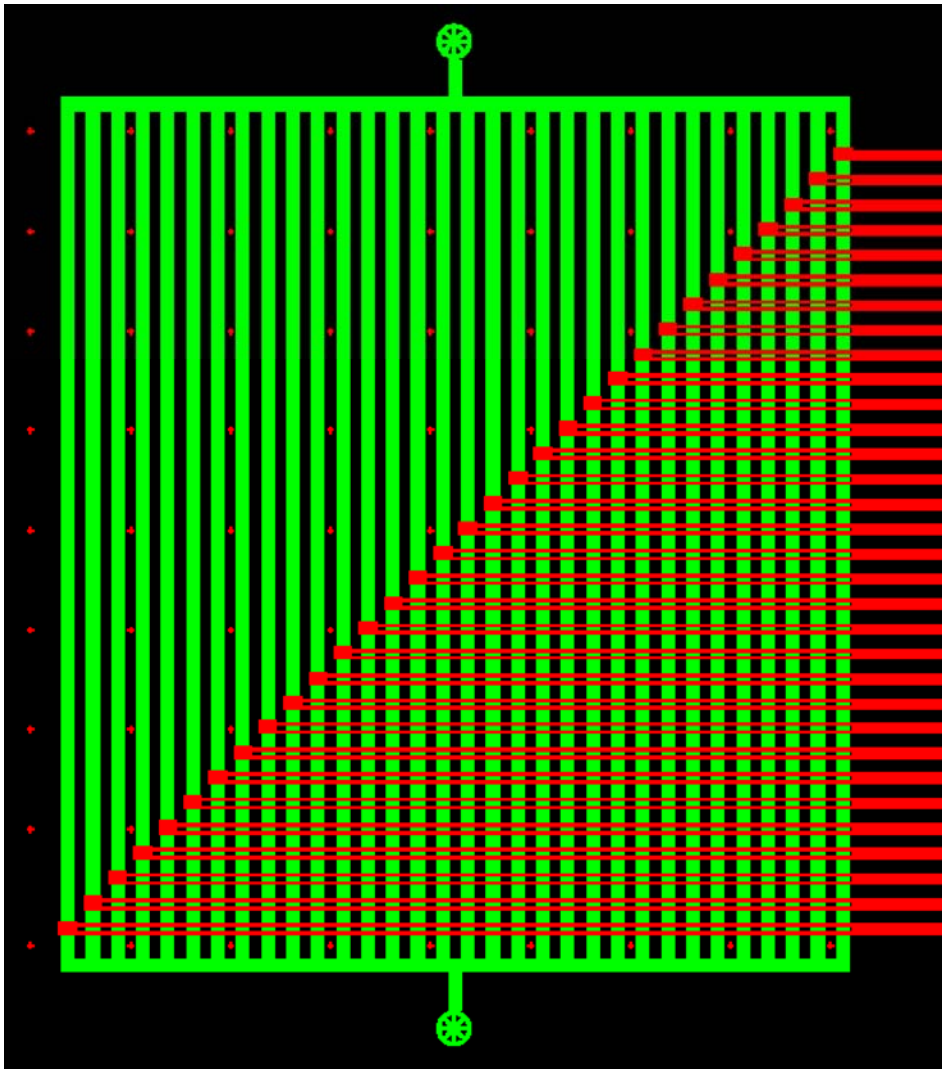

Figure 5-3: A 32 valve array controlled using DRAM

Regarding the dynamic aspect of the DRAM, the two most important attributes are the speed at which cells can be written and the length of time cells can hold their states before they lose their values. The former determines how fast the valves can be actuated, and the latter determines how often the DRAM has to be refreshed. The maximum number of valves that can be independently controlled will be the ratio of these two attributes. The speed at which the state of each chamber can change (write time) is highly dependent on the actuating time of the selection control lines. If a write event occurs before the proper chamber is selected, the wrong chamber might be assigned or

other chambers can be affected through cross talk. Using oil-filled selection lines, a minimum write time of approximately 1 second per chamber is achieved. This translates to about 0.5 min to completely set the state of the entire DRAM. For the specific application of DNA synthesis, each column valve has to actuate twice per four coupling steps. That averages to N/2 seconds of wait time before each coupling step, where N is the number of reactor columns. The wait time can be dramatically reduced by switching to a fluid with a lower viscosity or even an inert gas. While the use of oil is not optimal from the point of speed, the ability of the DRAM to maintain its states using oil is superb, as valves remained closed at the termination of a timing test which lasted over 2 hours. Because of the low vapor pressure of oil, it will not vaporize and escape through the porous PDMS matrix. With either water or inert gases, the loss of the pressure within the compartment would be much quicker. An ideal liquid to be used in the implementation of "control of control" should have low viscosity, low vapor pressure, and be compatible with PDMS.

Design Considerations

"Control of control" can be implemented in either a three-layer device or a two-layer device. Depending on the applications, one option might be more suitable than the other. For "control of control" to be implemented in a two-layer device, the thin layer that is normally used exclusively as the fluidic layer in the push down configuration needs to double as a control layer for the demux as well. Thus, one would use a push up configuration to implement the control of the demux in the thin layer. A hybrid or mold is used in the thick layer to create channels that have both square and round profiles. The round section would be the fluidic lines of the demux; the square section would become

the control channel to the fluidic lines in the thin layer. The different profiles make identification of the role of each channel easier; however, a round mold can be used as well.

While having both the thick and thin layers double as control and fluidic layers allows devices to be made using the normal protocol, routing could be problematic in devices with high valve density. This configuration should only be used if the fluidic channels have to come into direct contact with a modified glass surface, such as in a DNA array. Oxygen plasma bonding to the glass substrate is not an option because it would destroy the modified glass surface. Thus, the select control lines cannot be operated at a pressure greater than 20 psi. Assuming that actuation pressure is 5 psi for a push-up valve and 10 psi for a push-down valve, the highest pressure that can be used in the top level fluidic channel would only be 5 psi.

In a three-layer device, the control channels of the demux would be present in their own layer, simplifying routing. Because a push-up configuration is used for the top level fluidic layer, one is allowed to have greater channel height, which would be advantageous for applications requiring the use of large beads, or the manipulation of eukaryotic cells (13). Because oxygen plasma bonding could be used to bond to the glass substrate, the select control lines could operate at pressures as high as 35--40 psi. Assuming that actuation pressure for push-up valves is 5 psi, reagent pressure as high as 25 psi could be used. This is especially useful in DNA synthesis where 15 psi pressure is used during the washing step for quick removal of residual chemicals.

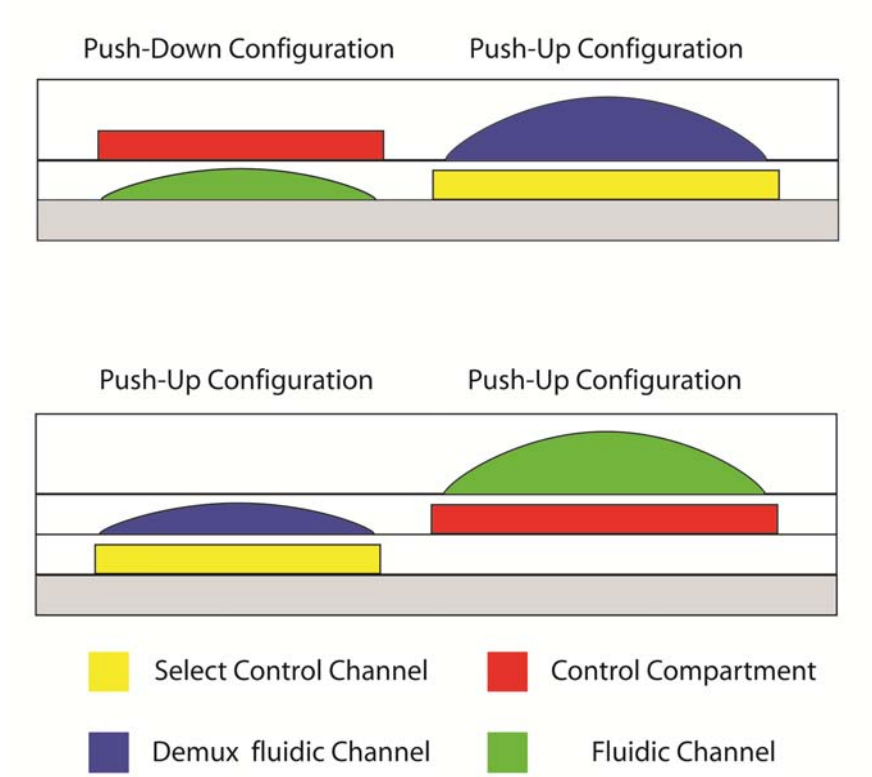

Figure 5-4: Cross-sectional view of two-layered and three-layered implementation of "control of control" device

Another consideration for the design of DRAM is the volume of the cell compartment. The size of the compartment is proportional to the capacitance of the DRAM cell. While smaller cell compartments can lead to a modest reduction in the write time, a critical volume is needed such that the states in each compartment cell can withstand a certain amount of noise and leakage. Using a conservative addressing scheme to cycle through all the cells in DRAM, the amount of oil trapped in a given compartment could increase by N times the valve volume, where N is the number of selection bits. If the compartment of the cell is small, the increase in amount of oil inside the compartment can cause a great enough pressure change so the state goes from low pressure to high pressure.

There are also instances where the number of control lines needed to implement a demux for use in a DRAM can be reduced further. In cases where the state of each cell is not important while it is being written, the number of control lines can be further reduced to N. Instead of having two control lines for each select bit, the complementary control line can be omitted as long as a special addressing scheme to write the cells is followed. For example, in a 3 bit system, one can write the state of line 0 into all lines with all control lines open (binary 000). In select state of (binary 001), and one can write the state of line 1 into lines 1--7. In select state of (binary 010), one can write the state of line 2 into lines 2--7. In select state of (binary 011), one can write the state of line 3 into lines 3--7. In select state of (binary 100), one can write the state of line 4 into lines 4--7. By the time select state of (111) is chosen, one sets the state of line 7 and the entire DRAM is now at the proper state.

Custom Sequence Specific Oligonucleotide Synthesizer

Instead of having a single valve that can be independently actuated to control the flow of reagent into a reaction column, one could have multiple valves that each control the flow of reagent into a reaction column for a particular step.

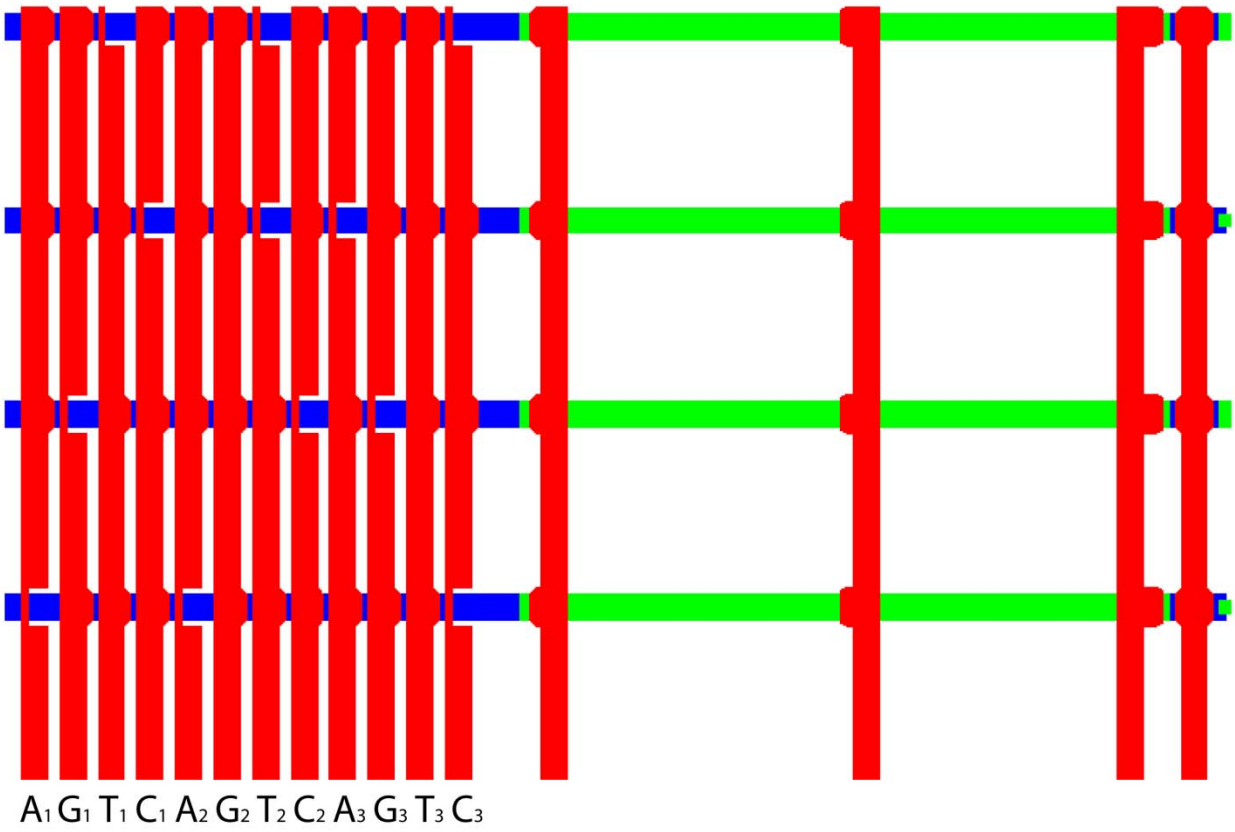

Figure 5-5: Schematic of control lines for sequence specific oligonucleotide synthesizer

The sequence information is directly encoded into the layout of the control lines, so there is no need for a complex program that changes depending on the oligonucleotides to be synthesized. The complex operation of determining which valves to actuate would be replaced by a straightforward sequential actuation of control lines.

Each control line controls fluid flows into all reactor columns for a single coupling step. For example, in Figure 5-5, the control line A_1 controls the coupling of the adenosine at the first position of oligonucleotide to be synthesized. Similarly, C_3 controls the coupling

of cytosine at the third synthesis position. Using the above control lines, the 4 sequences that will be synthesized from top to bottom are TTC, CTA, GCG, and AAC.

An advantage of using this control scheme is that the control lines can be extended to manage hundreds or even thousands of columns in parallel. The number of control lines needed is determined solely by the length of the desired sequence and not by the number of columns. Because each control line only controls a single coupling step, four lines are needed for each synthesis cycle. For 32 base oligonucleotides, 128 control lines would be needed. If one were to combine a demux with this control scheme, the total number of outside control valve for addressing the reactor columns be would reduced to 14.

Column Array Construction

The construction of a reactor arrays with uniform flow rate and capacity becomes increasingly challenging as the number of reactors increases. While serial packing of reactors can often ensure the quality of the bead column being formed, it leads to an increase in preparation time as well as the need for additional outside controls that are already scarce, especially when large numbers of columns are needed.

In order to save time and reduce the number of preparation procedures, a design that accommodates parallel loading is preferred. In an initial design beads fill a channel that has a large compartment (shown in red in Figure 5-6) dedicated to each column. Once all the compartments are filled, valves portion off each reactor, and the beads are flushed against the sieve valve by a binary tree to the left. The number of beads flushed into the column valve depends on the size of the compartments in the bead loading channel.

Multiple iterations of filling the compartments with beads and flushing the beads into the column will eventually fill the reactor columns with beads.

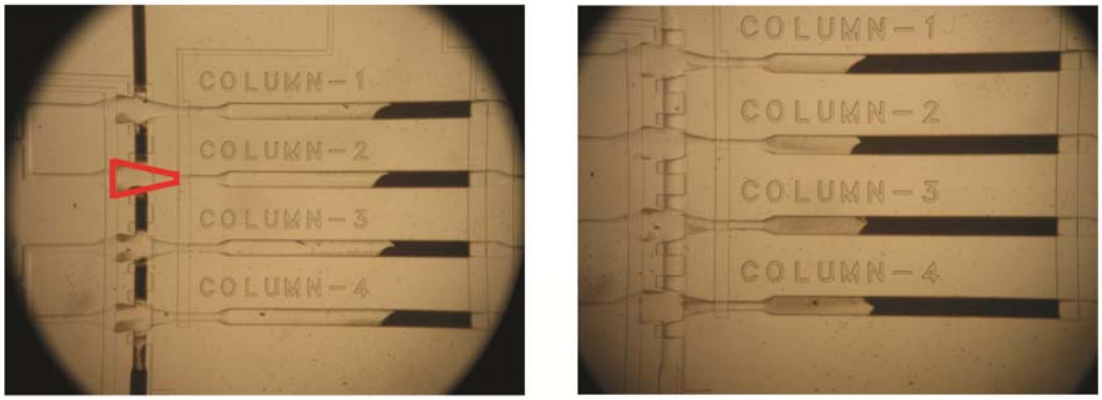

Figure 5-6: The red line marks the bead compartment within the vertical bead loading channel. (A) Valves are portioned of the compartment and the beads are pushed against the column valve to the right. (B) Two iterations of bead filling and flushing are completed. The leftover beads within the vertical bead loading channel run are flushed out.

In a later design, the compartments within the bead loading channel are removed to further streamline the process. Instead, the beads directly fill the reactor columns during the bead loading process. The size of the column reactor now controls the number of beads being loaded, not the size of the compartment in the previous design. The detailed process is shown in Figure 5-7.

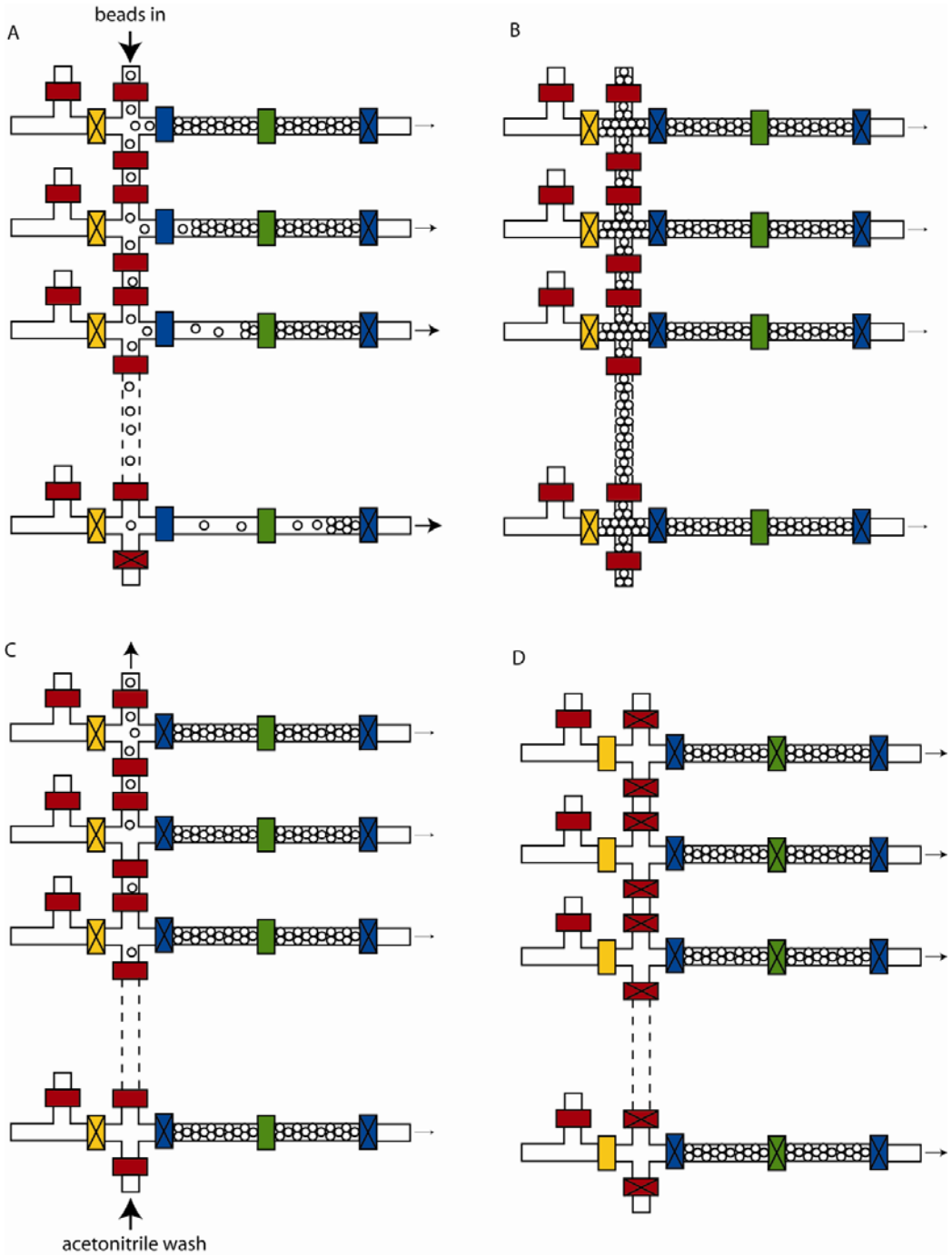

Figure 5-7: Schematic illustration for construction of the bead column in the microfluidic oligonucleotide synthesizer. Valves with cross bar indicate they are closed during that operation. Otherwise they remain open. (A) The addressable inlet valves are all closed and the bead suspension is loaded from the top. The top column fills first because it is closest to the bead inlet. However, as the beads pack, the resistance to the column increases and more beads are carried into the later columns. (B) Once all the columns are fully packed, the set of sieve valves closest to the inlet is closed to prevent beads from escaping. (C) Acentonitrile is flushed from the bottom to remove any excess beads that are not inside the column. (D) After the excess beads are removed, the valves between columns are closed to separate the columns from each other. The compression valves are also actuated to prevent rearrangement of beads when pressure drops occur between synthesis steps, thus minimizing bead loss.

During bead loading, it is important that the pressure within the column array is maintained or increased with each successive step until the columns have been packed. Otherwise, there is an increased probability of beads becoming trapped within the vertical channel, which may prevent the valves from fully closing and could lead to crosstalk between adjacent reactor columns. At higher pressures, the cross-sectional areas of the channels are larger due to the elastic nature of PDMS. If the pressure were to suddenly drop, the channel height would decrease and beads that could previously just barely pass through the section will now become clamped down and unable to move.

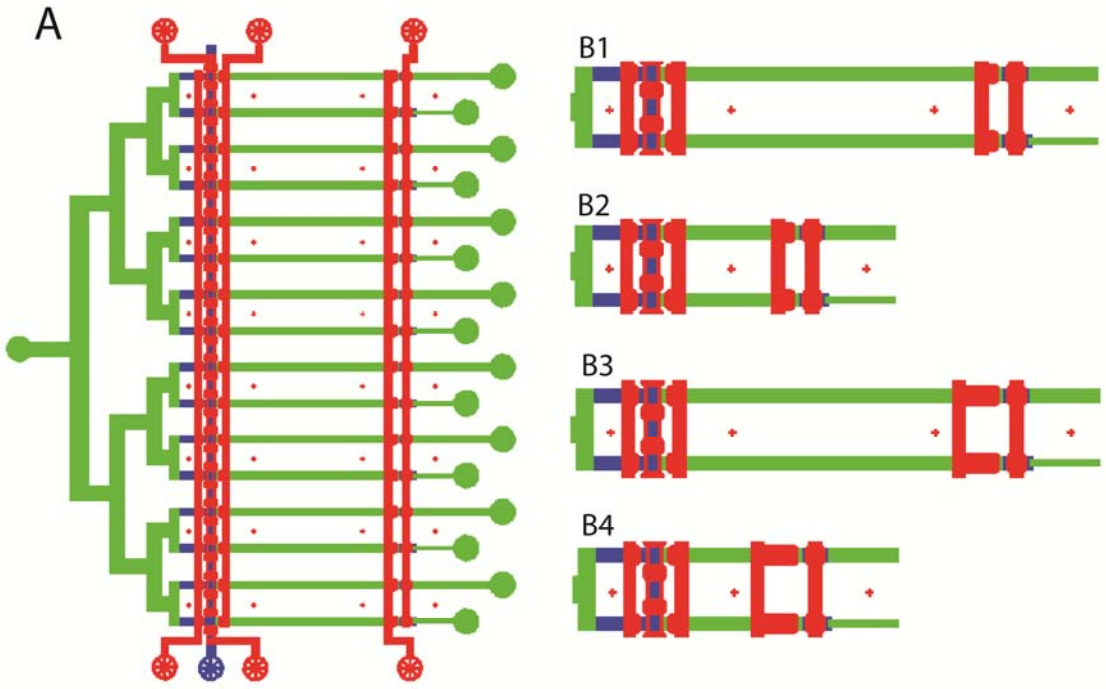

Figure 5-8: Schematics for the various column arrays tested. (A) Overview of the column array. (B) Close-up of various configurations tested. (B1) Long column length with small column valve. (B2) Short column length with small column valve. (B3) Long column length with big column valve. (B4) Short column length with big column valve

To optimize the performance of the column array, several parameters were tested, including the column valve sizes, the length of the reactor columns, and the profile of the

binary tree. The different configurations tested are shown in Figure 5-8. Actual flow rates of each column in each of the configurations were measured and normalized. Standard deviation is then computed to reflect the uniformity of the flow rate between columns. The values for the standard deviation are summarized in Table 0-1

Table 0-1: Measurement of flow rate uniformity between columns under various configurations

	Column Array Configuration			
	long column small valve	long column large valve	short column small valve	short column large valve
run 1	0.097	0.122	0.129	0.305
run 2	0.093	0.126	0.154	0.247
run 3	0.070	0.121	0.111	0.233

The results suggest that the uniformity increases with increasing column length. This finding is not surprising, as deviations due to irregular bead packing are more likely to be averaged out in longer columns. What is surprising is that the size of the column valve has a large impact as well. In designing the column valves, it is desirable that they be just large enough to trap the beads. While, having larger column valves can ameliorate the escape of beads between synthesis steps, it has an adverse affect on the uniformity of flow rate. This has to do with the size of the beads compared to the size of the opening at the edge of the columns when the column valve is deflected. Under the current valve geometry, the openings at the edges of the channel are larger than the beads. For the column to be packed, the opening is clogged by a stochastic staggering of beads that prevents them from passing through the opening one by one. Having a larger column valve can lead to more variability as seen in Figure 5-9.

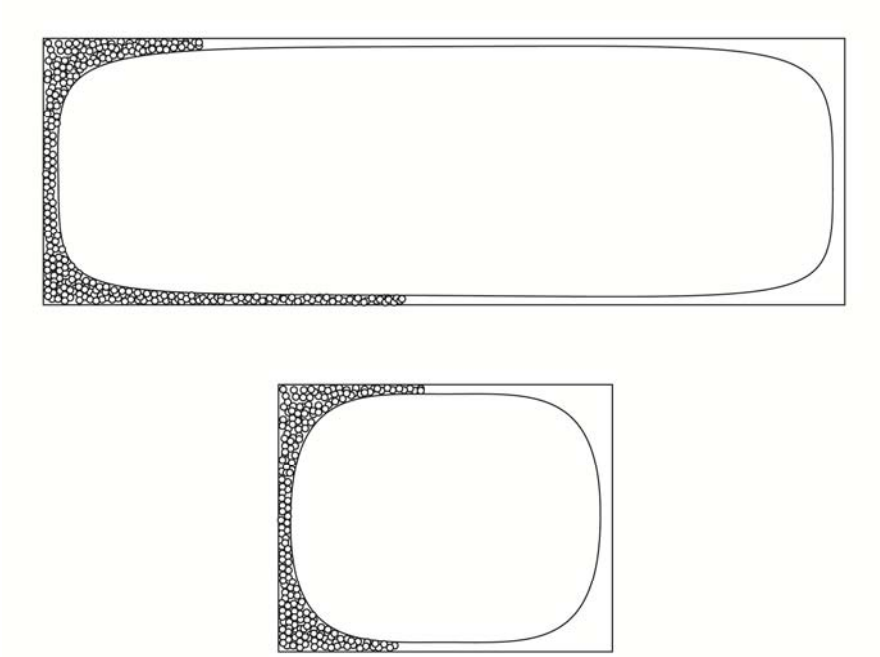

Figure 5-9: Illustration of how beads are packed against column valves with different valve size. As this figure shows, having a larger column valve permits more variability in the staggering arrangement of beads at the edges of the channel.

A problem that surfaces after many cycles of synthesis is the gradual loss of beads between steps. In between synthesis steps, pressure changes in the reactor column cause rearrangement of the packed spherical beads, and those at the edges of the column valve have a chance to escape through the opening. As discussed, a larger column valve cannot be used because it could contribute to uneven flow between the columns. Additional sieve valves, denoted as compression valves, were added to the middle of the columns to press down against the beads to prevent rearrangement of closely packed spherical beads. Using this design over 95% of resin was retained after 40 cycles (20 hr) of synthesis.

Squared profile channels are used in the construction of binary tree because flow velocity is much more constant across the width of a square channel compared to the parabolic

velocity profile associated with rounded channel. The final design is then implemented into the parallel microfluidic DNA synthesizer described in Chapter 4.

In Situ Construction of Reactive Sites

While a successful column array was designed and fabricated for 16 columns, it is difficult to envision parallel loading of similar column array scaling up to over 100 columns. The time needed to construct columns prior to use for thousands or hundreds of thousands of distinct oligonucleotides may be significant. Also if the columns were to continue to shrink in size so more could fit on a chip of a similar size, the flow rates in each column may become more uneven. One solution to these problems is to modify the PDMS surface so that it is much more glass-like, thus allowing further coupling of linker directly onto the column surfaces. The synthesis sites will now be directly on the device, and there is no longer any need to pack columns of solid phase support.

Oxidation of the PDMS channel walls is one of the most popular routes for covalently modifying the surface (73,74). Surface oxidation using an oxygen plasma is followed by simple silanol condensation chemistry for the attachment of 3-aminopropyl on the channel surface (75). However, the free silanol groups on the surfaces of PDMS are transient, and a progressive restoration of hydrophobicity occurs as free PDMS chains move to the surface and the silanol groups become buried (76). Thus any modification to the surface must be performed quickly and would face issues with longer term stability. From the standpoint of device fabrication, surface-modified PDMS poses additional challenges with device assembly and channel sealing because bonding can only occur after the appropriate chemistry has taken place. As a result, the current method of

bonding between partially cured layers is no longer applicable because it has to be done within 2 hr of curing.

Sol-Gel Modified Poly(dimethylsiloxane)

A potential alternative method for modifying the surface (and bulk) properties of PDMS is to use sol-gel process to form nanometer-sized particles throughout a polymerized PDMS matrix (77--79). To form the particles, an alkoxysilane precursor such as tetraethyl orthosilicate (TEOS), which is soluble in the polymerized PDMS, is first hydrolyzed. Particles are then formed through the condensation of the hydrolyzed silanes. The condensation is generally catalyzed using either an acid or base. Spherical particles are expected in the case of base-catalyzed reaction while linear chain growth is anticipated via acid catalysis. This process results in the generation of permanent free silanol groups at the surface as well as within the matrix of the PDMS, thereby allowing the wide range of surface modifications developed for glass to be used on these modified PDMS devices.

$$Si(OC_2H_5)_4 + 4\ H_2O \rightarrow Si(OH)_4 + 4\ C_2H_5OH \qquad \text{(hydrolysis)}$$
$$Si(OH)_4 + Si(OH)_4 \rightarrow (HO)_3Si\text{-}O\text{-}Si(OH)_3 + H_2O \qquad \text{(condensation)}$$

The diameter of the silica particles generally increases with increasing concentration of base (80). While the modified bulk PDMS displays a higher Young's modulus, the increase is not high enough to affect the closing of valves in push-up configuration. However, it could become a problem for push-down valves.

Evaluation of Amino-Grafted Reactor Chamber

The silanol-covered PDMS surfaces were treated with 3-Aminopropyltriethoxysilane (*APTES*). A constant flow of neat APTES was maintained for 1 hr at room temperature to complete the silanization reaction. Dry acetonitrile was used to remove unreacted silane. To quantify the amount of NH_2 on the surface of reactor, FAM fluorescein was coupled onto the surface though a peptide bond. For comparison, amine slides were purchased from ArrayIT® and coupled with FAM under the same conditions.

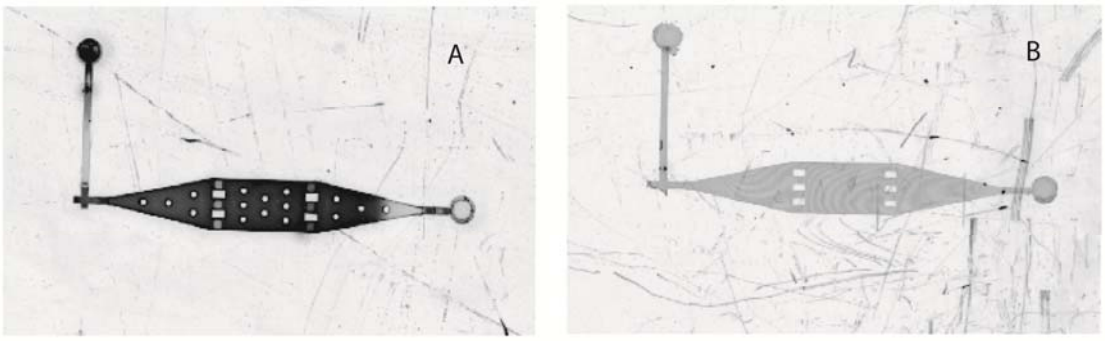

Figure 5-10: Quantification of Amino group present in sol-gel modified device compared to amine slide purchased from ArrayIt. (A) Sol-gel modified device coupled with FAM fluorescein. (B) Amine slide coupled with FAm fluorescein

The images were analyzed using ImageQuant (Amersham Biosciences). An amino group density of approximately 3.3 pmol/cm^2 was assigned to the signal strength obtained from the amine slides, based on their specifications. The density of amino group on the sol-gel device is calculated to be approximately 3.8 pmol/cm^2 by comparing the average signal intensity inside the reactors of the two images. The image appears much darker for the sol-gel device because amino groups are present on the floor and the ceiling of the reactor, compared to the amine glass slide, which only has amino groups on the floor.

While the density of the amino group in the sol-gel device compares favorably with that of commercialized amine slides, using this setup, one can only hope to double the amount of oligonucleotide synthesized using equivalent microarray technology. Yield can be further improved by increasing the surface area inside the reactor columns. One strategy is to construct an array of cylindrical posts to increase the total surface area inside the reactor. However, for each post the area of the wall created is $2\pi rh$ and the area lost from floor and ceiling is $4\pi r^2$. Thus the aspect ratio (height-to-width ratio) of the post must be greater than 1 for the total area to increase. In the various attempts to make such structures, the PDMS posts very often got stuck in the mold and would be torn off in the process of device fabrication. To address this problem, pyramids or cones could be used instead of posts, as their sloped surfaces are easier to peel off.

Materials and Methods

Device Preparation and Operation for "Control of Control"

The demux control lines were interfaced with computer-controlled solenoid valves (Pneumadyne, Plymouth, MN) through steel tubes connected to Tygon tubing, and were primed with Krytox oil through dead-end filling. The high pressure source for the DRAM was connected to the microfluidic device through Tygon tubing. The low pressure inlet of device was left open to the atmosphere. Before use the DRAM was also primed with Krytox oil through dead-end filling. The demux control lines actuation (35 psi) and the high pressure source for DRAM (20 psi) were controlled using nitrogen gas.

Sol-Gel Modification

A three-layer device is initially made without holes punched, and cured for 24 hours instead of the normal 8 hours before use. Next, it is immersed into pure TEOS for 2.5 min, allowing it to penetrate and swell the PDMS matrix. The device is taken out and dried completely. Then the device is immersed in a 4% methylamine solution in water for 5 hours and subsequently baked at 95 ºC for 1 hour. Finally, the inlet, outlet, and control holes are punched and the finished device plasma bonded to a glass slide (70 W, 300 mTorr, 15 sec).

Conclusion

We have discussed some issues with massive parallelization of DNA synthesis using our current microfluidics platform. The two most pressing problems are the need for additional control circuitry within the microfluidic device to eliminate the need for off-chip controllers that could be costly and difficult to interface, and the ability to construct thousands of reaction chambers with high uniformity to carry out the synthesis of a massive number of oligonucleotides. Possible solutions are proposed and tested. Using a custom synthesis device in conjunction with "control of control" the number of control lines needed to control an arbitrary number of reactors for synthesis of oligonucleotides 40 bases in length can be reduced to 14, which is two less than the number currently being used to control the 16 column device.

The issues associated with the construction of the bead columns are more complex. One can choose to deravitize the surface of PDMS with amino groups so that universal linkers

used in CPG can be directly coupled to the column surfaces. However, the scale at which the oligonucleotide can be synthesized is now similar to other microarray technology. The yield can be improved by making rough features that increase the overall surface area, however, it will be difficult to approach the scale of CPG.

Appendix A

Solution-Phase Surface Modification of Poly(Dimethylsiloxane) Microfluidic Devices

Introduction

In the last decade, there has been a shift away from glass and silicon microfluidic devices to those made of polymer substrate because of the time-consuming and expensive fabrication process associated with the former two (74). Some of the polymer materials that have been used for device fabrication are poly(methylmethacrylate) (PMMA), polyvinylchloride (PVC), polycarbonate (PC), polystyrene (PS), polyurethane and poly(dimethylsiloxane) (PDMS) (81--83). Of all the polymers used, PDMS has been the most popular for a number of reasons. By using soft lithography, a technique introduced by Whitesides' group, multiple PDMS devices can be made from a single master by replica molding (84). The elasticity of PDMS also allows active valves to be made in situ for further manipulation of fluids. PDMS is biologically inert and non-toxic, making it suitable for various biological applications. The porous matrix is permeable to gases, allowing various gases to be supplied into closed cell culture systems (85). Lastly, it has excellent optical properties, allowing transmission of light down to wavelengths of 280 nm.

In spite of the many advantages of PDMS, its application in microfluidics has not been without problems. The surface modification of PDMS is difficult because the material is inert. Furthermore, PDMS is extremely hydrophobic. As a result, PDMS readily absorbs nonpolar organic solvents and small hydrophobic analytes, causing fouling of the material (86). Several approaches have been developed to confer certain surface

properties such as hydrophilicity to PDMS to make it more attractive in certain applications. Grafting of common tethering groups such as amine and thiol (75,87) to the PDMS surface also allows subsequent attachments of molecules further altering its properties. The most common approach is to expose the PDMS to an energy source such as oxygen plasma, ultra-violet light, or corona discharges (76,88,89). While the exact mechanism is not clearly understood, exposure to corona or oxygen plasma causes formation of a SiO_xsilica-like layer with higher oxygen content than bulk PDMS through oxidation. At the end of this process, the silane groups on the PDMS are replaced by silanol groups. The effect is, however, transient, as progressive restoration of hydrophobicity is often observed minutes after the oxidative treatment. Further silanization of the freshly created silanol-covered surfaces introduces functional groups that enable desired surface properties and slow hydrophobicity recovery to weeks. From the standpoint of device fabrication, surface-modified PDMS poses additional challenges for device assembly and channel sealing because bonding can only occur after the appropriate chemistry has taken place. As a result, the current method of bonding between partially cured layers can no longer be used because it must be done within 2 hr of curing.

We propose an improved approach that consists of a solution-phase oxidation reaction in acidic H_2O_2 solution and a sequential silanization reaction using neat silane reagents for surface modification of intact microfluidic channels that are embedded in multilayered PDMS devices. In contrast to the conventional approaches, this method has the advantage of simple and convenient handling suitable for routine practices in both

chemistry and biology laboratories, with no need for specialized instruments such as oxygen plasma or UV light sources. Because the reaction takes place after the device has already been assembled, there are no issues with bonding between layers during device fabrication. And by switching to neat silane instead of diluted silane or vapor deposition, we also found that the resulting surface modification is more stable and remains intact for months after the derivatization.

Using this method, different functional groups were introduced onto PDMS surfaces for different purposes. PEG was used to limit nonspecific protein absorption onto the PDMS surface while amine groups were grafted for further attachment of bio-molecules and other chemical groups. X-ray electron spectroscopy (XPS) and contact angle measurements were used to characterize the surface of the PEG-grafted PDMS substrate and to track temporal changes. A variety of fluorescent protein solutions were flowed through the PEG-grafted PDMS channels to test whether the PEG group reduces nonspecific binding. Time-lapse images were taken showing that the protein repelling characteristic enhanced progressively over the initial 24 hour period and persisted for over two months.

Amino-grafted PDMS channels were created using similar protocols and further modified with tripeptide (RGD), and a soluble, recombinant form of prostate stem cell antigen, PSCA (90). Using these biomolecule-covered PDMS channels, cell immobilization and incubation and immunoassay were demonstrated on a miniature scale, with the additional benefits of chemical/sample economy and operational efficiency.

Solution-Phase Surface Modification

Modification of microfluidic channels starts from the solution-phase oxidation reaction of PDMS surface, which was carried out by continuously passing a mixture of H2O/H2O2/HCl (5:1:1) through the channel for 5 min. The channels were then purged with DI water and dried with argon, leaving the hydrophilic silanol-covered PDMS surfaces. After that 2 methoxy(polyethylenxy)propyl)trimethoxy-silane was injected into the silanol-covered channel to perform the silanization reaction at room temperature for 30 min. The unreacted silane was flushed from the channels by water to give the PEG-grafted channel surfaces, which were dried by argon flow and preserved in a ambient condition for various periods of time prior to the protein repelling studies.

Similar to the preparation of the PEG-grafted microfluidic channels, the silanol-covered channels were reacted with (3-aminopropyl)trimethoxy silane to generate the amino-grafted PDMS surface. The surface-grafted amino groups were converted to isothiocyanate groups by introducing a 0.5% thiophsgen solution in acetonitrile into the amino-grafted channels. Again, after purging with DI water and dry Argon, the isothiocyanate-grafted PDMS channels were subjected to attachment reactions with amino-terminated tripeptides or prostate stem cell antigens. These biomolecule-grafted channels were subsequently washed with phosphate-buffered saline (PBS, pH 7.4) or Tris-buffer solutions (pH 7.4) and preserved at 4 C for at least 24 hr prior to their respective studies.

Surface Characterization using XPS and Contact Angle Measurements

Bulk PDMS substrates were treated using the same surface modification protocol to give silanol-covered substrate and PEG-grafted substrate for subsequent surface characterizations. XPS was utilized to validate the functional group transformation on the PDMS substrates. The XPS spectra of the untreated PDMS substrate exhibits a ratio of 1.3:1 between O 1s and C 1s photoemissions, while the spectra of the PEG-grafted substrate exhibits a ratio of 1.6:1. In the high-resolution XPS spectra (shown in inset of Figure A-1), an O-linked C 1s peak centered at 281.3 eV, characteristic of PEG chains, emerges for the PEG-grafted PDMS but not for the unmodified PDMS.

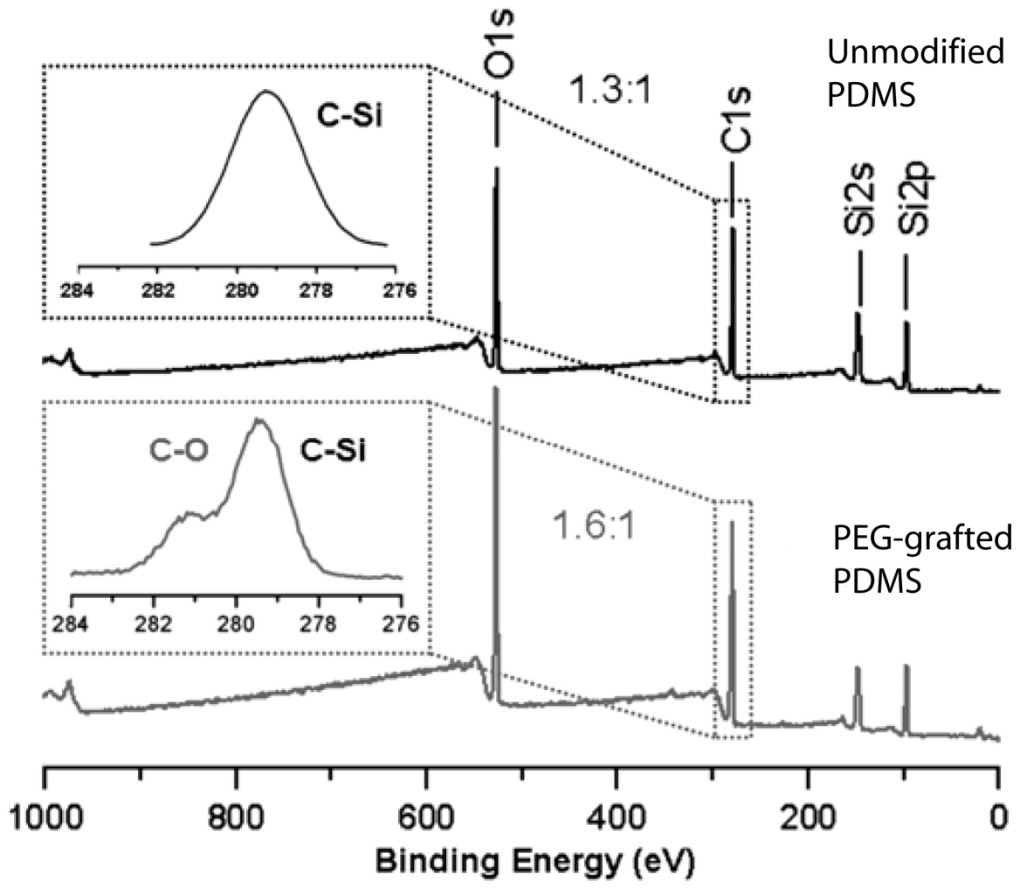

Figure A-1: XPS spectra of unmodified PDMS substrate and PEG-grafted substrate

Temporal contact angle measurements were used to monitor the dynamic surface characteristics of the silanol-covered substrates as well as of the PEG-grafted substrates. For comparison, the untreated PDMS substrate served as a control. Similar to the oxygen-plasma-treated PDMS surfaces, the silanol-covered substrates obtained by the H_2O_2/HCl treatment shows gradual recovery of their hydrophobicity characteristics within 24 hours when the substrates were stored in an ambient environment.

The PEG-grafted substrates exhibited a relative lower hydrophilicity after initial surface modification. However, the recovery of hydrophobicity in the PEG-grafted substrates was slower. At their steady states, the PEG-grafted substrates have lower contact angles than substrates that only underwent oxidative treatment. These results suggest that a robust cross-linked PEG silane layer using neat silane reagent exhibits long-lasting hydrophilicity. Control experiments in which diluted silane solution were employed for the PEG modification showed poor fidelity in surface stability.

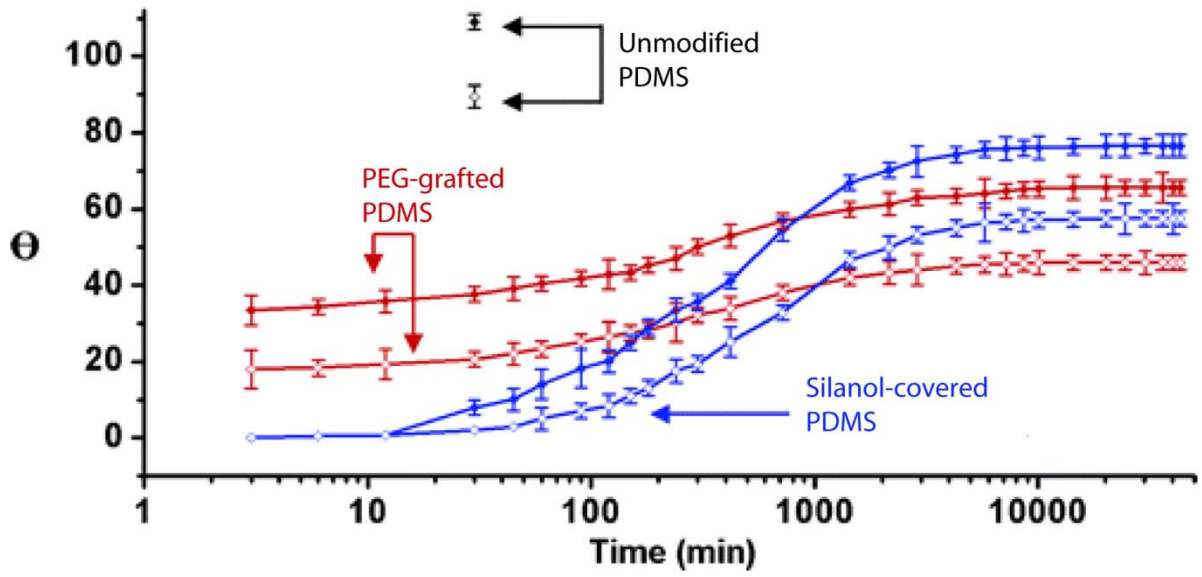

Figure A-2: Measurement of advancing (blank square) and receding (solid square) contact angles of water on PEG-grafted substrates and silanol-covered substrate compared to unmodified PDMS.

Protein Repelling Characteristics of PEG-Grafted Substrate

To further investigate the surface properties of these PEG-grafted PDMS surfaces, time-dependent measurements on the protein repelling characteristics of the PEG-grafted channels were performed. The study was carried out by first filling the channels with a concentrated solution of fluorophore-labeled proteins and incubating the microfluidic device at 37 ˚C for 1 hour. In our studies, two fluorophore-labeled proteins, avidin and fibronectin, were utilized. The resulting protein-contaminated device was then cleaned by flushing a PBS solution through the channels. Finally, the nonspecific absorption of the fluorophore-labeled proteins was quantified using fluorescent microscopy. For each channel, more than 30 fluorescent measurements were carried out at different locations and averaged.

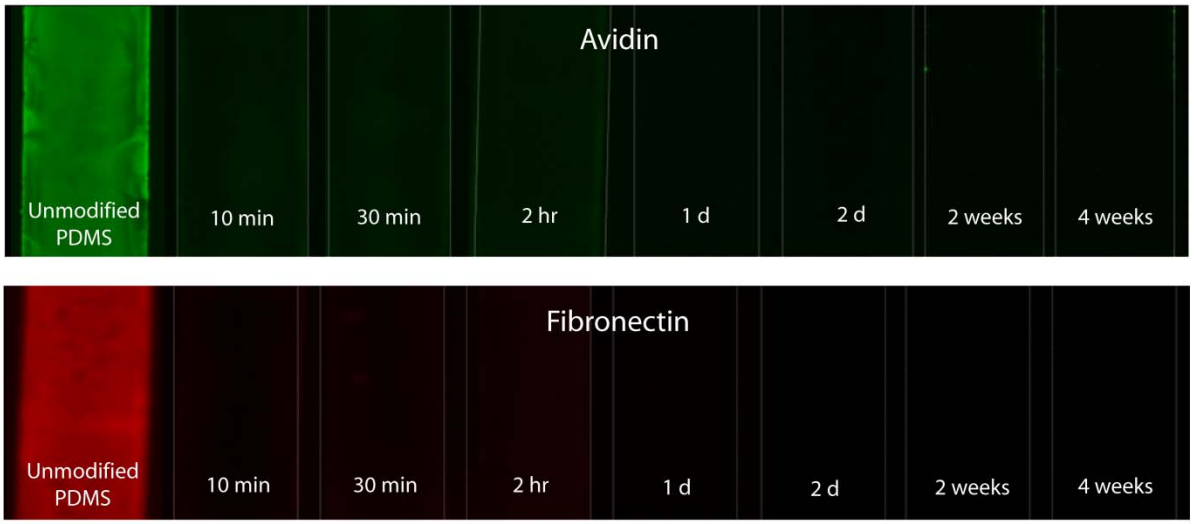

Figure A-3: Fluorescent micrographs of PEG-grafted PDMS channels preserved at different time after treating the channels with concentrated fluorophore-labeled protein solutions followed by PBS washing

The time-dependent profiles for the protein-repelling characteristics of the channels are similar for both avidin and fibronectin solutions. During the initial 24 hrs the protein-repelling property of the channels improved progressively; thereafter, the protein-repelling property reached steady state and lasted for more than two months. This suggests the robust cross-linked silane layers bear well-oriented PEG chains exhibiting excellent protein-repelling properties. The change in protein repellency over time occurred on a time scale similar to that observed for the temporal contact angle measurements.

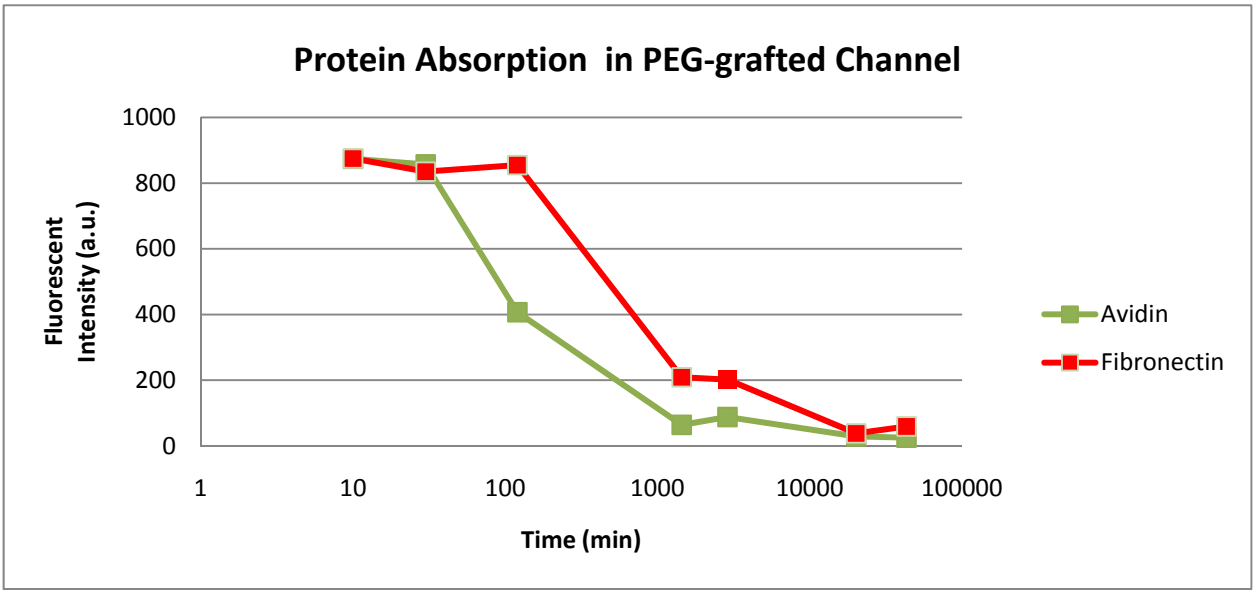

Figure A-4: Fluorescent intensity of PEG-grafted channels after exposure to florescein-labeled avidin and Alexa 5940labeled fibronectin

Cell Adhesion

Being able to specifically control cell immobilization and passivation would be beneficial to many types of cell cultures, cellular assays, and tissue engineering studies in microfluidic systems. Tripeptide RGD is the smallest active fragment found in the extracellular matrix and is known to be an important ligand for cell immobilization through the RGD-integrin interaction (91). The RDG-grafted channels were produced to test the feasibility of immobilizing cells in PDMS-based microfluidic channels. A427 cells (colon cancer cell line, ATCC) suspended in Dulbecco's modified Eagle medium (DMEM) cell culture media (Invitrogen) were introduced into the RGD-grafted channels, and allowed to incubate at 37 °C for 4 h. Culture medium was then used to slowly flush out unattached A427 cells. As shown in Figure A-5 a large number of A427 cells were immobilized on the RGD-grafted microchannels. Similar tests are also performed in amine-grafted, PEG-grafted, and unmodified PDMS channels for comparison. While some cells are attached to the channel walls in the amine-grafted channels, no cells were

immobilized in the PEG-grafted channel s. The unmodified PDMS channel retained very few cells,

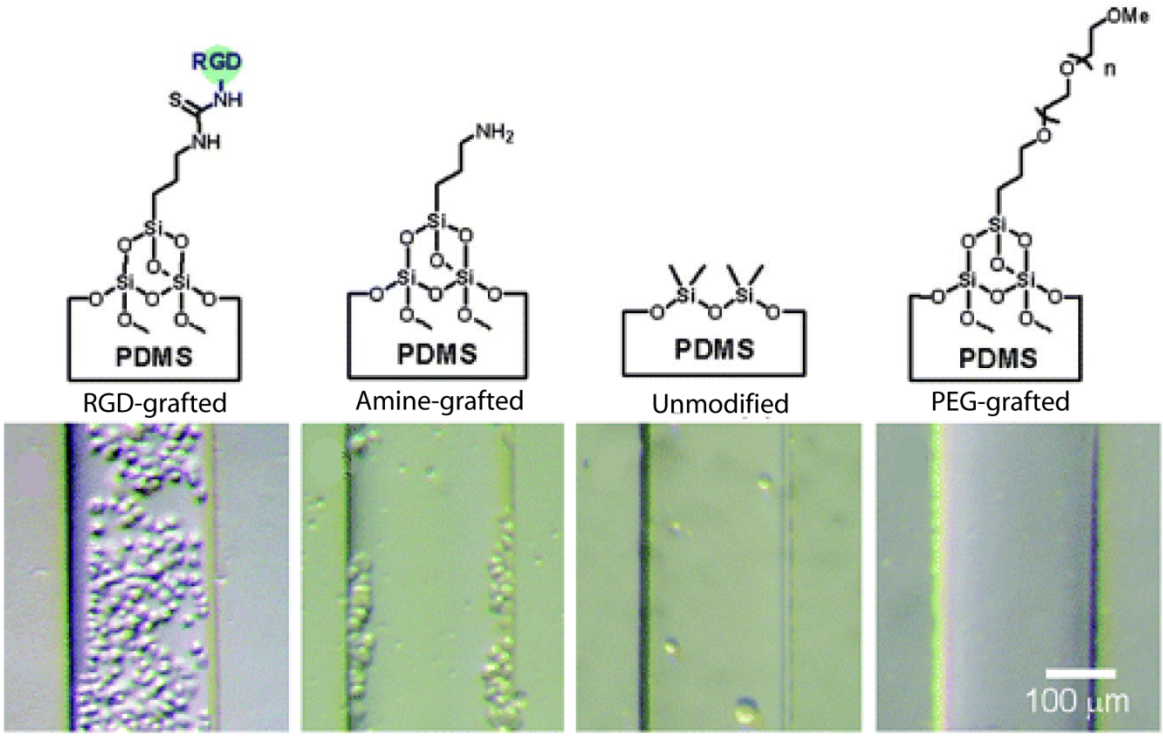

Figure A-5: Optical micrographs showing enhanced cell adhesion in the RGD-grafted channel and cell passivation in the PEG-grafted channels. Unmodified PDMS channel serves as control.

Immunoassay

Immunoassays are used to detect protein molecules with high selectivity and specificity. A conventional immunoassay is generally carried out in a 96-well plate, using microliter-level samples. Performing a miniaturized immunoassay on a microfluidic device offers the advantages of lower sample and reagent consumption, enhanced reaction efficiency, reduced operation time, and a portable point of care platform. The PSCA-grafted channels were utilized to demonstrate an immunoassay for detection and quantification of a prostate cancer biomarker, anti-PSCA. The PSCA-grafted channels trapped the anti-PSCA molecules from anti-PSCA solutions (PBS, pH 7.4) of three different

concentrations (1.6, 3.2, and 12.5 nM). Fluorophore-labeled secondary anti-PSCA (fluorescent Ab goat anti-human IgG (H+L), Molecular Probes, 6.7 nM) was then applied to the channel and allowed to incubate at room temperature for 1 hour. The fluorescent intensity measured using fluorescent microscopy increased with higher anti-PSCA concentration, as shown in Figure A-6.

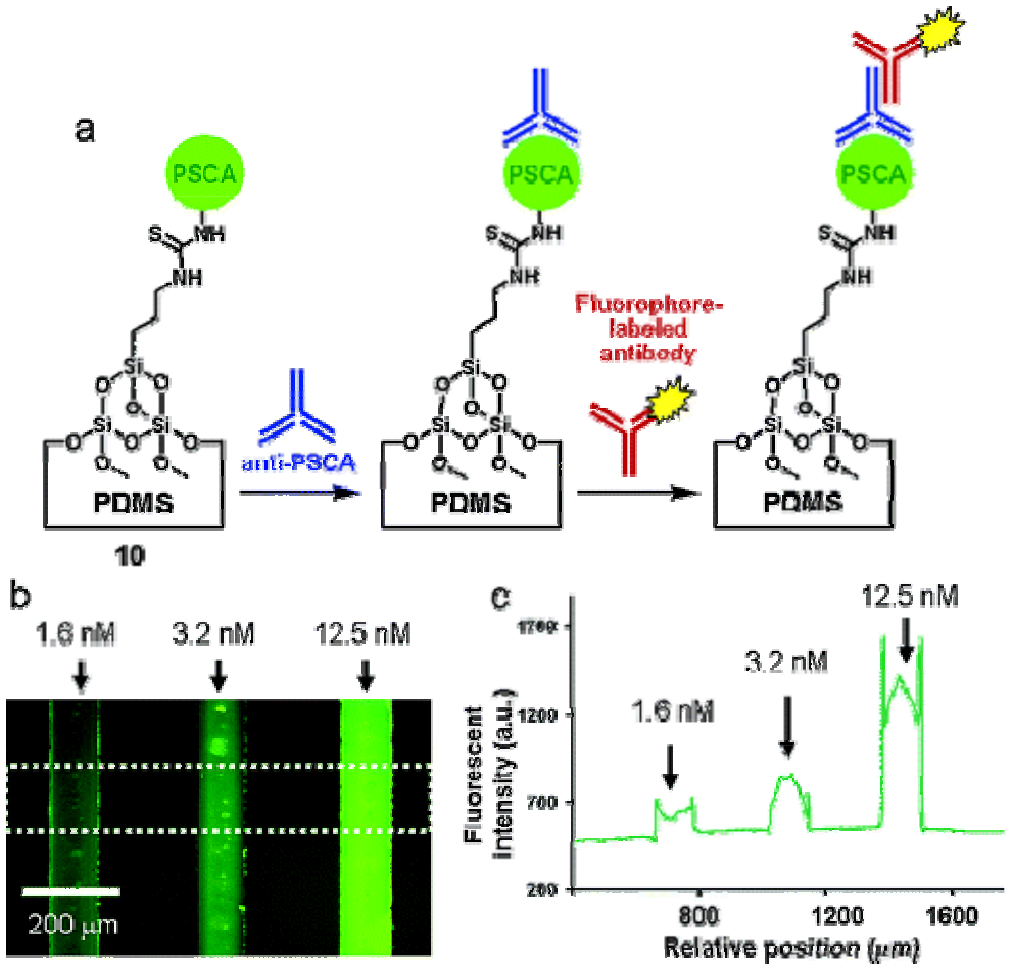

Figure A-6: Demonstration of immunoassay in PDMS channels. (a) Schematic representation of immunoassay for detection and quantification of anti-PSCA using PSCA-grafted channel surfaces. (b) Fluorescent micrograph of channels after performing immunoassays using target anti-PSCA solutions of different concentrations. (c) Plot of fluorescent intensity across channel integrated for the area of the dotted box

Conclusion

We have successfully demonstrated an improved approach for surface modification of microfluidic channels embedded in assembled multilayer devices. This solution-phase

approach is simple and convenient for routine analytical applications in chemistry and biology laboratories without additional equipment. In addition, the resulting surface modifications exhibit great stability. We have also successfully introduced functional groups, including PEG, amino group, isothiocyanate, peptide, and proteins onto the surfaces of microfluidic channels. The PEG-grafted channels are well suited for cell passivation, while the RDG-grafted channels showed improved cell adhesion. Introduction of amino and subsequent isothiocynate groups is especially useful for attachment of other molecules.

Materials and Methods

DI water (Milli-Q, Millipore, Bedford, MA) was used in all aqueous solutions, as well as for cleaning. PDMS prepolymer RTV615 (AB kit) was purchased from General Electric Co. (Waterford, NY). Hydrogen peroxide (Sigma-Aldrich, St, Louis, MO), 2-[methoxy(polyethylenxy)propyl]-trimethoxysilane (90% Gelest, Morrisville, PA), (3-aminopropyl)trimethoxysilane (97%, Sigma-Aldrich), thiophosgen (Sigma-Aldrich), arginine-glycine-aspartic acid (Sigma-Aldrich), fluorescein-labeled avidin (Fisher, Pittsburgh, PA), PBS (pH 7.4, Fisher), and Tris-buffer (pH 7.4, Fisher) were used as received. Fibronectin (Invitrogen, Carlsbad, CA) was treated with AlexaFluo 594 Labeling Kit (Invitrogen). Bovine serum (Invitrogen) was treated with AlexaFluo 555 Labeling Kit (Invitrogen).

Surface Modifications

Conversion of surface Si-CH3 groups into Si-OH was accomplished through an oxidative reaction. A mixture of H2O/H2O2/HCl (5:1:1) was flowed through PDMS channels through the connected Tygon tubing for 5 min. After the reaction was completed, the

channels were purged with DI water and dried using argon (5 psi), creating a surface covered with silanols.

PEG-Grafted Microfluidic Channels

2-[methoxy(polyethylenoxy)propyl]terimethoxysilane was injected into the silanol-covered channel by a microsyringe and kept at ambient temperature for 30 min until the silanization reaction was complete. DI water was continuously flowed through the channels to remove any unreacted silane, resulting in the final PEG-grafted channels.

Amino-Grafted Microfluidic Channels

(3-aminopropyl)-trimethoxy silane was injected into the silanol-covered channel by a mcirosyringe and kept at ambient temperature for 30 min until the silanization reaction was complete. DI water was continuously flowed through the channels to remove any unreacted silane, resulting in the final amino-grafted channels.

Isothiocyanate-Grafted Microfluidic Channels:

Thiophosgen solution in acetonitrile (0.5%) was introduced into amino-grafted channels and heated to 40 ˚C for 20 min. The channel was subsequently purged with with DI water and argon gas to obtain the final isothiocyanate-grafted channels.

Appendix B

Fabrication Protocols

FDG Device Design

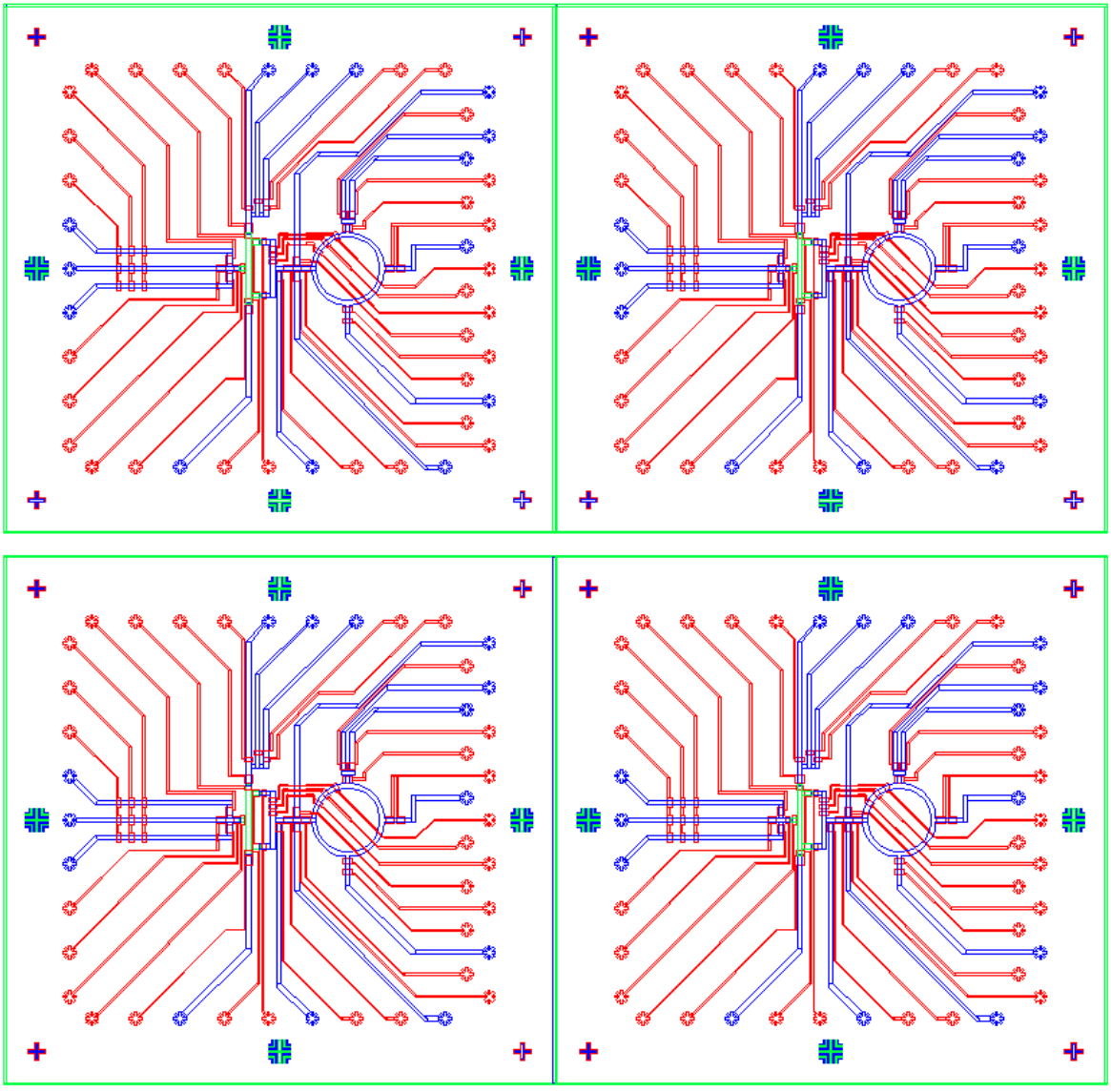

Figure B-1: Assembled FDG device

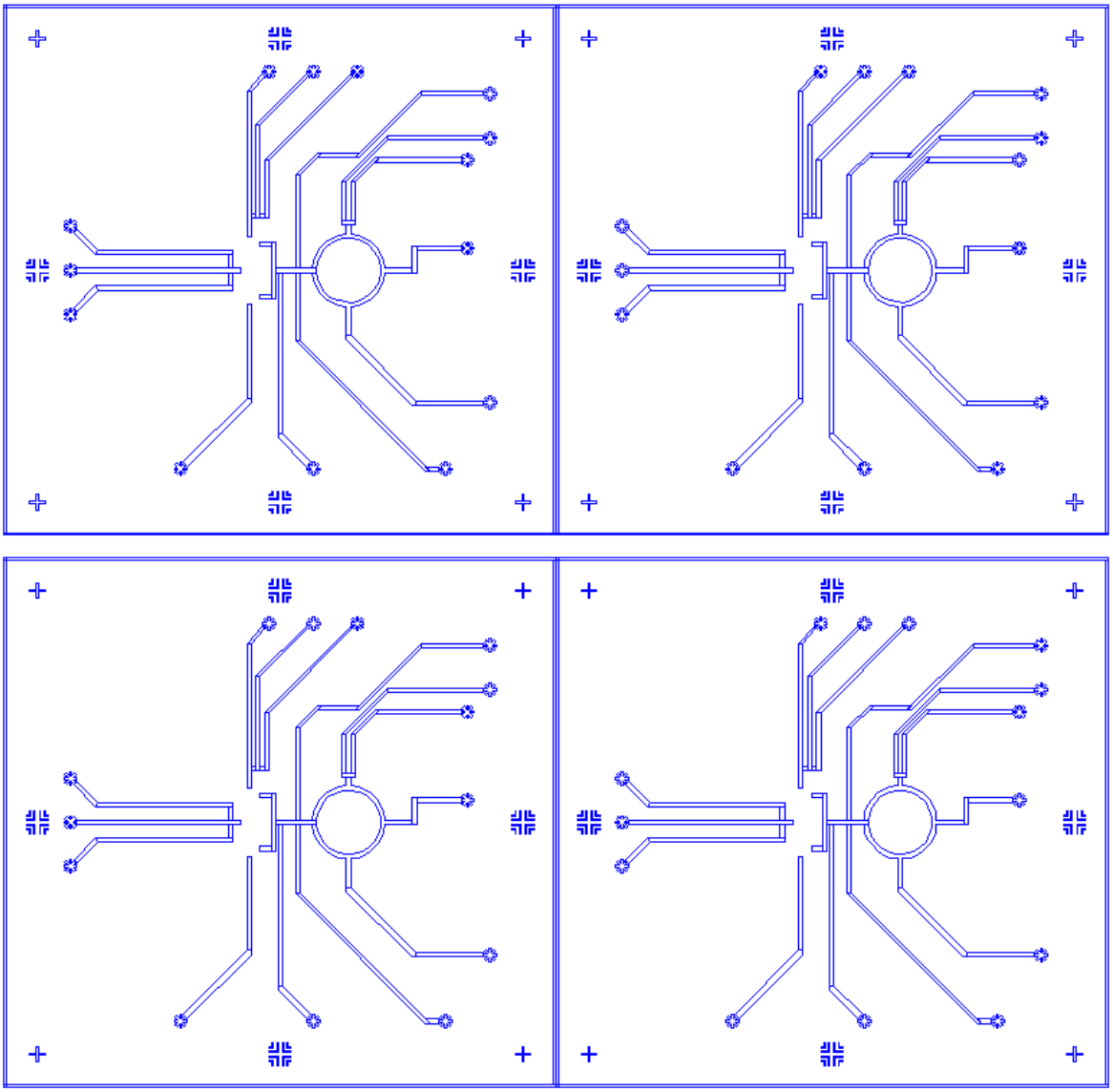

Figure B-2: FDG device rounded channel flow layer mask

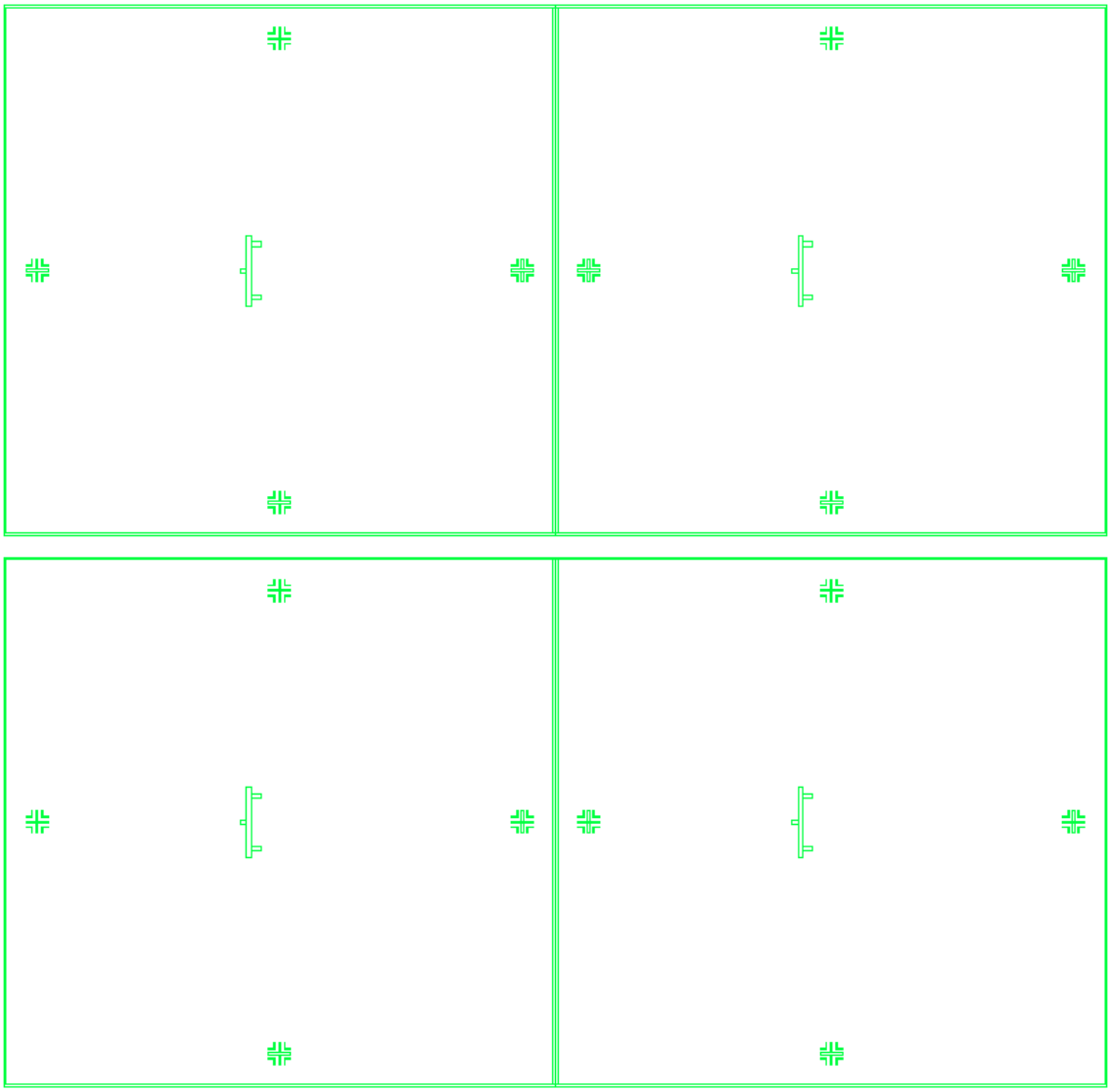

Figure B-3: FDG device column flow layer mask

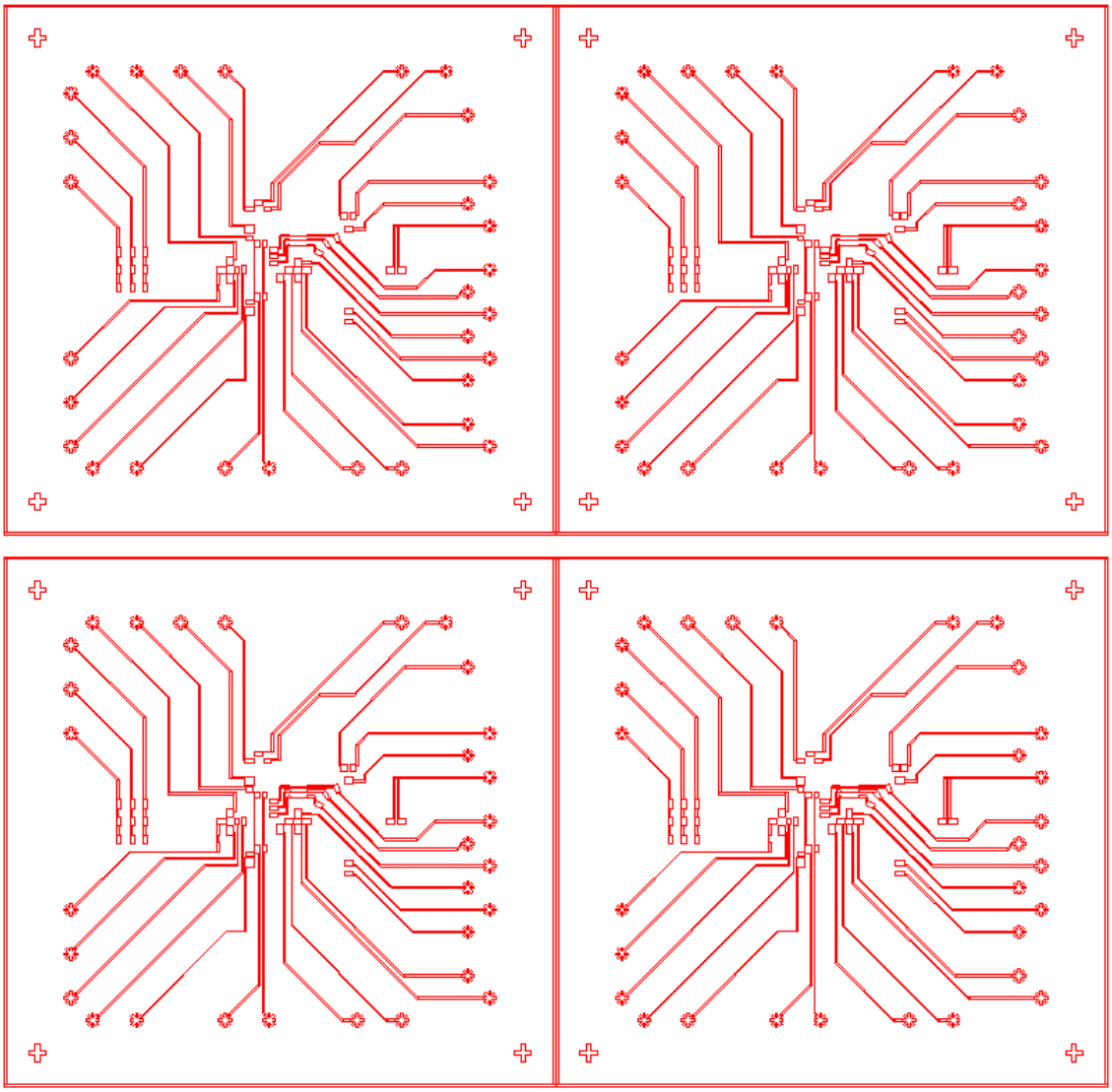

Figure B-4: FDG device control layer mask

FDG Device Mold Fabrication

I. Flow Mold--Rounded Channels

a.	Clean Wafers:	Rinse with acetone, isopropanol and dry
b.	Primer Wafers:	2 min hexamethyldisilazane (HMDS) vapor treatment
c.	Spin AZ100:	1000 rpm for 60 sec; 136 rpm/sec ramp. Film thickness = 45 μm
d.	Pre-Exposure Bake:	90 sec 65 ˚C/ 5 min 115 ˚C/ 90 sec 65˚C
e.	Expose Wafer:	85 sec at 8mW/cm^2
f.	Initial Develop:	2:1 DI water and AZ Developer till only thin film is left
g.	Final Develop:	5:1 DI water and AZ developer till completion
h.	Hard Bake:	Ramp from 65 ˚C to 190 ˚C; Bake for 5 hr at 190 ˚C

II. Flow Mold--Column

a.	Spin SU8-2050:	500 rpm for 15 sec; 136 rpm/sec ramp. 3800 rpm for 1 min, 136 rpm/sec ramp Film thickness = 45 μm
b.	Pre-Exposure Bake:	90 sec 65 ˚C/ 5 min 95 ˚C/ 90 sec 65˚C
c.	Expose Wafer:	45 sec at 8mW/cm^2
d.	Post-Exposure Bake:	90 sec 65 ˚C/ 10 min 95 ˚C/ 90 sec 65˚C
e.	Develop:	SU-8 developer till completion Rinse with acetone, isopropanol, and dry
f.	Hard Bake:	Bake for 1 hr at 150 ˚C

III. Control Mold

a.	Spin SU8-2025:	500 rpm for 15 sec; 136 rpm/sec ramp. 3200 rpm for 1 min, 136 rpm/sec ramp Film thickness = 25 μm
b.	Pre-Exposure Bake:	90 sec 65 ˚C/ 5 min 95 ˚C/ 90 sec 65˚C
c.	Expose Wafer:	45 sec at 8mW/cm^2
d.	Post-Exposure Bake:	90 sec 65 ˚C/ 10 min 95 ˚C/ 90 sec 65˚C
e.	Develop:	SU-8 developer till completion Rinse with acetone, isopropanol, and dry
f.	Hard Bake:	Bake for 1 hr at 150 ˚C

FDG Device: Device Fabrication

1. TMCS Treat Molds:	Expose flow mold and control mold to trimethylchlorosilane(TMCS) for 2 min
2. Prepare Flow Layer:	Combine 5:1 GE 615 RTV (30g A: 6 g B) Mix in hybrid mixer: 3 min mix/ 5 min degas Pour 32 g 5:1 onto flow mold Degas for 30 min in bell jar
3. Prepare Control Layer:	Start while flow layer is degassing Combine 20:1 GE 615 RTV (20 g A: 1 g B) Mix in hybrid mixer: 3 min mix/ 5 min degas Pour 5 ml 20:1 onto control mold Spin at 1800 rpm for 75 sec, 136 rmp/sec ramp Let PDMS relax for 30 min before curing
4. Cure Flow Layer:	Bake for 60 min at 80˚C
5. Cure Control Layer:	Bake for 45 min at 80˚C
6. Control/Flow Bonding:	Remove flow layer from mold Punch inlet and outlets with 20 gauge punch Cut devices out and clean with tape Align flow layer onto control layer Bake for 60 min at 80˚C
7. Prepare Blank Layer:	Start While flow/control bonding Combine 20:1 GE 615 RTV (20 g A: 1 g B) Mix in hybrid mixer: 3 min mix/ 5 min degas Pour 5 ml 20:1 onto clean glass slide Let PDMS relax for 10 min before curing Bake for 30 min at 80˚C
8. Assemble Device:	Remove bonded device from control mold Punch control inlets with 20 gauge punch Clean with tape Place bonded device onto blank layer Remove trapped air bubbles Cure assembled device at 80˚C for 24hr

PFPE DNA Synthesizer Design

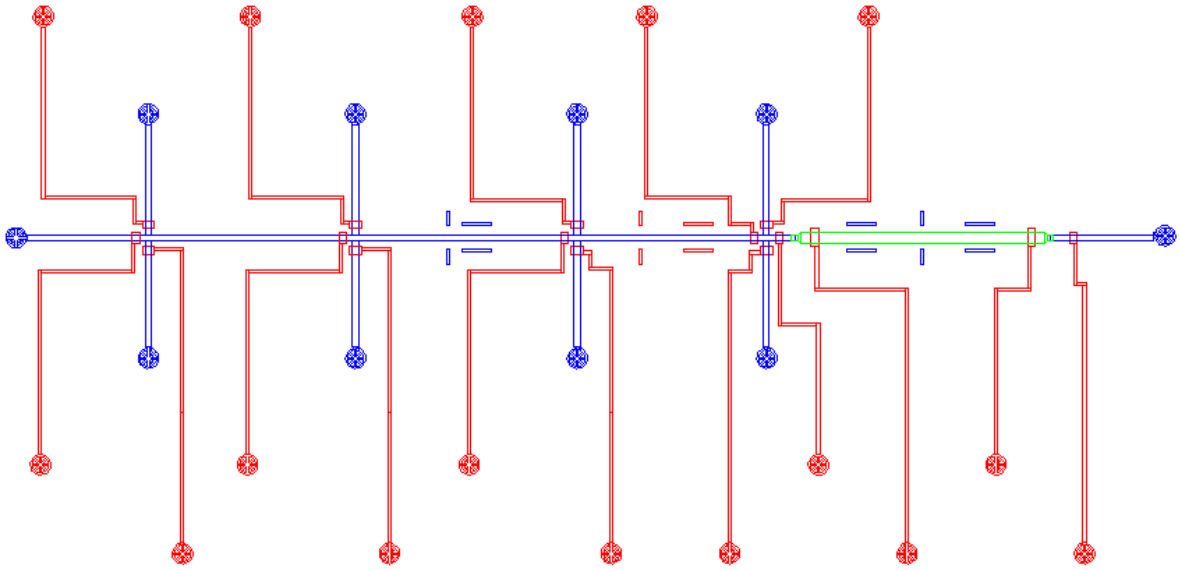

Figure B-5: Assembled PFPE DNA synthesizer device

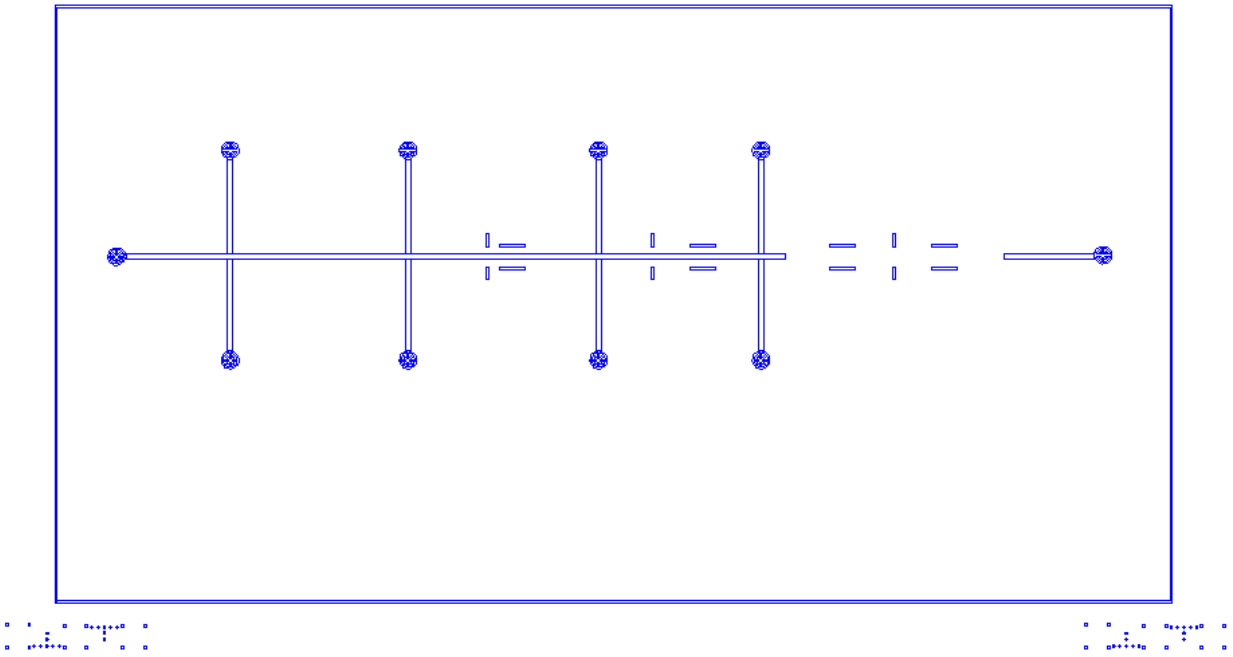

Figure B-6: PFPE DNA synthesizer rounded channel flow layer mask

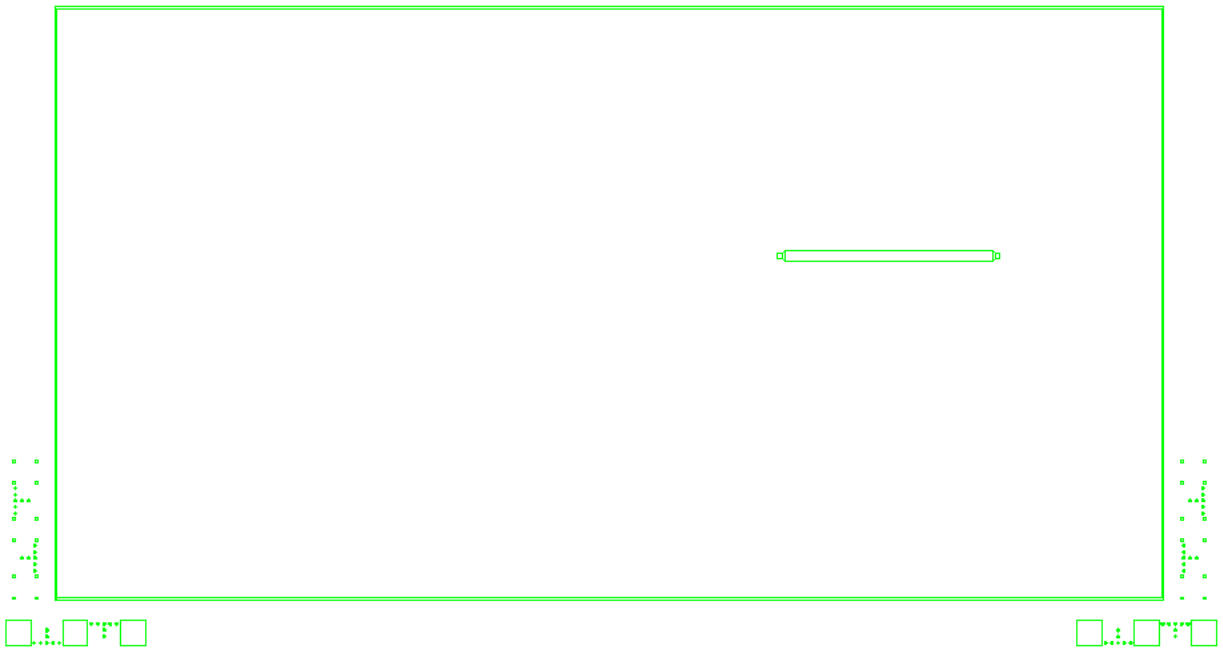

Figure B-7: PFPE DNA synthesizer column flow layer mask

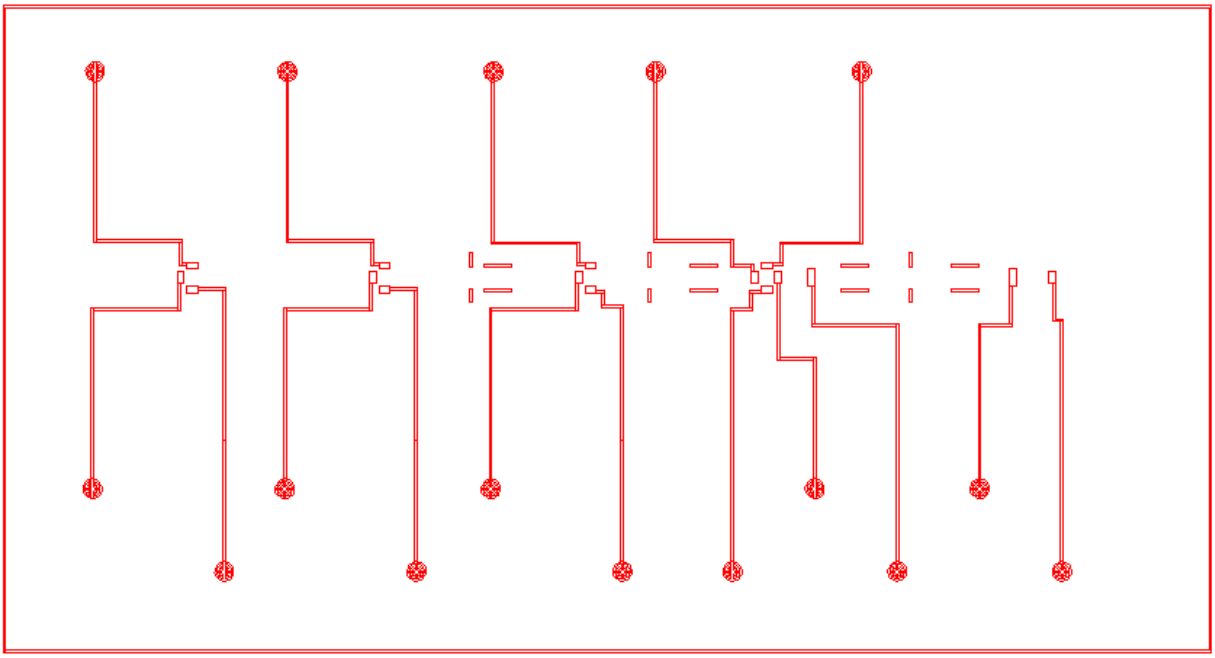

Figure B-8: PFPE DNA synthesizer control layer mask

PFPE DNA Device Mold Fabrication

I. Flow Mold--Rounded Channels

a.	Clean Wafers:	Rinse with acetone, isopropanol and dry
b.	Primer Wafers:	2 min hexamethyldisilazane (HMDS) vapor treatment
c.	Spin AZ100:	1000 rpm for 60 sec; 136 rpm/sec ramp. Film thickness = 45 μm
d.	Pre-Exposure Bake:	90 sec 65 ˚C/ 5 min 115 ˚C/ 90 sec 65˚C
e.	Expose Wafer:	85 sec at 8mW/cm^2
f.	Initial Develop:	2:1 DI water and AZ Developer till only thin film is left
g.	Final Develop:	5:1 DI water and AZ developer till completion
h.	Hard Bake:	Ramp from 65 ˚C to 190 ˚C; Bake for 5 hr at 190 ˚C

II. Flow Mold--Column

a.	Spin SU8-2050:	500 rpm for 15 sec; 136 rpm/sec ramp. 3800 rpm for 1 min, 136 rpm/sec ramp Film thickness = 45 μm
b.	Pre-Exposure Bake:	90 sec 65 ˚C/ 5 min 95 ˚C/ 90 sec 65˚C
c.	Expose Wafer:	45 sec at 8mW/cm^2
d.	Post-Exposure Bake:	90 sec 65 ˚C/ 10 min 95 ˚C/ 90 sec 65˚C
e.	Develop:	SU-8 developer till completion Rinse with acetone, isopropanol, and dry
f.	Hard Bake:	Bake for 1 hr at 150 ˚C

III. Control Mold

a.	Spin SU8-2025:	500 rpm for 15 sec; 136 rpm/sec ramp. 3200 rpm for 1 min, 136 rpm/sec ramp Film thickness = 25 μm
b.	Pre-Exposure Bake:	90 sec 65 ˚C/ 5 min 95 ˚C/ 90 sec 65˚C
c.	Expose Wafer:	45 sec at 8mW/cm^2
d.	Post-Exposure Bake:	90 sec 65 ˚C/ 10 min 95 ˚C/ 90 sec 65˚C
e.	Develop:	SU-8 developer till completion Rinse with acetone, isopropanol, and dry
f.	Hard Bake:	Bake for 1 hr at 150 ˚C

PFPE DNA Device: Device Fabrication

1.	TMCS Treat Molds:	Expose flow mold, control mold, reservoir mold, and one blank wafer to trimethylchlorosilane(TMCS) for 2 min
2.	Prepare Flow Layer:	Combine 5:1 GE 615 RTV (30g A: 6 g B) Mix in hybrid mixer: 3 min mix/ 5 min degas Pour 32 g 5:1 onto flow mold Degas for 30 min in bell jar
3.	Prepare Control Layer:	Start while flow layer is degassing Combine 20:1 GE 615 RTV (20 g A: 1 g B) Mix in hybrid mixer: 3 min mix/ 5 min degas Pour 5 ml 20:1 onto control mold Spin at 1800 rpm for 75 sec, 136 rmp/sec ramp Let PDMS relax for 30 min before curing
4.	Cure Flow Layer:	Bake for 60 min at 80˚C
5.	Cure Control Layer:	Bake for 45 min at 80˚C
6.	Control/Flow Bonding:	Remove flow layer from mold Punch inlet and outlets with 20 gauge punch Cut devices out and clean with tape Align flow layer onto control layer Bake for 60 min at 80˚C
7.	Prepare Blank Layer:	Start While flow/control bonding Combine 20:1 GE 615 RTV (20 g A: 1 g B) Mix in hybrid mixer: 3 min mix/ 5 min degas Pour 5 ml 20:1 onto clean glass slide Let PDMS relax for 10 min before curing Bake for 30 min at 80˚C
8.	Assemble Device:	Remove bonded device from control mold Punch control inlets with 20 gauge punch Clean with tape Place bonded device onto blank layer Remove trapped air bubbles Cure assembled device at 80˚C for 24hr

PDMS-Based Parallel DNA Synthesizer Design

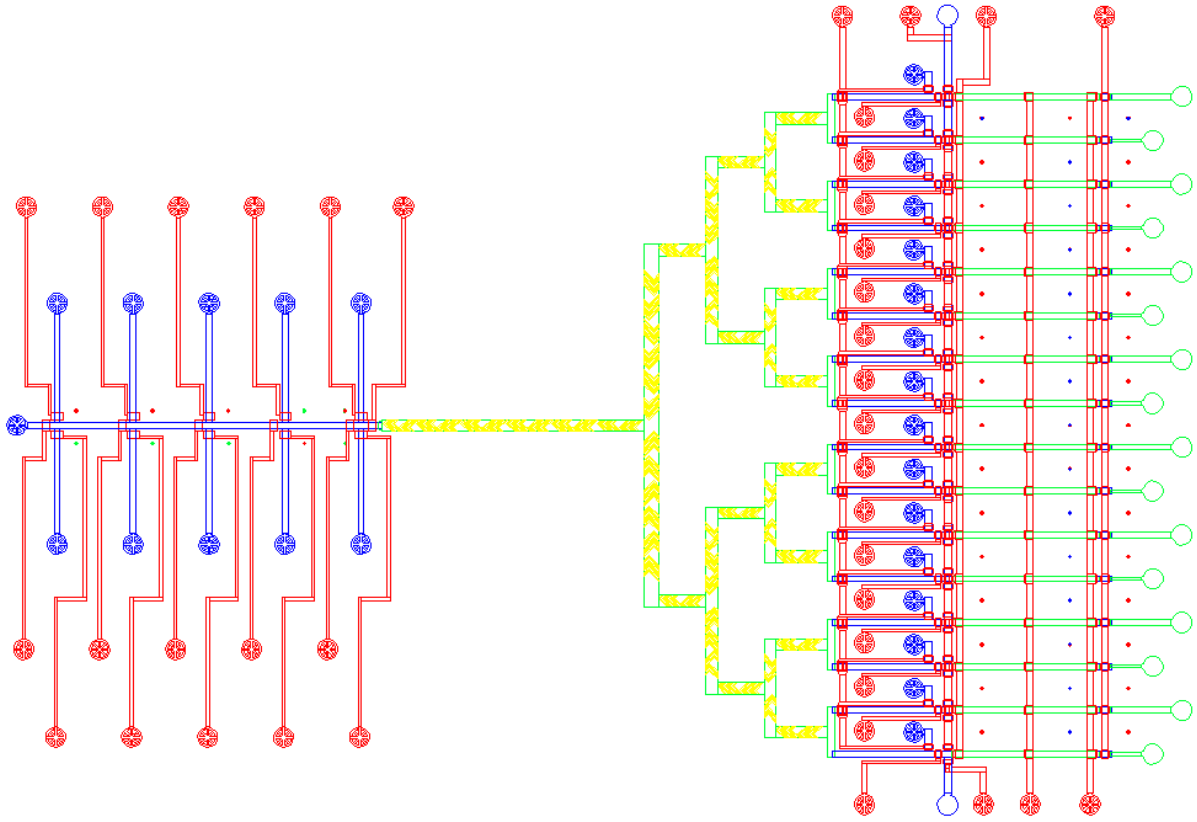

Figure B-9: Assembled PDMS-based parallel DNA synthesizer

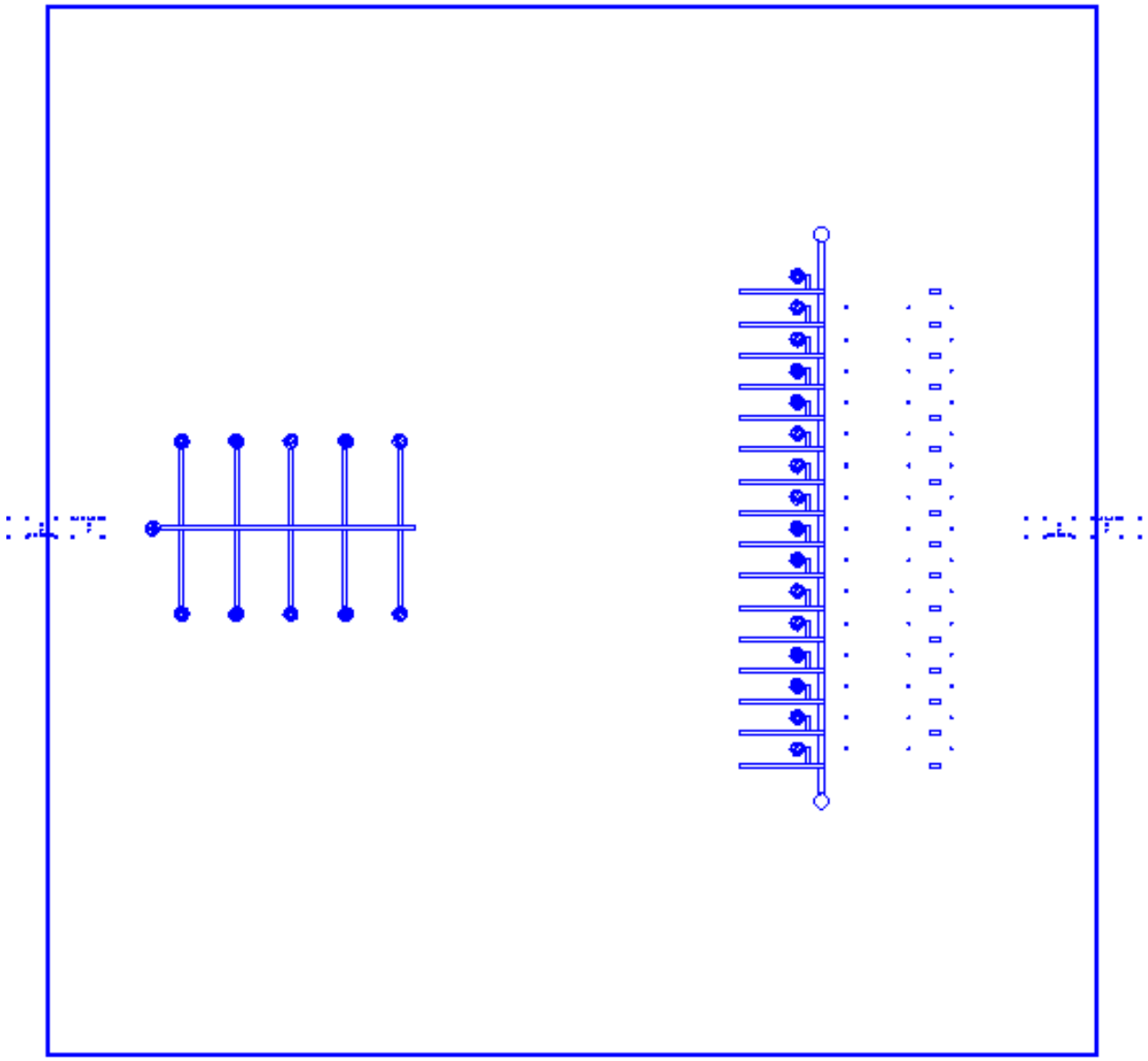

Figure B-10: PDMS-based parallel DNA synthesizer rounded channel flow layer mask

Figure B-11: PDMS-based parallel DNA synthesizer herringbone mixer mask

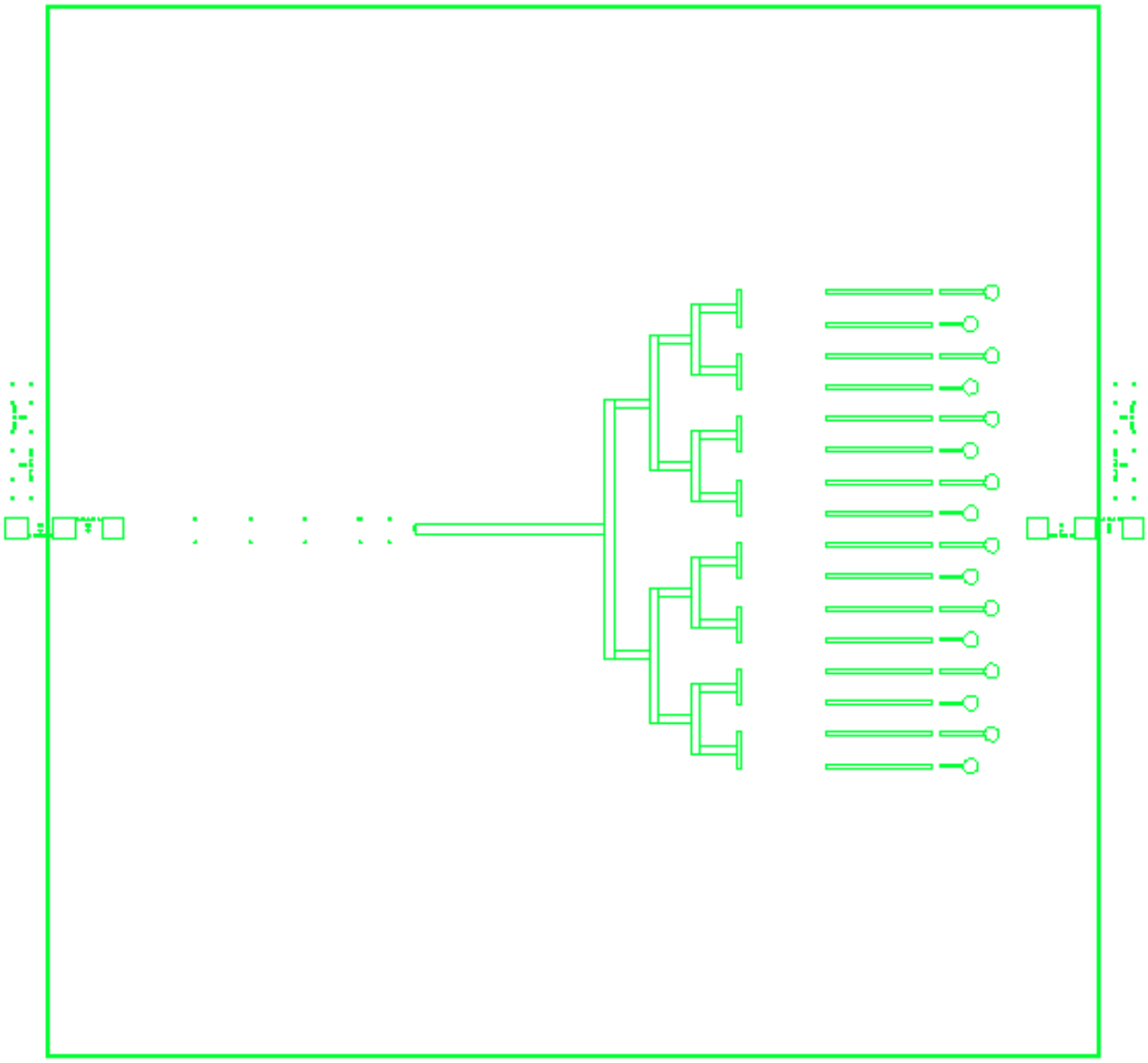

Figure B-12 PDMS-based parallel DNA synthesizer binary tree and column channel flow layer mask

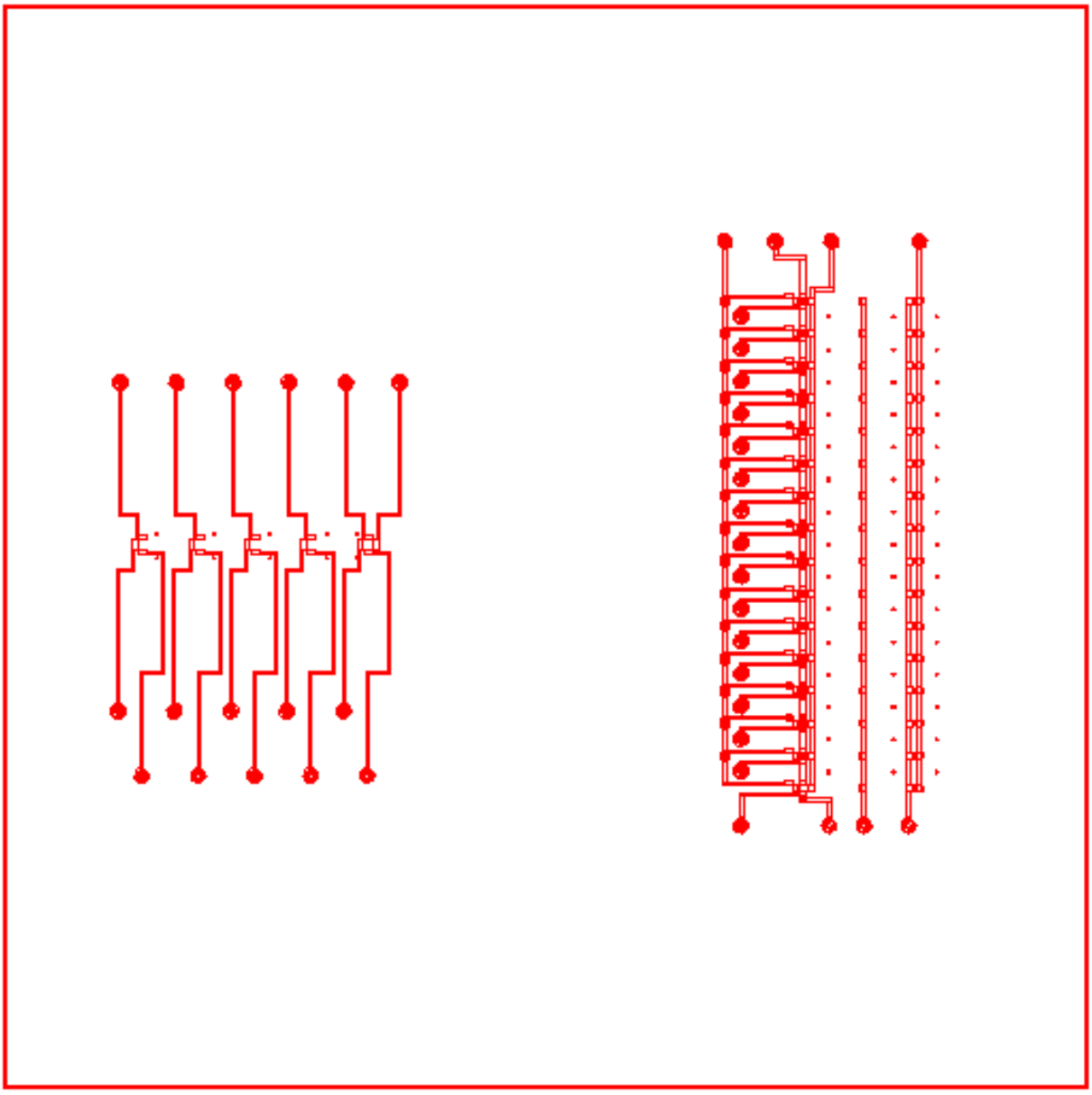

Figure B-13: PDMS-based parallel DNA synthesizer control layer mask

PDMS-Based Parallel DNA Synthesizer: Mold Fabrication

I. Flow Mold--Rounded Channels

a.	Clean Wafers:	Rinse with acetone, isopropanol and dry
b.	Primer Wafers:	2 min hexamethyldisilazane (HMDS) vapor treatment
c.	Spin AZ100:	1000 rpm for 60 sec; 136 rpm/sec ramp. Film thickness = 45 μm
d.	Pre-Exposure Bake:	90 sec 65 ˚C/ 5 min 115 ˚C/ 90 sec 65˚C
e.	Expose Wafer:	85 sec at 8mW/cm^2
f.	Initial Develop:	2:1 DI water and AZ Developer till only thin film is left
g.	Final Develop:	5:1 DI water and AZ developer till completion
h.	Hard Bake:	Ramp from 65 ˚C to 190 ˚C; Bake for 5 hr at 190 ˚C

II. Flow Mold--Column

a.	Spin SU8-2050:	500 rpm for 15 sec; 136 rpm/sec ramp. 3800 rpm for 1 min, 136 rpm/sec ramp Film thickness = 45 μm
b.	Pre-Exposure Bake:	90 sec 65 ˚C/ 5 min 95 ˚C/ 90 sec 65˚C
c.	Expose Wafer:	45 sec at 8mW/cm^2
d.	Post-Exposure Bake:	90 sec 65 ˚C/ 10 min 95 ˚C/ 90 sec 65˚C
e.	Develop:	SU-8 developer till completion Rinse with acetone, isopropanol, and dry
f.	Hard Bake:	Bake for 1 hr at 150 ˚C

III. Control Mold

a.	Spin SU8-2025:	500 rpm for 15 sec; 136 rpm/sec ramp. 3200 rpm for 1 min, 136 rpm/sec ramp Film thickness = 25 μm
b.	Pre-Exposure Bake:	90 sec 65 ˚C/ 5 min 95 ˚C/ 90 sec 65˚C
c.	Expose Wafer:	45 sec at 8mW/cm^2
d.	Post-Exposure Bake:	90 sec 65 ˚C/ 10 min 95 ˚C/ 90 sec 65˚C
e.	Develop:	SU-8 developer till completion Rinse with acetone, isopropanol, and dry
f.	Hard Bake:	Bake for 1 hr at 150 ˚C

PDMS-Based Parallel DNA Synthesizer: Device Fabrication

1.	TMCS Treat Molds:	Expose flow mold and control mold to trimethylchlorosilane(TMCS) for 2 min
2.	Prepare Flow Layer:	Combine 5:1 GE 615 RTV (45 g A: 9 g B) Mix in hybrid mixer: 3 min mix/ 5 min degas Pour 52 g 5:1 onto flow mold Degas for 30 min in bell jar
3.	Prepare Control Layer:	Start while flow layer is degassing Combine 20:1 GE 615 RTV (20 g A: 1 g B) Mix in hybrid mixer: 3 min mix/ 5 min degas Pour 5 ml 20:1 onto control mold Spin at 1800 rpm for 75 sec, 136 rmp/sec ramp Let PDMS relax for 30 min before curing
4.	Cure Flow Layer:	Bake for 60 min at 80˚C
5.	Cure Control Layer:	Bake for 45 min at 80˚C
6.	Control/Flow Bonding:	Remove flow layer from mold Punch inlet and outlets with 20 gauge punch Cut devices out and clean with tape Align flow layer onto control layer Bake for 60 min at 80˚C
7.	Prepare Blank Layer:	Start While flow/control bonding Combine 20:1 GE 615 RTV (20 g A: 1 g B) Mix in hybrid mixer: 3 min mix/ 5 min degas Pour 5 ml 20:1 onto clean glass slide Let PDMS relax for 10 min before curing Bake for 30 min at 80˚C
8.	Assemble Device:	Remove bonded device from control mold Punch control inlets with 20 gauge punch Clean with tape Place bonded device onto blank layer Remove trapped air bubbles Cure assembled device at 80˚C for 24hr

32 Compartment DRAM Device Design

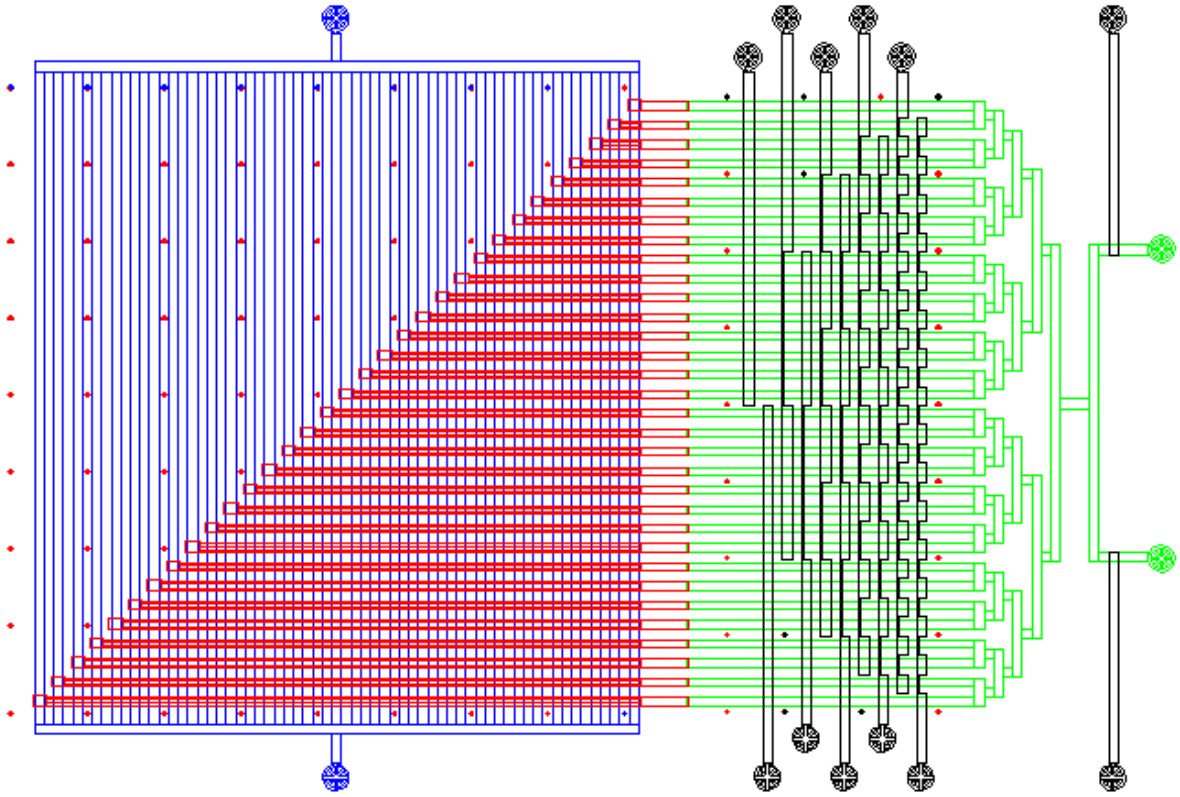

Figure B-14: Assembled 32 comparment DRAM device

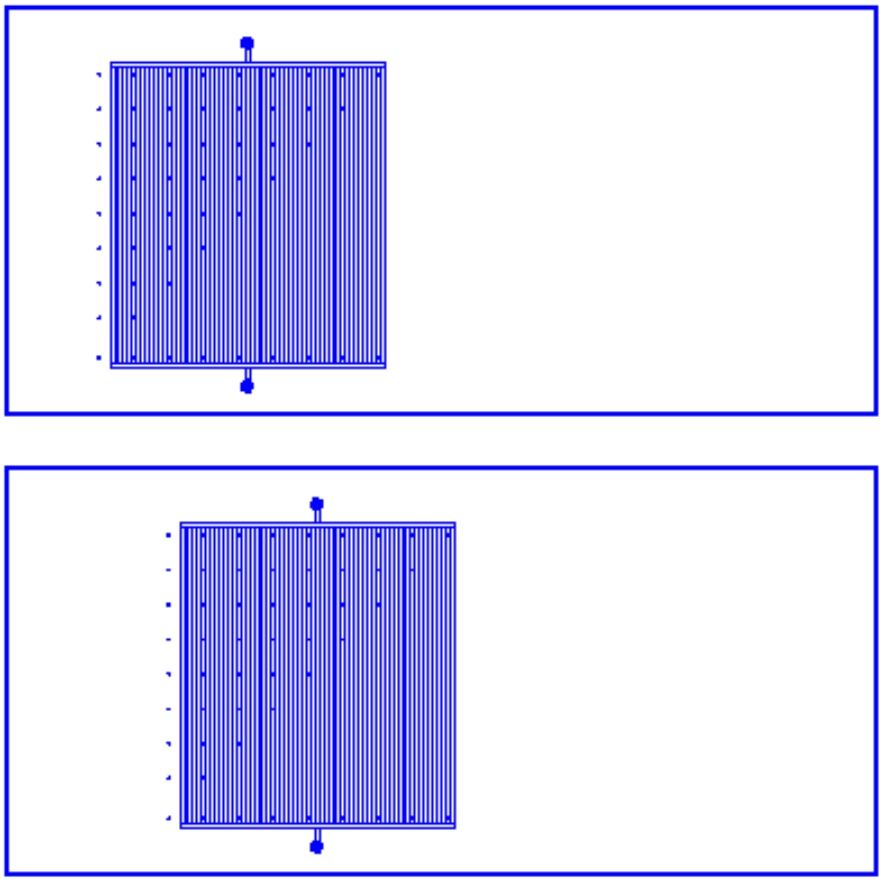

Figure B-15 32 compartment DRAM device rounded channel flow layer mask

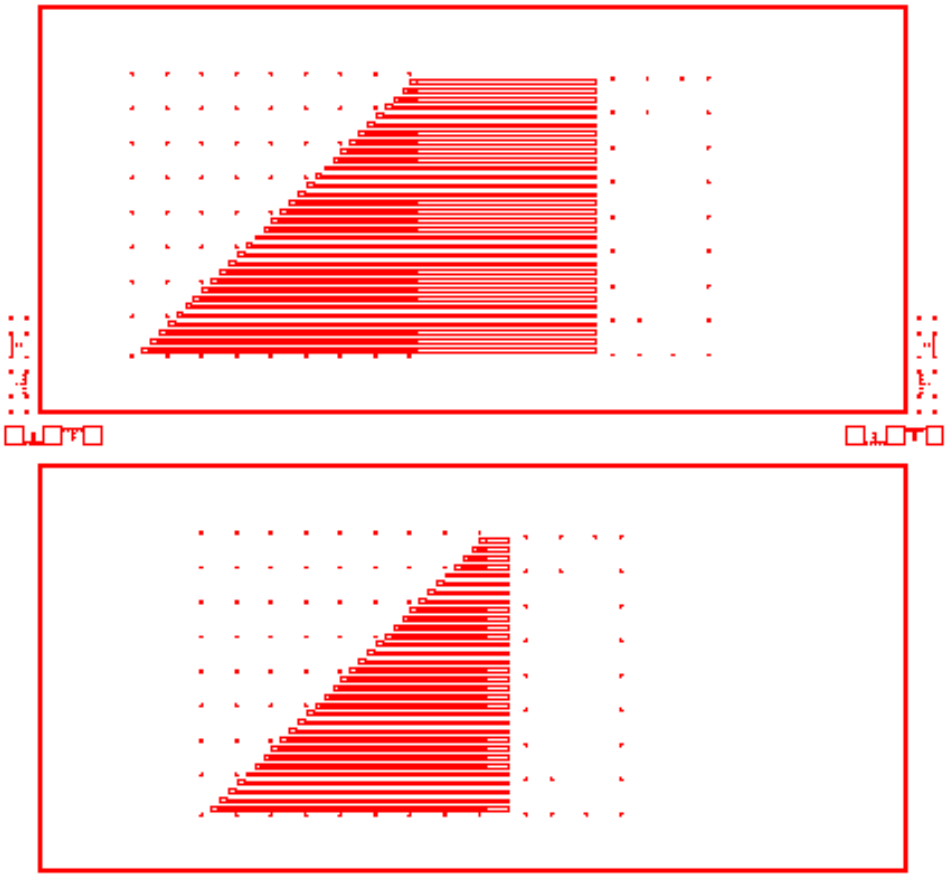

Figure B-16: 32 compartment DRAM device intermediate control layer mask

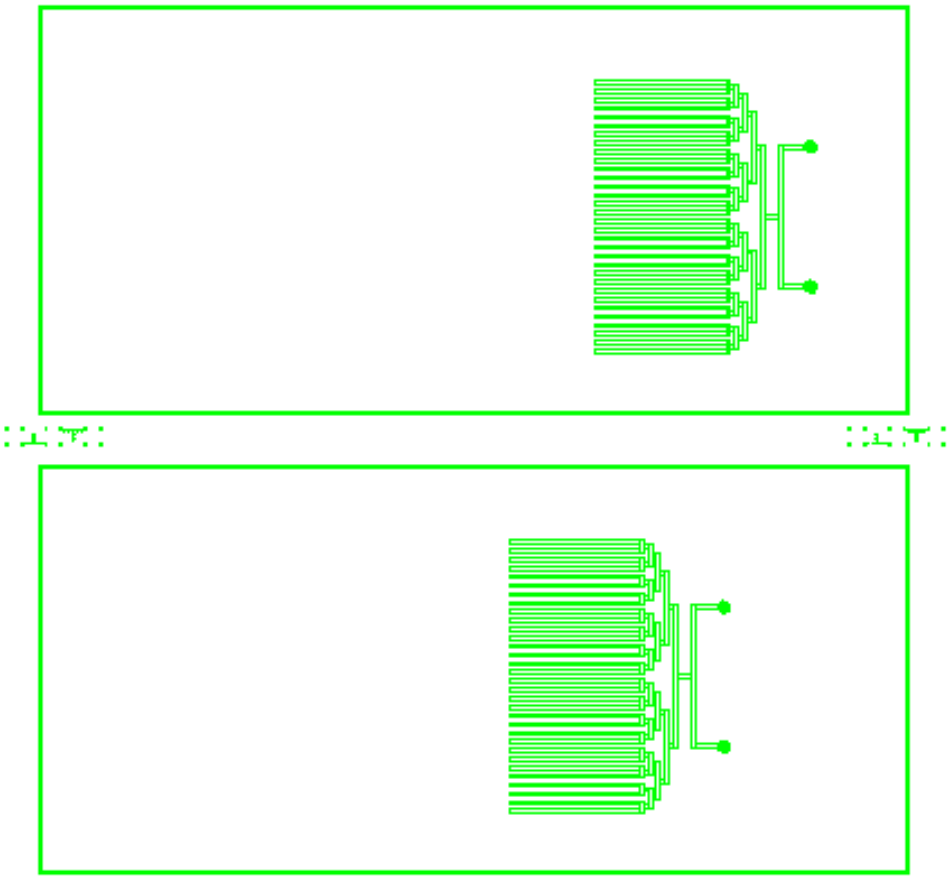

Figure B-17: 32 compartment DRAM device bottom level rounded channel flower layer mask

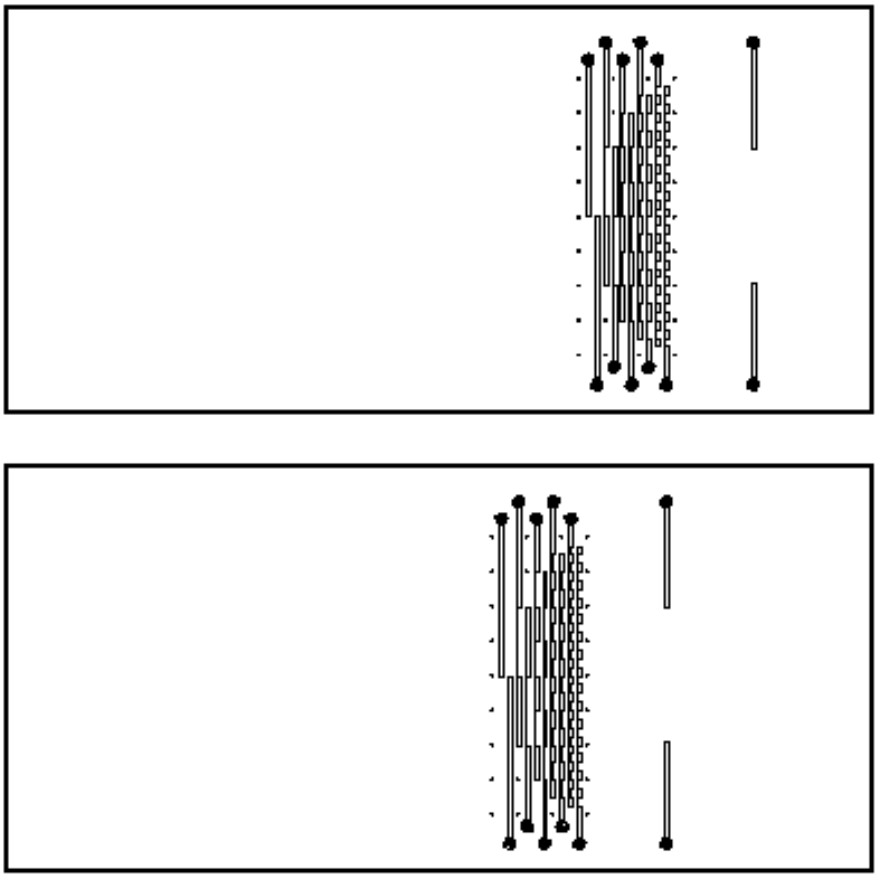

Figure B-18: 32 compartment DRAM bottom level control layer mask

32 Compartment DRAM Device: Mold Fabrication

I. Top Flow Mold--Rounded Channels

a.	Clean Wafers:	Rinse with acetone, isopropanol and dry
b.	Primer Wafers:	2 min hexamethyldisilazane (HMDS) vapor treatment
c.	Spin AZ100:	1000 rpm for 60 sec; 136 rpm/sec ramp. Film thickness = 45 μm
d.	Pre-Exposure Bake:	90 sec 65 ˚C/ 5 min 115 ˚C/ 90 sec 65˚C
e.	Expose Wafer:	85 sec at 8mW/cm^2
f.	Initial Develop:	2:1 DI water and AZ Developer till only thin film is left
g.	Final Develop:	5:1 DI water and AZ developer till completion
h.	Hard Bake:	Ramp from 65 ˚C to 190 ˚C; Bake for 5 hr at 190 ˚C

II. Intermediate Mold--Rounded Channels

a.	Clean Wafers:	Rinse with acetone, isopropanol and dry
b.	Primer Wafers:	2 min hexamethyldisilazane (HMDS) vapor treatment
c.	Spin AZ100:	1000 rpm for 60 sec; 136 rpm/sec ramp. Film thickness = 45 μm
d.	Pre-Exposure Bake:	90 sec 65 ˚C/ 5 min 115 ˚C/ 90 sec 65˚C
e.	Expose Wafer:	85 sec at 8mW/cm^2
f.	Initial Develop:	2:1 DI water and AZ Developer till only thin film is left
g.	Final Develop:	5:1 DI water and AZ developer till completion
h.	Hard Bake:	Ramp from 65 ˚C to 190 ˚C; Bake for 5 hr at 190 ˚C

III. Intermediate Control Mold

a.	Spin SU8-2050:	500 rpm for 15 sec; 136 rpm/sec ramp. 3800 rpm for 1 min, 136 rpm/sec ramp Film thickness = 45 μm
b.	Pre-Exposure Bake:	90 sec 65 ˚C/ 5 min 95 ˚C/ 90 sec 65˚C
c.	Expose Wafer:	45 sec at 8mW/cm^2
d.	Post-Exposure Bake:	90 sec 65 ˚C/ 10 min 95 ˚C/ 90 sec 65˚C
e.	Develop:	SU-8 developer till completion Rinse with acetone, isopropanol, and dry
f.	Hard Bake:	Bake for 1 hr at 150 ˚C

IV. Bottom Level Control Mold

a.	Spin SU8-2025:	500 rpm for 15 sec; 136 rpm/sec ramp. 3200 rpm for 1 min, 136 rpm/sec ramp Film thickness = 25 μm
b.	Pre-Exposure Bake:	90 sec 65 ˚C/ 5 min 95 ˚C/ 90 sec 65˚C
c.	Expose Wafer:	45 sec at 8mW/cm^2
d.	Post-Exposure Bake:	90 sec 65 ˚C/ 10 min 95 ˚C/ 90 sec 65˚C
e.	Develop:	SU-8 developer till completion Rinse with acetone, isopropanol, and dry
f.	Hard Bake:	Bake for 1 hr at 150 ˚C

32 Compartment DRAM Device: Device Fabrication

1.	TMCS Treat Molds:	Expose Top flow mold, Intermediate control mold and bottom control mold to trimethylchlorosilane(TMCS) for 2 min
2.	Prepare Top Flow Layer:	Combine 5:1 GE 615 RTV (30g A: 6 g B) Mix in hybrid mixer: 3 min mix/ 5 min degas Pour 32 g 5:1 onto flow mold Degas for 30 min in bell jar
3.	Prepare Int. Layer:	Start while flow layer is degassing Combine 20:1 GE 615 RTV (20 g A: 1 g B) Mix in hybrid mixer: 3 min mix/ 5 min degas Pour 5 ml 20:1 onto control mold Spin at 1800 rpm for 75 sec, 136 rmp/sec ramp Let PDMS relax for 30 min before curing
4.	Cure Top Flow Layer:	Bake for 60 min at 80˚C
5.	Cure Intermediate Layer:	Bake for 45 min at 80˚C
6.	Int./Top Flow Bonding:	Remove flow layer from mold Punch inlet and outlets with 20 gauge punch Cut devices out and clean with tape Align flow layer onto intermediate layer Bake for 60 min at 80˚C
7.	Prepare Bottom Layer:	Start while top/intermediate bonding Combine 20:1 GE 615 RTV (20 g A: 1 g B) Mix in hybrid mixer: 3 min mix/ 5 min degas Pour 5 ml 20:1 onto clean glass slide

	Let PDMS relax for 10 min before curing
	Bake for 30 min at 80˚C
8. Assemble Device:	Remove bonded device from intermediate mold
	Punch control and flow inlets with 20 gauge punch
	Clean with tape
	Place bonded device onto bottom control layer
	Remove trapped air bubbles
	Cure assembled device at 80˚C for 24hr
9. Prepare Glass Slide:	Wash glass slide using Micro-90 cleaner
	Rinse with DI water and dry
10. O_2 Plasma Treatment:	70 W, 300 mTorr, 15 sec
11. Final Assembly:	Bond the device onto the glass slide
	Bake at 80˚C overnight

Bibliography

1. Watts, P., and Haswell, S.J. (2003) Microfluidic combinatorial chemistry. *Curr. Opin. Chem. Biol.*, **7**, 380--387.
2. Cullen, C.J., Wootton, R.C.R., and de Mello, A.J. (2004) Microfluidic systems for high-throughput and combinatorial chemistry. *Curr. Opin. Drug Discov. Dev.*, **7**, 798--806.
3. Roberge, D.M., Ducry, L., Bieler, N., Cretton, P., and Zimmermann, B. (2005) Microreactor technology: A revolution for the fine chemical and pharmaceutical industries? *Chem. Eng. Technol.*, **28**, 318--323.
4. DeMello, A.J. (2006) Control and detection of chemical reactions in microfluidic systems. *Nature*, **442**, 394--402.
5. Aota, A., Nonaka, M., Hibara, A., and Kitamori, T. (2007) Countercurrent laminar microflow for highly efficient solvent extraction. *Angewandte Chemie (International ed.)*, **46**, 878--880.
6. de Mas, N., Gunther, A., Schmidt, M.A., and Jensen, K.F. (2003) Microfabricated multiphase reactors for the selective direct fluorination of aromatics. *Industrial & Engineering Chemistry Research*, **42**, 698--710.
7. Kobayashi, J., Mori, Y., Okamoto, K., Akiyama, R., Ueno, M., Kitamori, T., and Kobayashi, S. (2004) A microfluidic device for conducting gas-liquid-solid hydrogenation reactions. *Science*, **304**, 1305--1308.
8. Knight, J.B., Vishwanath, A., Brody, J.P., and Austin, R.H. (1998) Hydrodynamic focusing on a silicon chip: Mixing nanoliters in microseconds. *Physical Review Letters*, **80**, 3863--3866.
9. Hye Yoon, P., Kim, S.A., Korlach, J., Rhoades, E., Kwok, L.W., Zipfel, W.R., Waxham, M.N., Webb, W.W., and Pollack, L. (2008) Conformational changes of calmodulin upon Ca/sup 2+/ binding studied with a microfluidic mixer. *Proc. Nat. Acad. Sci. USA*, **105**, 542--547.
10. Dittrich, P.S., and Manz, A. (2006) Lab-on-a-chip: microfluidics in drug discovery. *Nature Reviews Drug Discovery*, **5**, 210--218.
11. Mueller, S., Coleman, J.R., and Wimmer, E. (2009) Putting Synthesis into Biology: A Viral View of Genetic Engineering through De Novo Gene and Genome Synthesis. *Chemistry & Biology*, **16**, 337--347.
12. Unger, M.A., Chou, H.P., Thorsen, T., Scherer, A., and Quake, S.R. (2000) Monolithic microfabricated valves and pumps by multilayer soft lithography. *Science*, **288**, 113--116.
13. Melin, J., and Quake, S.R. (2007) Microfluidic large-scale integration: The evolution of design rules for biological automation. *Annual Review of Biophysics and Biomolecular Structure*, **36**, 213--231.
14. Fu, A.Y., Chou, H.P., Spence, C., Arnold, F.H., and Quake, S.R. (2002) An integrated microfabricated cell sorter. *Analytical Chemistry*, **74**, 2451--2457.
15. Hansen, C.L., Skordalakes, E., Berger, J.M., and Quake, S.R. (2002) A robust and scalable microfluidic metering method that allows protein crystal growth by free interface diffusion. *Proc. Nat. Acad. Sci. USA*, **99**, 16531--16536.

16. Liu, J., Enzelberger, M., and Quake, S. (2002) A nanoliter rotary device for polymerase chain reaction. *Electrophoresis*, **23**, 1531--1536.
17. Hong, J.W., Studer, V., Hang, G., Anderson, W.F., and Quake, S.R. (2004) A nanoliter-scale nucleic acid processor with parallel architecture. *Nat. Biotechnol.*, **22**, 435--439.
18. Marcus, J.S., Anderson, W.F., and Quake, S.R. (2006) Parallel picoliter RT-PCR assays using microfluidics. *Analytical Chemistry*, **78**, 956--958.
19. Maerkl, S.J., and Quake, S.R. (2007) A systems approach to measuring the binding energy landscapes of transcription factors. *Science*, **315**, 233--237.
20. Hamacher, K., Coenen, H.H., and Stocklin, G. (1986) Efficient stereospecific synthesis of no-carrier-added 2-[F-18]-fluoro-2-deoxy-d-glucose using aminopolyether supported nucleophilic-substitution. *Journal of Nuclear Medicine*, **27**, 235--238.
21. Letsinger, R.L., and Lunsford, W.B. (1976) Synthesis of thymidine oligonucleotides by phosphite triester intermediates. *Journal of the American Chemical Society*, **98**, 3655--3661.
22. Matteucci, M.D., and Caruthers, M.H. (1981) Nucleotide chemistry .4. synthesis of deoxyoligonucleotides on a polymer support. *Journal of the American Chemical Society*, **103**, 3185--3191.
23. Pawloski, A.R., McGall, G., Kuimelis, R.G., Barone, D., Cuppoletti, A., Ciccolella, P., Spence, E., Afroz, F., Bury, P., Chen, C. et al. (2007) Photolithographic synthesis of high-density DNA probe arrays: Challenges and opportunities. *Journal of Vacuum Science & Technology B*, **25**, 2537--2546.
24. Tian, J.D., Gong, H., Sheng, N.J., Zhou, X.C., Gulari, E., Gao, X.L., and Church, G. (2004) Accurate multiplex gene synthesis from programmable DNA microchips. *Nature*, **432**, 1050--1054.
25. Phelps, M.E. (2002) Molecular imaging with positron emission tomography. *Annual Review of Nuclear and Particle Science*, **52**, 303--338.
26. Sharma, V., and Piwnica-Worms, D. (2002) Molecular imaging of gene expression and protein function in vivo with PET and SPECT. *Journal of Magnetic Resonance Imaging*, **16**, 336--351.
27. Massoud, T.F., and Gambhir, S.S. (2003) Molecular imaging in living subjects: seeing fundamental biological processes in a new light. *Genes & Development*, **17**, 545--580.
28. Rudin, M., and Weissleder, R. (2003) Molecular imaging in drug discovery and development. *Nature Reviews Drug Discovery*, **2**, 123--131.
29. Hamacher, K., Coenen, H.H., and Stocklin, G. (1986) Efficient Stereospecific Synthesis of No-Carrier-Added 2- F-18 -Fluoro-2-Deoxy-D-Glucose Using Aminopolyether Supported Nucleophilic-Substitution. *Journal of Nuclear Medicine*, **27**, 235--238.
30. Padgett, H.C., Schmidt, D.G., Luxen, A., Bida, G.T., Satyamurthy, N., and Barrio, J.R. (1989) Computer-Controlled Radiochemical Synthesis--a Chemistry Process-Control Unit for the Automated Production of Radiochemicals. *Applied Radiation and Isotopes*, **40**, 433.
31. Quake, S.R., and Scherer, A. (2000) From micro- to nanofabrication with soft materials. *Science*, **290**, 1536--1540.

32. Chan, E.M., Mathies, R.A., and Alivisatos, A.P. (2003) Size-controlled growth of CdSe nanocrystals in microfluidic reactors. *Nano Letters*, **3**, 199--201.
33. Bird, R.B., Stewart, W.E., and Lighttfoot, E.N. (2002) *Transport Phenomena*. John Wiley & Sons, New York, NY.
34. Dertinger, S.K.W., Chiu, D.T., Jeon, N.L., and Whitesides, G.M. (2001) Generation of gradients having complex shapes using microfluidic networks. *Analytical Chemistry*, **73**, 1240--1246.
35. Lee, J.N., Park, C., and Whitesides, G.M. (2003) Solvent compatibility of poly(dimethylsiloxane)-based microfluidic devices. *Analytical Chemistry*, **75**, 6544--6554.
36. McDonald, J.C., Duffy, D.C., Anderson, J.R., Chiu, D.T., Wu, H.K., Schueller, O.J.A., and Whitesides, G.M. (2000) Fabrication of microfluidic systems in poly(dimethylsiloxane). *Electrophoresis*, **21**, 27--40.
37. Wagner, M., Seitz, U., Buck, A., Neumaier, B., Schultheiss, S., Bangerter, M., Bommer, M., Leithauser, F., Wawra, E., Munzert, G. et al. (2003) 3 '-[F-18]fluoro-3 '-deoxythymidine ([F-18]-FLT) as positron emission tomography tracer for imaging proliferation in a murine B-cell lymphoma model and in the human disease. *Cancer Research*, **63**, 2681--2687.
38. Whitesides, G.M. (2006) The origins and the future of microfluidics. *Nature*, **442**, 368--373.
39. Jahnisch, K., Hessel, V., Lowe, H., and Baerns, M. (2004) Chemistry in microstructured reactors. *Angew Chem Int Edit*, **43**, 406--446.
40. Pal, R., Yang, M., Lin, R., Johnson, B.N., Srivastava, N., Razzacki, S.Z., Chomistek, K.J., Heldsinger, D.C., Haque, R.M., Ugaz, V.M. et al. (2005) An integrated microfluidic device for influenza and other genetic analyses. *Lab on a Chip*, **5**, 1024--1032.
41. Wang, Y.J., Lin, W.Y., Liu, K., Lin, R.J., Selke, M., Kolb, H.C., Zhang, N.G., Zhao, X.Z., Phelps, M.E., Shen, C.K.F. et al. (2009) An integrated microfluidic device for large-scale in situ click chemistry screening. *Lab on a Chip*, **9**, 2281--2285.
42. Wang, J.Y., Sui, G.D., Mocharla, V.P., Lin, R.J., Phelps, M.E., Kolb, H.C., and Tseng, H.R. (2006) Integrated microfluidics for parallel screening of an in situ click chemistry library. *Angew Chem Int Edit*, **45**, 5276--5281.
43. Rolland, J.P., Van Dam, R.M., Schorzman, D.A., Quake, S.R., and DeSimone, J.M. (2004) Solvent-resistant photocurable "liquid teflon" for microfluidic device fabrication. *Journal of the American Chemical Society*, **126**, 2322--2323.
44. Hasty, J., McMillen, D., and Collins, J.J. (2002) Engineered gene circuits. *Nature*, **420**, 224--230.
45. Kobayashi, H., Kaern, M., Araki, M., Chung, K., Gardner, T.S., Cantor, C.R., and Collins, J.J. (2004) Programmable cells: Interfacing natural and engineered gene networks. *Proc. Nat. Acad. Sci. USA*, **101**, 8414--8419.
46. Chang, M.C.Y., and Keasling, J.D. (2006) Production of isoprenoid pharmaceuticals by engineered microbes. *Nature Chemical Biology*, **2**, 674--681.
47. Cello, J., Paul, A.V., and Wimmer, E. (2002) Chemical synthesis of poliovirus cDNA: Generation of infectious virus in the absence of natural template. *Science*, **297**, 1016--1018.

48. Gibson, D.G., Benders, G.A., Andrews-Pfannkoch, C., Denisova, E.A., Baden-Tillson, H., Zaveri, J., Stockwell, T.B., Brownley, A., Thomas, D.W., Algire, M.A. et al. (2008) Complete chemical synthesis, assembly, and cloning of a Mycoplasma genitalium genome. *Science*, **319**, 1215--1220.
49. Kong, D.S., Carr, P.A., Chen, L., Zhang, S.G., and Jacobson, J.M. (2007) Parallel gene synthesis in a microfluidic device. *Nucleic Acids Research*, **35**.
50. Ugi, I., Jacob, P., Landgraf, B., Rupp, C., Lemmen, P., and Verfurth, U. (1988) Phosphite oxidation and the preparation of 5-membered cyclic phosphorylating reagents via the phosphites. *Nucleosides & Nucleotides*, **7**, 605--608.
51. Dorsett, Y., and Tuschl, T. (2004) siRNAs: Applications in functional genomics and potential as therapeutics. *Nature Reviews Drug Discovery*, **3**, 318--329.
52. Rothemund, P.W.K. (2006) Folding DNA to create nanoscale shapes and patterns. *Nature*, **440**, 297--302.
53. Liao, S.P., and Seeman, N.C. (2004) Translation of DNA signals into polymer assembly instructions. *Science*, **306**, 2072--2074.
54. Condon, A. (2006) Designed DNA molecules: principles and applications of molecular nanotechnology. *Nature Reviews Genetics*, **7**, 565--575.
55. Au, L.C., Yang, F.Y., Yang, W.J., Lo, S.H., and Kao, C.F. (1998) Gene synthesis by a LCR-based approach: High-level production of leptin-L54 using synthetic gene in Escherichia coli. *Biochemical and Biophysical Research Communications*, **248**, 200--203.
56. Stemmer, W.P.C., Crameri, A., Ha, K.D., Brennan, T.M., and Heyneker, H.L. (1995) Single-step assembly of a gene and entire plasmid from large numbers of oligodeoxyribonucleotides. *Gene*, **164**, 49--53.
57. Gao, X.L., Gulari, E., and Zhou, X.C. (2004) In situ synthesis of oligonucleotide microarrays. *Biopolymers*, **73**, 579--596.
58. Fodor, S.P.A., Read, J.L., Pirrung, M.C., Stryer, L., Lu, A.T., and Solas, D. (1991) Light-directed, spatially addressable parallel chemical synthesis. *Science*, **251**, 767--773.
59. Butler, J.H., Cronin, M., Anderson, K.M., Biddison, G.M., Chatelain, F., Cummer, M., Davi, D.J., Fisher, L., Frauendorf, A.W., Frueh, F.W. et al. (2001) In situ synthesis of oligonucleotide arrays by using surface tension. *Journal of the American Chemical Society*, **123**, 8887--8894.
60. Hughes, T.R., Mao, M., Jones, A.R., Burchard, J., Marton, M.J., Shannon, K.W., Lefkowitz, S.M., Ziman, M., Schelter, J.M., Meyer, M.R. et al. (2001) Expression profiling using microarrays fabricated by an ink-jet oligonucleotide synthesizer. *Nature Biotechnology*, **19**, 342--347.
61. Huang, M.C., Ye, H., Kuan, Y.K., Li, M.H., and Ying, J.Y. (2009) Integrated two-step gene synthesis in a microfluidic device. *Lab Chip*, **9**, 276--285.
62. Ye, H.Y., Huang, M.C., Li, M.H., and Ying, J.Y. (2009) Experimental analysis of gene assembly with TopDown one-step real-time gene synthesis. *Nucleic Acids Research*, **37**.
63. Thorsen, T., Maerkl, S.J., and Quake, S.R. (2002) Microfluidic large-scale integration. *Science*, **298**, 580--584.
64. Huang, Y.Y., Castrataro, P., Lee, C.C., and Quake, S.R. (2007) Solvent resistant microfluidic DNA synthesizer. *Lab Chip*, **7**, 24--26.

65. Wang, Z.W., Olsen, P., and Ravikumar, V.T. (2007) A novel universal linker for efficient synthesis of phosphorothioate oligonucleotides. *Nucleosides Nucleotides & Nucleic Acids*, **26**, 259--269.
66. Paul, C.H., and Royappa, A.T. (1996) Acid binding and detritylation during oligonucleotide synthesis. *Nucleic Acids Research*, **24**, 3048--3052.
67. Moorcroft, M.J., Meuleman, W.R.A., Latham, S.G., Nicholls, T.J., Egeland, R.D., and Southern, E.M. (2005) In situ oligonucleotide synthesis on poly(dimethylsiloxane): a flexible substrate for microarray fabrication. *Nucleic Acids Research*, **33**.
68. Tuma, R.S., Beaudet, M.P., Jin, X.K., Jones, L.J., Cheung, C.Y., Yue, S., and Singer, V.L. (1999) Characterization of SYBR gold nucleic acid gel stain: A dye optimized for use with 300-nm ultraviolet transilluminators. *Analytical Biochemistry*, **268**, 278--288.
69. Septak, M. (1996) Kinetic studies on depurination and detritylation of CPG-bound intermediates during oligonucleotide synthesis. *Nucleic Acids Research*, **24**, 3053--3058.
70. Garland, P.B., and Serafinowski, P.J. (2009) High yield detritylation of surface-attached nucleosides with photoacid generated in an overlying solid film: roles of translational diffusion and scavenging. *Organic & Biomolecular Chemistry*, **7**, 451--459.
71. Li, G., Ran, R., Zhao, J.L., and Xu, Y.S. (2007) Design, simulation, and optimization of a miniaturized device for size-fractioned DNA extraction. *Electrophoresis*, **28**, 4661--4667.
72. Hua, Z.S., Xia, Y.M., Srivannavit, O., Rouillard, J.M., Zhou, X.C., Gao, X.L., and Gulari, E. (2006) A versatile microreactor platform featuring a chemical-resistant microvalve array for addressable multiplex syntheses and assays. *Journal of Micromechanics and Microengineering*, **16**, 1433--1443.
73. Duffy, D.C., McDonald, J.C., Schueller, O.J.A., and Whitesides, G.M. (1998) Rapid prototyping of microfluidic systems in poly(dimethylsiloxane). *Analytical Chemistry*, **70**, 4974--4984.
74. Makamba, H., Kim, J.H., Lim, K., Park, N., and Hahn, J.H. (2003) Surface modification of poly(dimethylsiloxane) microchannels. *Electrophoresis*, **24**, 3607--3619.
75. Vaidya, A.A., and Norton, M.L. (2004) DNA attachment chemistry at the flexible silicone elastomer surface: Toward disposable microarrays. *Langmuir*, **20**, 11100--11107.
76. Fritz, J.L., and Owen, M.J. (1995) Hydrophobic recovery of plasma-treated polydimethylsiloxane. *Journal of Adhesion*, **54**, 33--45.
77. Wen, J.Y., and Wilkes, G.L. (1996) Organic/inorganic hybrid network materials by the sol-gel approach. *Chem Mater*, **8**, 1667--1681.
78. Yuan, Q.W., and Mark, J.E. (1999) Reinforcement of poly(dimethylsiloxane) networks by blended and in-situ generated silica fillers having various sizes, size distributions, and modified surfaces. *Macromolecular Chemistry and Physics*, **200**, 206--220.
79. Roman, G.T., Hlaus, T., Bass, K.J., Seelhammer, T.G., and Culbertson, C.T. (2005) Sol-gel modified poly(dimethylsiloxane) microfluidic devices with high

electroosmotic Mobilities and hydrophilic channel wall characteristics. *Analytical Chemistry*, **77**, 1414--1422.

80. Roman, G.T., and Culbertson, C.T. (2006) Surface engineering of poly(dimethylsiloxane) microfluidic devices using transition metal sol-gel chemistry. *Langmuir*, **22**, 4445--4451.
81. Roberts, M.A., Rossier, J.S., Bercier, P., and Girault, H. (1997) UV laser machined polymer substrates for the development of microdiagnostic systems. *Analytical Chemistry*, **69**, 2035--2042.
82. McCormick, R.M., Nelson, R.J., AlonsoAmigo, M.G., Benvegnu, J., and Hooper, H.H. (1997) Microchannel electrophoretic separations of DNA in injection-molded plastic substrates. *Analytical Chemistry*, **69**, 2626--2630.
83. Martynova, L., Locascio, L.E., Gaitan, M., Kramer, G.W., Christensen, R.G., and MacCrehan, W.A. (1997) Fabrication of plastic microfluid channels by imprinting methods. *Analytical Chemistry*, **69**, 4783--4789.
84. Qin, D., Xia, Y.N., and Whitesides, G.M. (1996) Rapid prototyping of complex structures with feature sizes larger than 20 mu m. *Advanced Materials*, **8**, 917.
85. Regehr, K.J., Domenech, M., Koepsel, J.T., Carver, K.C., Ellison-Zelski, S.J., Murphy, W.L., Schuler, L.A., Alarid, E.T., and Beebe, D.J. (2009) Biological implications of polydimethylsiloxane-based microfluidic cell culture. *Lab on a Chip*, **9**.
86. Toepke, M.W., and Beebe, D.J. (2006) PDMS absorption of small molecules and consequences in microfluidic applications. *Lab on a Chip*, **6**, 1484--1486.
87. Liu, D.J., Perdue, R.K., Sun, L., and Crooks, R.M. (2004) Immobilization of DNA onto poly(dimethylsiloxane) surfaces and application to a microelectrochemical enzyme-amplified DNA hybridization assay. *Langmuir*, **20**, 5905--5910.
88. Efimenko, K., Wallace, W.E., and Genzer, J. (2002) Surface modification of Sylgard-184 poly(dimethyl siloxane) networks by ultraviolet and ultraviolet/ozone treatment. *Journal of Colloid and Interface Science*, **254**, 306--315.
89. Hillborg, H., and Gedde, U.W. (1998) Hydrophobicity recovery of polydimethylsiloxane after exposure to corona discharges. *Polymer*, **39**, 1991--1998.
90. Reiter, R.E., Gu, Z.N., Watabe, T., Thomas, G., Szigeti, K., Davis, E., Wahl, M., Nisitani, S., Yamashiro, J., Le Beau, M.M. et al. (1998) Prostate stem cell antigen: A cell surface marker overexpressed in prostate cancer. *Proc. Nat. Acad. Sci. USA*, **95**, 1735--1740.
91. Roberts, C., Chen, C.S., Mrksich, M., Martichonok, V., Ingber, D.E., and Whitesides, G.M. (1998) Using mixed self-assembled monolayers presenting RGD and (EG)(3)OH groups to characterize long-term attachment of bovine capillary endothelial cells to surfaces. *Journal of the American Chemical Society*, **120**, 6548--6555.